Reply to interactive reviewer comment by reviewer 1 (Pedro Costa)

We appreciate the constructive comments and suggestions on our manuscript. Below, we will reply to each of them separately (please note: line numbers refer to the revised version with track changes).

Comment: Your manuscript is very well prepared. It is nicely written and fits perfectly within the scope of the journal. The figures serve their purposes very well. In fact they illustrate with high-quality the reasoning forwarded and facilitates the reader's job because they are very informative. Nevertheless, their number seems a bit excessive and a couple of them couple be merged (e.g.A14-A15-A16).

Reply: We decided to use a large number of figures to document our findings to the reader as comprehensive as possible. However, we agree that an excessive use of figures may be rather distracting from the main aspects of the paper and have merged and excluded some of the supplement figures.

Changes in revised version: We have merged figures of the appendix where possible in the revised version. Figs A14 to A16 were simplified by only presenting average values and omitting individual measurement data (as also recommended by reviewer 2). This allows the IRSL data presented in Fig. A16 to be merged with the associated plots in Figs A14 and A15. Figures A18 and A19 have been excluded from the manuscript, since they duplicate data from Figure 5.

Comment: The text flows well and, with the exception of very few misspelling words, it is impeccable to read. References seem to be updated and formulas used are properly formatted.

Regarding science, this manuscript focus on one key issue on storm and marine deposits, namely in boulder deposits. It is a known problem to accurately date the transport of these boulders in coastal settings and it is a theme that have constrained the accurate establishment of return periods and hazard assessments in many locations worldwide. The authors used a well-controlled setting within a short-time window of observation which allowed comparison with aerial/satellite imagery. Thus, narrowing time-interval of transport being studied. The concept and the example selected is interesting and very sound. However, several question still remain to be answered. I will raise a few below but first would like to stress that I feel this manuscript clearly addresses a relevant topic and, with the results presented, moves science forward.

The "new" OSL methodology presented is robust and should/needs to be further tested in other locations. A shame we do not have this methodology compared with other dates from other previously studied locations. The fact that is from specific locations clearly puts forward its potential but still leaves some doubts regarding its reliability. It would be interesting to have further direct age comparisons.

Reply: We absolutely agree that independent age control is required to better evaluate the reliability of the dating approach. Unfortunately, most alternative dating techniques that have been used for determining boulder chronologies so far (i.e. mainly radiocarbon and U/Th dating of coral boulders or attached organisms) are associated with pure limestone lithologies, which cannot be used for OSL dating. Cosmogenic nuclide dating that would work on the same rocks, is not sensitive enough to provide useful age control due to low production rates at sea level and the comparatively short time scales of a few centuries or less. There are currently plans to try to establish a lichen chronometry for the study site, an approach that showed large potential for the time scales we are talking about in a recently published study (Oliveira et al., 2020, Progress in Physical Geography). But even if this attempt should be successful, it will take years to work robustly.

Similar constraints apply to most other boulder deposits. So when we selected the site for this study, we chose boulders with potentially adequate properties for OSL-RSED (which excludes pure limestone boulders due to the lack of quartz and feldspar, and magmatic boulders due to problems with clearly identifying overturning), for which at least age control in form of satellite data and observations for the last decades was available. Since this age control is undoubtedly limited, the presented study is of course only a first attempt to better understand the potential and the challenges associated with the dating approach. More case studies are definitely required to further evaluate the reliability of the dating approach, and we think that the selection of future sites will significantly benefit from the conclusions drawn from our data.

Changes in revised version: We realized that the reasoning for site selection may not have been explained explicitly enough in the original manuscript. In the revised version, we added some explaining sentences to the introduction in lines 72-77.

Comment: One aspect that concerns me is the obvious dependence on mineralogy. Limestone coastal areas will still be a challenge and one that needs to be addressed. Nevertheless, this manuscript clearly points very interesting future research directions.

Reply: Indeed OSL-RSED cannot be applied to pure limestone boulders, which unfortunately excludes a large portion of all boulder deposits, particularly in tropical regions. However, the approach promises to provide chronological information for boulder sites with quartz and/or feldspar bearing lithologies, such as sandstones, calcarenites and igneous boulders, which also account for a significant number of boulder sites. In other words, we do not pretend to present a dating solution that is applicable to all boulder deposits, but a technique that might provide chronological information for some of them. It is, however, important to highlight, that OSL-RSED can address boulders which are specifically hard to date with alternative approaches so far. Most existing chronologies for Holocene boulders are restricted to limestone boulders that are composed of or associated with calcareous organisms datable by radiocarbon or U/Th.

Changes in revised version: We now document the lithology-related limitations and chances of OSL-RSED more explicitly in the introduction (lines 66-68) and conclusions (lines 588-590) of the revised version.

Comment: The mineralogy-dependence is an obvious constrain to this methodology. This is also evident when we have weathering or erosion. There are micro-erosion meters and they should have been used. I am aware erosion meters have slow rates and require a larger time-window of observation, nevertheless the modelled erosion rates represent for me a huge degree of uncertainty that might have been avoided with empirical data. Furthermore, these rates are highly controlled by lithology, mineralogy and texture. So, this section of the manuscript is valuable but would benefit from a larger discussion on its shortcomings. Furthermore, this is a key issue in the new OSL methodology: before dating the surface, one must very accurately establish the erosion since deposition.

Reply: We appreciate the suggestions to improve the discussion of erosion as a key factor for reliable OSL-RSED ages. Micro-erosion meters are a very good idea that we unfortunately did not consider when starting the study, but which should be included in systematic future studies on OSL-RSED as a possible means of better evaluating modelled erosion rates inferred from the OSL data. We already discussed the uncertainties introduced by dating unstable (eroding) surfaces and consider the influence of texture and mineralogy on erosion rates, since these are inherent factors controlling the model output of individual samples. We, however, agree that the paper would also benefit from a critical discussion of the approach we used to determine erosion rates and about benefits of potential alternative approaches, such as erosion meters.

Changes in revised version: We extended the discussion of erosion rates in the revised version of the manuscript by implementing a critical view on the limitations of modelling and the potential benefits of alternative approaches (lines 458-466).

Comment: Regarding the study case, it has been widely established that in many coasts along the North Atlantic from Iceland (Etienne and Paris, 2010), Ireland (Cox et al., 2019) to Portugal (Oliveira et al., 2020) boulder deposits are essentially associated with storm events. There are occasional cases where tsunami origin has been discussed but many times with caution. In that sense, the authors should be less bold on lines 470-475 in particular when comparing case studies with multiple dating methodologies with others with a single methodology or even with just a single measurement. So, the dominance of short-lived and frequent storms on the creation and shaping of boulder deposits is natural in particular in areas not so prone to tsunami events like the North Atlantic. This raises the issue of poor and difficult recognition of tsunami boulder deposits except when very specific dates are obtained (which is very difficult) or when size of boulders and its heights allows to disregard storm origin...but even then, there is the possibility of being palaeo-storm signatures of past higher sea-levels. So, to conclude the data provided from the study case reinforces the reasoning above and I recommend the authors to stress this aspects by adding a couple of sentences on this.

Replay: Thank you for this comment. We agree that the aspect of discriminating between storm and tsunami origin might need a bit longer discussion. In essence, our data support the reviewer's opinion that in most regions the majority of coastal boulders are associated with storms and that a tsunami origin at such locations is usually hard to verify with the chronological data available. As such, our data also support that boulders identified along the Atlantic coasts of Morocco and Iberia have to be treated with caution when it comes to discussing their tsunami origin, since the associated chronologies usually do not allow to precisely differentiate specific events. It is, however, right that most of the associated studies already acknowledge storms as an alternative transport mechanism. We apologize, if our formulation has implied something else.

Changes in revised version: We used a more cautious wording with regard to the interpretation of coastal boulders in other studies in the revised version of the manuscript (lines 558-566). This also includes a brief but more detailed discussion of the difficulties related to tsunami boulder recognition (lines 509-513).

Reply to interactive reviewer comment by reviewer 2 (anonymous)

While we disagree with most of the conceptual concerns raised by reviewer 2, we however appreciate the detailed comments and suggestions on our manuscript. We will reply separately to each of the concerns below (note: line numbers refer to the revised version with track changes).

Comment: This study attempts to determine the exposure ages of some large wave-transported boulders at the coast of Rabat, Morocco, using OSL rock surface exposure dating (OSL-RSED). The final exposure ages are however deemed as unreliable (i.e. imprecise and inaccurate) because of large data scatter, resulting in significant fitting uncertainties, and underestimated due to the erosion of boulder surfaces. This is altogether not very surprising, given that neither the selected lithology nor the chosen geomorphic settings are suitable for OSL-RSED technique.

OSL-RSED requires sensitive quartz and feldspar minerals, while the target boulders in this study are calcarenite, a type of limestone that is predominantly composed of carbonate, which does not have the required luminescent properties for OSL dating. OSL-RSED is also based on the sunlight-driven evolution of mm- to cm-scale luminescence-depth profiles beneath rock surfaces, and is thus very susceptible to the effect of erosion, down to sub-mm scales. Such erosion-sensitive profiles cannot be used to derive reliable surface exposure ages from boulders undergoing wave and bio-erosion at rates of ~1 mm a-1, as is the case in this study.

Reply: We will address the 5 major points of criticism separately after this general comment, but we feel it is necessary to reply to this specific conceptual comment on site selection already here.

We fully agree that the boulder lithology and the coastal setting used in this study do not provide circumstances that are ideal for OSL-RSED. However, our reasoning for conducting this study was not to apply OSL-RSED to a geomorphological/geological context with ideal preconditions, but to evaluate the potential of the approach for coastal boulder deposits. These deposits indeed potentially represent an important archive for coastal hazard assessment, but they often lack chronological information to be fully exploited. In the absence of alternative dating approaches (which is the case for numerous boulder fields worldwide), any (even relative) chronological information that might be provided by OSL-RSED is useful, because in many locations it is the only chronological information available. In this study we make a first attempt to evaluate the potential of the approach for coastal boulders in general (please note: this is not a dating study), and this includes to accept the challenging conditions and to document how they affect the reliability of the dating approach.

Therefore, we were completely aware of the rather difficult conditions for OSL-RSED of coastal boulders in general when we started the study, and we selected a site that (although not ideal compared to other geomorphological contexts) offered all indispensable prerequisites for the evaluation of OSL-RSED: A lithology containing quartz and feldspar, unambiguous signs of boulder overturning in their taphonomy, and age control at least for some of the boulders. Boulder sites with more appropriate lithologies for OSL-RSED typically lack clear indication of boulder movement and age control, and coastal boulders with better independent chronologies are typically composed of pure limestone that cannot be used for OSL dating.

Although not ideal, the properties of these boulders are not as poor as implied by the reviewer comment. Calcarenites are carbonate-dominated and/or carbonate-cemented sandstones (they are predominantly, i.e. > 50 %, composed of carbonate grains). This means that they can contain up to 50 % non-carbonate grains such as quartz and feldspar. At the Rabat coast, the calcarenites generally do contain sensitive quartz and feldspar. This is shown in our study using pure quartz and feldspar extracts, and it was already documented in other publications prior to this study, e.g. by Barton et al. (2009, Quaternary Science Reviews).

Furthermore, as to the comment on wave- and bio-erosion on boulder surfaces, we have to note that we explicitly did not sample surfaces that were affected by wave- or bio-erosion (except for one case, VAL 1, to investigate the effects of wave- or bio-erosion) under regular/typical non-storm conditions. The samples that are considered for dating are all well above the zone of wave- and bio-erosion. Erosion of their surfaces is driven by atmospheric weathering of the calcarenite, independent of wave- and bio-erosion. Since we selected apparently smooth surfaces with no clear signs of erosion, the quantification of erosion (which in retrospect is larger than expected at least for some of the surfaces) was one aim of this evaluation study.

Changes in the revised version: We realized that the reasoning of site selection may not have been explained explicitly enough in the original submission and, therefore, added two sentences with regard to this topic in the introduction of the revised version (lines 72-77).

Comment: While I appreciate the amount of effort the authors have put to overcome the challenges arising from this adverse combination of poor luminescence properties and erosion, I am afraid their manuscript, at its present form, is not rigorous enough to be considered for publication in Esurf. I could consider this study as a useful methodological contribution to the rapidly growing literature on OSL-RSED if the OSL methods were sound and the data were treated properly. But in my view, this is unfortunately not the case here. In the following, I give an account of both conceptual and methodological issues, which particularly seem problematic to me and try to explain how they could be dealt with differently, where possible. In my opinion, the manuscript may only be considered for publication after addressing these issues properly in a new submission.

Reply: Our study is meant as a methodological contribution, not a dating paper. We think we have addressed all methodological concerns in the revised version, why we think it is suitable for publication. In the following, we will address the five main points, on which the criticism is based on.

Geomorphology and process/hazard information:

Comment: The application of OSL-RSED to coastal boulders as is shown in Fig. 1 is oversimplified, as it does not take the effect of reworking into account. If storm surges have enough energy to detach fresh boulders from bedrock, it is very likely that they can rework (slide and overturn) the previously detached boulders sitting loose on the beach as well. It is thus quite conceivable to imagine that some of the surfaces have undergone multiple burial and exposure events, and not only a single continuous exposure event after detachment, as is conceptualised in Fig. 1. In this environment however, the dose rates are low and the burial events are too short (because storm events have high frequency and occur on decadal timescales) to leave a record in the shape of the OSL-depth profiles. Thus, an observed OSL-depth profile measures the cumulative exposure time since the detachment event, and has no record of the subsequent storm events that might have reworked the surface. Consequently, even in the absence of complications due to e.g. erosion and poor luminescence characteristics, such profiles are not particularly useful for deriving process information in similar geomorphic settings. They cannot be used for reconstructing boulder transport histories (as the title suggests), because they do not have a memory of the burial events.

Reply: We agree that we can only date the first overturning event of each boulder and not the subsequent movements. So yes, it is right that OSL-RSED of the boulders cannot be used to reconstruct the multiple transportation events that might have moved them to their final position (we admit that the present title indeed may be misleading). This is, however, not because of problems to differentiate multiple overturning events. The boulders targeted in this study have most likely been overturned only once. All of the sampled boulders weigh several tons and have a platy shape, corresponding to FI (i.e., flatness index, Nandasena and Tanaka, 2013) values of >1 or mostly even >2. It is documented in boulder literature that such clasts are usually overturned during storms when detached from the cliff (in this situation storm waves can attack the boulders from below, e.g. Noormets et al. 2004), but that it needs waves with much larger velocities and heights to overturn them once they rest scattered on the supratidal platform (e.g. Nandasena, 2020). The predominant transport mode for a non-cubic subaerial boulder (i.e., such as most boulders in this study, with FI >2) is sliding, not rolling (Imamura et al. 2008;

Nandasena and Tanaka, 2013; Liu et al., 2015). While we admit that this could be explained more explicitly in the manuscript, the current state of the art in boulder transport by storms clearly supports the transport model shown in Figure 1 and contradicts any biasing of our OSL-RSED data by multiple overturning events. Movement of the boulders subsequent to cliff detachment can happen and probably has happened to most of the sampled boulders. But due to the boulder's shape, mass and distance from the cliff, sliding is the most plausible transport mode.

Changes in the revised version: We changed the title of the manuscript to "Evaluating OSL rock surface exposure dating as a novel approach for reconstructing coastal boulder movement on decadal to centennial timescales" in order to better reflect the limitations of the approach with regard to dating sliding motion after cliff detachment. Furthermore, we improved the description of boulder transport at the study site, to clarify that boulders have been overturned only once (lines 59-63 and lines 106-120).

Comment: They are not good proxy for storm events either, because they only record the single event that detached them from the cliff and not any of the subsequent storm events. One could argue that subsequent events of similar or higher energy are expected to pluck fresh blocks that could also be dated in a similar manner to give a chronology for the storm events. In that scenario, one would expect to see an overall trend of longer exposure events (the so-called "transport ages" here) and thus deeper OSL profiles as one moves farther from the coast, because the storms should gradually push the older boulders inland with time. But this does not seem to be the case; at least not here. For example, according to the age control, sample VAL 6 at a distance of _80 m from the cliff seems to be younger than sample VAL 4, which is located only _25 m from the cliff. This presumably implies that boulder detachment is not merely driven by wave power, but is also controlled by other factors such as joint formation and orientation. This inherent geomorphic character can limit the use of OSL-RSED to derive process/hazard information from coastal boulders.

Reply: We completely disagree with this opinion, since it contradicts all research on coastal boulder records. The reviewer's argument is clearly opposed by the existing literature on coastal boulders (see e.g. the latest review by Lau and Autret, 2020 and references therein). Coastal boulders have frequently been used as an archive for long-term tsunami and storm hazard assessment (e.g. Terry et al., 2013 and references therein). Regardless of the dating approach used (mainly radiocarbon, U/Th and ESR dating), all of these studies are based on ages for the initial onshore transport of the boulders, i.e. due to detachment from the cliff/reef or due to lifting from subtidal areas to the supratidal platform (e.g. Zhao et al., 2009; Engel and May, 2012; Araoka et al., 2013; Rixhon et al., 2017). While the data presented in these publications do not allow to date each transportation event and consequently not every storm, they show that (i) this limitation is not restricted to OSL-RSED but an inherent problem of all established dating approaches applicable to coastal boulders; (ii) ages of initial onshore transport can give a good impression of the recurrence patterns of storms/tsunami if sufficient boulders are dated, particularly since with increasing age specific events cannot be discriminated chronologically anyway (the fact that the scenario described by the reviewer is not reflected by the small number of ages presented in this study does not mean that the principles behind it do not generally apply); and (iii) boulder movement is often not controlled exclusively by wave power, but it is typically the dominant factor. This means that using coastal boulder records for reconstructing the history of extreme wave events may be limited by some of your concerns, but since they are the best (and often only) archive available for the reconstruction of storm/tsunami impact over geological timescales, these limitations (which apply to all dating approaches, not only OSL-RSED) are widely accepted.

To sum up our reply to the general conceptual issues, it is particularly the potential of OSL-RSED that makes it a promising candidate for providing chronological information on non-limestone, quartz- and/or feldspar-bearing boulder deposits and to make use of the coarse clast record for reconstructing extreme event histories. The exposure dating has also the potential to provide depositional ages, which is preferred in comparison to dating of marine organisms prone to reworking. We consider this a chance to explore the coastal coarse clast record, and this paper shall present a step forward by evaluating and testing the potential. As we have argued before, the conceptual concerns of reviewer 2 are unsubstantiated.

OSL-RSED data presentation:

Comment: I find the presentation of profile data in Figs. 4, A14-16 cluttered and obscure. The mean data points with standard errors include all the information one needs to evaluate the reliability of individual data points and the overall progress of the bleaching front in a given surface. These are also the data points that are fitted to derive either the exposure age or erosion rate. So, in my view, the presentation of individual aliquots and cores in the way it is done in Figs. 4, A14-16 does not provide any useful information and impedes a proper assessment of the quality of the data.

The fits to the profile data that are used to derive the parameter values in Table 2 are not shown. Without the fits, one cannot evaluate their goodness and the reliability of the resulting parameter values.

In order to enable a clear evaluation of the data, my suggestion is to only present the mean data points with standard errors and the fits to the mean data.

Reply: Thank you for this comment. We understand the criticism of the way the OSL signal-depth data of the individual samples was presented. Our reasoning for presenting the data the way it was done in the original submission was to show the reader the entire data set he analyses is based on. We, however, realized that this may rather distract from the important information, which are the mean values and the fit of the data.

Changes in the revised version: In the revised version we followed the suggestion of reviewer 2 and adjusted Figures A14 and A15 by (i) presenting only average values for each depth, (ii) plotting the associated fit of the data to allow evaluation of its reliability, and (iii) providing the values for μ and sigmaphi_0 used for fitting each sample.

OSL-RSED calibration:

Comment: The data from calibration sample RAB 5-1 CAL in Fig. 5 seem to reach a plateau at _0.8 and not 1. This makes me wonder i) why this sample was normalised differently and ii) how this apparently different normalisation must have affected the calibration values derived from this sample, and hence the mean calibrated parameter values used to derive the exposure ages/erosion rates. I note that the same (mean) data presented in Fig. A18 seem to have been normalised correctly. This needs to be revised, in case the authors choose the keep this sample in a new analysis of calibration data. Please see my comment below.

Reply: Sorry for the confusion. There has been a mistake in the axis configuration of this sample in Figure 5. The data set used for model calibration in the original submission was, however, based on values normalized to 1.0 already. Thus, the calibration results were not affected by this issue.

Changes in revised version: The axis configuration in figure 5 was adjusted.

Comment: The data from calibration samples VAL 4-1 CAL 2 and RAB 5-1 CAL seem to be much more scattered than those from the other samples. Given the goodness (badness?) of the fits to such poor-quality data, I do not think that the parameter values derived from these samples can be deemed as reliable. It is also intriguing that although the data from these samples are much more scattered than those from e.g. sample TEM 3-1 CAL, the relative uncertainties on sample-specific sigmaphi_0 values derived from these samples are smaller than the uncertainty on the corresponding value obtained for sample TEM 3-1 CAL.

Reply: It is absolutely right that these two samples are much more scattered than the others and we agree that individual values fitted using the data are not reliable. We therefore only used them in combination with the two other samples with flat surfaces to fit mutual sigmaphi_0 values.

Changes in the revised version: As suggested, we excluded samples VAL 4-1 CAL 2 and RAB 5-1 CAL from model calibration in the revised version.

Comment: It is argued that the sample-specific μ values have "huge uncertainties", and therefore site-specific values of μ have been derived instead as "a reasonable and necessary compromise". This argument is not supported by the presented data, and is not in accordance with our understanding of μ as a physical parameter.

Firstly, the relative standard deviation (RSD) of sample-specific μ values derived from the calibration samples in Fig. 5 is ~34%, while the RSD of the corresponding sigmanphi_0 values is ~210%. So, if sample-specific μ values can be dismissed because of large uncertainties and overdispersion, how can sample-specific sigmaphi_0 values, which have even greater uncertainties and are more dispersed, be acceptable and taken as a shared parameter between the calibration samples?

Secondly, if μ is dependent on lithology and all samples come from the same calcarenite bedrock, why not sharing μ between all the samples from all the sites? There is no evidence (or at least not presented here) that bedrock lithology varies from one site to another, so I cannot really see the logic behind sharing μ between samples from individual sites, but not between all the samples.

Reply: We cannot really follow the argument in this comment. We did not use sample-specific sigmaphi_0 values for calibration. We used a mutual value for all samples (otherwise we would need individual calibration samples for each targeted boulder). Thus we followed the same approach as for μ, i.e. improving the reliability of fitting by sharing the same value for several samples.

While mutual sigmaphi values are, according to current knowledge, a realistic assumption for boulder surfaces from the same area and with the same surface inclination, mutual μ values indeed do not reflect the heterogeneity of rocks even from the same lithological formation (e.g. Gliganic et al., 2019). This is also the case for the study site. Although the lithology is generally

similar (all calcarenite) for all boulders targeted in this study, it is not completely uniform along the entire coastline. There are slight differences in granulometry and content of bioclasts. As we explain in the original manuscript version, the best way to account for expected differences in lithology would be to use a sample-specific μ value for each sample. This is, however, impeded by fitting uncertainties, which lead to unreliable sample-specific values. We therefore have to use several samples to derive a mutual μ value. To account at least for lithological differences between the different study sites, for each of which a sufficient number of samples is available, we decided to calculate site-specific μ values in the original submission. We, however, realized that the reasoning for site-specific μ-values was not explicitly mentioned and that using a mutual μ value for all samples, as suggested by the reviewer, might indeed improve the robustness of the data (the number of samples the value is based on is much larger).

Changes in the revised version: In the revised version we followed the suggestion of the reviewer and used a mutual μ value of 1.39±0.15 for all samples. All analysis (calibration, age calculation, erosion modelling) were redone with this value. All figures and tables were updated accordingly.

Comment: The issues mentioned above make me wonder about the robustness of the calibration approach undertaken here and the reliability of the resulting parameter values. To address these issues, I would reanalyse the calibration data by i) excluding the inferior data of samples VAL 4-1 CAL 2 and RAB 5-1 CAL, and ii) sharing μ between all samples or leaving it as a free sample-specific parameter in fitting.

Reply: According to our replies above, we reanalysed the calibration data. While these modifications change the individual ages of each boulder, the overall chronological pattern of the boulders and, thus, our main conclusions are not affected.

Changes in the revised version: To reanalyse the calibration data we (1) excluded the strongly scattered samples VAL 4-1 CAL 2 and RAB 5-1; (2) started with the calculation of a mutual μ value of 1.39±0.15 mm^{-1} for all samples by simultaneously fitting all samples (calibration samples and samples of unknown age) with μ as free and shared parameter and age x sigmaphi_0 (see e.g. Sohbati et al., 2015) as a single free and unshared parameter; and (3) calculated the mutual sigmaphi_0 using the calibration samples and the mutual μ (lines 325-355). All analysis based on the signal-depth data and all data resulting from them were recalculated with these new values. While the exact numbers are different, the main conclusions do not change.

Erosion rate modelling:

Comment: The authors have followed a numerical approach (not “analytical” as is mentioned in line 333) to model the OSL erosion rates. But, the OSL erosion rate equation has an exact analytical solution that is already published (see Sohbati et al., 2018). So, there is no need and no scientific justification for making guesses at the solution numerically as is done here. The parameter values derived from the calibration samples can simply be inserted in the erosion rate equation and fitted to the profiles to give erosion rates.

Reply: The approach of Lehmann et al. (2019) that we applied to our samples is indeed a numerical approach. We, however, completely disagree that the application of a numerical approach lacks scientific justification while an analytical approach exists. We are aware that an analytical solution for the quantification of erosion from OSL rock surface data was already

presented by Sohbati et al. (2018). The numerical approach of Lehmann et al. (2019) that is used in this study was later published in Earth Surface Dynamics, acknowledging the analytical approach but providing an alternative solution for the erosion problem. Both approaches have their advantages and there is no approach that is absolutely superior compared to the other. The analytical solution of Sohbati et al. (2018) might be more elegant and faster, but the numerical approach chosen in this study (which is not guessing, but inferring results from our data) is able to resolve the problem in time and provides a quantification of misfits and thus uncertainties on the results.

Changes in revised version: We refer to the Lehmann et al. (2019) model as a numerical approach in the revised version of the manuscript (line 389).

Minor comments:

Comment, Line 17: I suggest "wave-driven" instead of "wave-emplaced". The boulders cannot be "emplaced" by waves and "transported" at the same time.

Changes in the revised version: The wording was changed to "wave-driven".

Comment, Lines 48-49: "...these approaches are restricted to certain boulder lithologies and time scales.". So is OSL RSED; it is largely restricted to lithologies that "contain quartz and/or feldspar" and to timescales of "decades, centuries up to a few millennia" as is mentioned later in lines 61-62.

Reply: Thank you for this comment. We realized that we have to be more specific here. Palaeomagnetic dating still suffers from a number of intrinsic methodological limitations, and cosmogenic nuclide dating typically cannot provide sufficient resolution on Late Holocene time scales and is, therefore, of limited benefit for the vast majority of coastal boulders.

Changes in the revised version: We added a sentence explaining the limitations of the two dating approaches more specifically in the revised version of the manuscript (lines 49-53).

Comment, Line 63: Does the statement "...to reconstruct...tsunami frequency patterns..." imply that the tsunami events are expected to follow some sort of temporal/spatial patterns?

Reply: Yes, tsunamis typically show temporal patterns if they are generated by earthquakes. Since the 1755 Lisbon tsunami was triggered by an offshore earthquake, it is not unlikely that potential predecessors follow a certain temporal pattern that is controlled by the accumulation of seismic strain.

Comment, Lines 71-72: Consider to change "...erosion of post-transport exposed boulder surfaces..." to "erosion of boulder surfaces exposed after transportation" or something like that.

Changes in the revised version: The wording was changed accordingly.

Comment, Line 79: Add "buried" before "sediment".

Changes in the revised version: Will be changed as suggested.

Comment, Line 94: What Fig. 1 is actually showing is a boulder that is detached from a wave-cut platform and overturned by waves. There is no “transportation” involved in the depicted scenario.

Reply: The relocation of the boulder from the cliff edge to the supratidal coastal platform in an overturning movement clearly involves transportation. In Figure 1 the process of overturning during transport is illustrated by showing two successive stages of boulder movement.

Changes in the revised version: We nevertheless changed the wording in the revised version to better express the fact that we always date the cliff detachment of overturned boulders and not potential transport events following afterward, which typically take place as a sliding movement for plate-shaped boulders as selected in this study (lines 105-120).

Comment, Line 147: I cannot see how 2-3 m-high spring tides can reach and exceed the 5-m high first ridge (as is mentioned in line 154) to flood Oulja.

Reply: While the first calcarenite ridge shows average heights of about 5 m above sea level, this barrier occasionally shows sections with lower elevations or can even be breached at river mouths. This is where water can enter the depression of the Oulja during high tides.

Comment, Lines 189-196: The preheat temperature should also be mentioned somewhere in these lines as Table A2 is in the Appendix.

Changes in the revised version: In the revised version, we now mention the preheat condition, i.e. 220 °C for 10 s (line 221).

Comment, Line 191: The stimulation time in Table A2 is 150 s and not 160 s.

Reply: Sorry for this mistake. This should be 160 s as stated in the main text.

Changes in the revised version: Table A2 was updated accordingly.

Comment, Lines 197-208: I suppose the dose recovery and preheat plateau tests described in this paragraph were carried out to guide decision on the most suitable measurement protocol. In that case, this paragraph must precede the previous paragraph in which the actual measurement protocol is explained.

Changes in the revised version: We changed the order of arguments to clarify that these experiments were used as a basis for final protocol selection.

Comment, Line 207: The “burial ages” suddenly appear here. So far, only OSL RSED is discussed. It is also mentioned (in lines 104-105) that the buried sides of the boulders are inaccessible and “not tried in this study”. So, speaking of burial ages here is confusing to me. In fact, it is first 60 lines further down in the text (line 267) that a careful reader may find out that what here is referred to as burial age, is actually the rock formation age, calculated by dating quartz extracts from deep layers within the boulders that have never seen light after rock formation. These should not be confused by boulder surface burial ages.

Reply: Sorry for the confusion. While the ages indeed reflect the timing of sand grain burial during ridge formation, we agree that the term “burial age” may be ambiguous in this study.

Changes in the revised version: To differentiate rock surface burial ages (which were not determined in this study) from conventional OSL dating of the sandstone formation (which we refer to here), we replaced "burial ages" by "ages for sandstone formation" in the revised version.

Comment, Line 212: I find the use of the term "background level" inappropriate here. Background level in OSL dating is commonly referred to while discussing the stimulation curves. I suggest "plateau" instead.

Reply: We absolutely agree that the term "background" may be misleading in this context.

Changes in the revised version: The wording will be changed as suggested.

Comment, Lines 214-215: This sounds to be a subjective and qualitative approach towards removing the outliers, while there are various quantitative methods to identify them. One common approach that could also be used here is to remove those data points that are different than the mean by three standard deviations.

Reply: Thank you for the suggestion. Our approach was indeed somehow subjective.

Changes in the revised version: We revised our rejection criteria as follows: (i) Entire cores were excluded, if they did not show any signs of bleaching with depth, while all other cores from the same sample did. (ii) All other data points were classified as outliers according to a deviation from the mean of more than 2 standard deviations (lines 245-247). We use this new data set for all analysis in the revised version. The data, however, did not change significantly.

Comment, Line 229: Not sure what is meant by "comparable preconditions for sunlight exposure". If the scenario is as simple as shown in Fig. 1, then all the boulders must have experienced comparable conditions (i.e. detachment and overturn). But if they are likely to have been reworked (i.e. moved and turned over multiple times) then it is very difficult to imagine how they could have had comparable exposure conditions.

Reply: The meaning of this term is explained in the second part of this sentence. While all boulders used for this study have been overturned only once (see reply to main comment: the platy boulders used in this study were overturned when detached from the cliff, but moved by sliding only or not at all afterwards), sunlight exposure may also be different due to differential shielding after deposition or due to different exposure angles.

Changes in the revised version: We changed "preconditions" to "conditions", since this term seems more appropriate.

Comment, Line 252: How about "target" instead of "dated"?

Changes in the revised version: Changed as suggested in the revised version.

Comment, Lines 253-256: It is difficult for me to judge this inference by the way the data are presented in Fig. A12. The pure quartz BSL, K-rich feldspar IRSL and polymineral post-IRSL-BSL signals must be normalised and shown on the same graph to enable a direct comparison.

Reply: We do not agree with this opinion. What we want to document is: (1) Post-IRSL-BSL signals of polymineralic aliquots are significantly stronger than the IRSL signals measured on

the same polymineralic aliquots. This is documented in Fig. A12a, where normalized values of both signals are compared in the same plot (as asked for by the reviewer). (2) The post-IRSL-BSL signals of polymineralic aliquots are dominated by a quartz signal with only minor influence of feldspar signals. This is documented in Fig. A12d, which shows that the IRSL stimulation used in our protocol reduces the potassium feldspar signal to 60% of its initial value (more details are given in the caption of Fig. A12).

Comment, Lines 274-275: I assume that calibration was carried out before fitting the actual data? Please present the steps in data analysis in the logical order.

Reply: We used this sentence as an introduction to the explanation, why calibration is necessary.

Changes in revised version: To avoid confusion, we changed the wording to "To estimate boulder ages with OSL-RSED, measured post-IRSL-BSL signal-depth data must be fitted with the bleaching model described in Equation (1)".

Comment, Line 279: Sohbati et al. (2011) is the correct reference.

Changes in revised version: The reference was changed accordingly.

Comment, Lines 293-295: This is an interesting observation that the calibration sample TEM 3-1 CAL that is collected from an inclined surface yields a sigmanphi_0 value that is ~3 orders of magnitude larger than the corresponding values estimated for the horizontal surfaces. If this conclusion still stands after data reanalysis (see my comments above), it would be useful to report the tilt angle of the surface. At the moment, there is no data on the dependence of sigmanphi_0 on the incident angle of solar radiation in the literature.

Reply: After reanalysing the data by excluding the two calibration samples with poorly defined bleaching fronts, there is still a significant difference of one order of magnitude between the horizontal calibration samples and the inclined calibration sample (the angle of the surface is already reported in Table 1 with ~25°). We agree that such an observation has not been reported and would be worth a more detailed investigation. We are, however, aware that our assumption is only based on a single sample (and a total set of 5 calibration samples even without excluding RAB 5-1 CAL and VAL 4-1 CAL2). It obviously needs a larger dataset and more controlled conditions (e.g. in a bleaching experiment) to evaluate the assumed relationship between inclination of the surface and sigmaphi_0.

Comment, Line 307: What is meant by "inadequate" here?

Changes in revised version: We changed "inadequate" to "incorrect".

Comment, Line 333: The approach of Lehmann et al. (2019) is numerical not analytical.

Changes in revised version: We changed "analytical" to "numerical" in the revised version.

Comment, Line 356: "observed" instead of "achieved"?

Changes in revised version: The wording was changed accordingly.

Comment, Line 365: It seems unlikely to me that "mineralogy-induced dose rate differences" can result in the observed scatter in data from such samples. Hot minerals such as zircon and

K-rich feldspars are rare, if not non-existent, in calcarenite. Meyer et al. (2018) have attributed similar scatters in their data to the presence of opaque minerals and iron hydroxides, which strongly impede the penetration of light with depth. In the absence of any independent evidence, this seems more reasonable to me as an explanation here.

Reply: We agree that this argument will definitely not explain most of the observed scatter. While it may add to the observed scatter of signals (that is why we included the argument originally), it is likely of very minor importance and might involuntarily make the discussion more complicated than necessary.

Changes in revised version: We decided to abstain from using this argument in the revised version of the manuscript.

Comment, Lines 366-368: I am not sure I follow. How can the aliquot-to-aliquot variation in feldspar content can give rise to additional scatter in profile data? Does it mean that test dose is not adequately correcting for this possible variation? Why not? What is the evidence?

Reply: We do not have direct evidence for this argument. We however know that the IRSL stimulation of our post-IRSL-BSL protocol is removing most of the feldspar signal, but not all of it. Although we assume that the feldspar contribution is insignificant based on our test measurements, it must be expected that the contribution of feldspar signals to the post-IRSL-BSL signal will be slightly different for polymineralic aliquots with different percentages of feldspar.

Changes in revised version: Since this potential source of scatter will again explain (if at all) only a very minor part of the observed scatter, we again decided to abstain from using this argument in the revised version of the manuscript and focus on the most plausible arguments (lines 420-435).

Comment, Lines 375-378: While the interpretation that age underestimation could have been caused by unreliable sigmaphi values and erosion of the boulder surfaces may be right, it would nevertheless be interesting to see what erosion rates one would get by applying the erosion rate model to samples that do not seem to suffer from age underestimation. The erosion rate of such samples must be negligible compared to the erosion rates of the samples showing age underestimation. This should provide a good basis for your interpretation.

Reply: The point developed by reviewer 2 is fair and was tackled during revision of the manuscript. The erosion rates provided by the model are indeed negligible (i.e. < 0.01 mm/year). This is, however, not surprising given the fact that the depth profiles of these samples can be explained without any erosion.

Comment, Line 377: Does “inadequate” mean “unreliable” here?

Changes in revised version: We replaced “inadequate” by “unreliable”.

Comment, Line 388: What is meant by “environmental factors beyond the exposure time”?

Reply: The factors refereed to here, i.e. post-transport erosion and occasional shielding of the post-transport surface by e.g. water, are explained in the following sections of the manuscript.

Changes in revised version: We changed the wording to “factors different than exposure time” to avoid any confusion.

Comment, Lines 418-419: It may be worth mentioning here that, in retrospect, IRSL signals were likely to work better than the post-IRSL-BSL signals for these samples.

Changes in revised version: We added a short reference regarding the potential benefits of IRSL signals for some of our samples: “While IRSL signals were not used in this study due to insufficiently bright signals for most samples, in retrospect their use might be advantageous to post-IRSL-BSL signals at least for some of the investigated samples” (lines 499-501).

Comment, Line 422: What is considered as “insufficiently bright signals”? If the post-IRSL-BSL signals shown in Fig. A12 are typical for these samples, they are all well above background by more than 3.

Reply: The term “insufficiently bright” refers to the IRSL signals of polymineralic samples. Those shown in Figure A12a are representative for the samples of the different sites and hardly distinguishable from the background (signal <3 times background for most aliquots).

Comment, Line 431-434: 1) The ages obtained from eroding surfaces are “apparent” surface exposure ages. The fact that they underestimate the expected ages, does not mean that they are inaccurate. They may be accurate, but they simply do not reflect the age of the event of interest. 2) There is no scientific basis to support this general statement that the ages from inclined surfaces are inaccurate. Surfaces can be dated regardless of their orientation provided that suitable calibration samples are available.

Reply: We agree with and appreciate these arguments. What we want to express is that apparent ages do not agree with age control due to erosion or unreliable calibration samples.

Changes in revised version: We changed the phrasing of the section to better reflect this argumentation in the revised version (lines 514-515).

Evaluating OSL rock surface exposure dating as a novel approach for reconstructing ~~transport histories of~~ coastal boulder~~s~~ movement ~~over~~ on decadal to centennial timescales

Dominik Brill[1]*, Simon Matthias May[1], Nadia Mhammdi[2], Georgina King[3], Benjamin Lehmann[4], Christoph Burow[1], Dennis Wolf[1], Anja Zander[1], Helmut Brückner[1]

[1] Institute of Geography, University of Cologne, Köln, Germany
[2] Institut Scientifique, Laboratory LGRN and GEOPAC Research Center, Université Mohammed V, Rabat, Rabat, Morocco
[3] Institute for Geology, University of Lausanne, Switzerland
[4] Centro de Estudios Avanzados en Zonas Áridas (CEAZA), ULS-Campus Andrés Bello, Raúl Brítán 1305, La Serena, Chile

Correspondence to: Dominik Brill (brilld@uni-koeln.de)

Abstract. Wave-transported boulders represent important records of storm and tsunami impact over geological timescales. Their use for hazard assessment requires chronological information on their displacement that in many cases cannot be achieved by established dating approaches. To fill this gap, this study investigated, for the first time, the potential of optically stimulated luminescence rock surface exposure dating (OSL-RSED) for estimating cliff-detachment~~transport~~ ages of wave-~~emplaced~~ driven coastal boulders. The approach was ~~applied to~~tested on calcarenite clasts at the Rabat coast, Morocco. Calibration of the OSL-RSED model was based on samples with rock surfaces exposed to sunlight for ~2 years, and OSL exposure ages were evaluated against age control deduced from satellite images. Our results show that the dating precision is limited for all targeted boulders due to the local source rock lithology which has low amounts of quartz and feldspar. The dating accuracy may be affected by erosion rates on boulder surfaces of 0.02~~6~~-0.18~~2~~ mm/year. Nevertheless, we propose a robust relative chronology for boulders that are not affected by significant post-depositional erosion and that share surface angles of inclination with the calibration samples. The relative chronology indicates that (i) most boulders were ~~moved~~ detached from the cliff by storm waves; (ii) these storms lifted boulders with masses of up to ~~20~~ 24 t; and (iii) the role of storms for the formation of boulder deposits along the Rabat coast is ~~much~~ more significant than previously assumed. Although OSL-RSED cannot provide reliable absolute exposure ages for the coastal boulders in this study, the approach has large potential for boulder deposits composed of rocks with larger amounts of quartz or feldspar~~, older formation histories~~ and less susceptibility to erosion.

1. Introduction

Coastal boulders with masses of up to tens or hundreds of tons, located well above high tide level or far inland from the shoreline, are impressive evidence for the occurrence and impact of tsunamis and extreme storms (e.g. Engel and May, 2012; May et al., 2015; Cox et al., 2019). Such geological imprints may be preserved over periods that significantly exceed instrumental and historical records (Yu et al., 2009; Ramalho et al., 2015), making them valuable ~~archives~~ records for long-term hazard assessment. Compared to sandy tsunami and storm deposits, which are used more commonly for this purpose, wave-transported boulders are abundant along rocky coastlines and can be preserved over geological time scales even in settings dominated by erosion (Paris et al., 2011). Furthermore, boulder~~s~~ ~~transport~~ may provide information on the magnitude of prehistoric tsunamis and storms that cannot be deduced from sandy sediments (Nandasena et al., 2011).

For coastal boulders to be valuable for hazard assessment, they have to provide information on the frequency of the associated flooding events, which in turn requires chronological information on boulder displacement. Since boulders unlike sandy storm and tsunami deposits typically lack a stratigraphic context, dating approaches rely on chronometers related to the boulder rock itself or on constructive features attached to the boulder, such as marine organisms or flow stones. Established dating approaches are based on radiocarbon (^{14}C) and U-series ($^{230}Th/^{234}U$) dating of organic carbonates (e.g. Zhao et al., 2009; Araoka et al., 2013), and thus require coral boulders or the presence of attached marine organisms, as well as coincidence between the death of these organisms and the ~~transportation event~~onshore transport of the boulder. Direct ages for the transport of coastal boulders were achieved by using terrestrial cosmogenic nuclide surface exposure dating (Ramalho et al., 2015; Rixhon et al., 2017) and palaeomagnetic dating (Sato et al., 2014)~~.~~, ~~but~~ However, palaeomagnetic dating still suffers from ~~due to~~a number of intrinsic methodological limitations, ~~and~~ cosmogenic nuclide dating cannot provide sufficient resolution on Late Holocene time scales and is, therefore, of limited benefit for the vast majority of coastal boulders. ~~these approaches are restricted to certain boulder lithologies and time scales.~~

The recently developed optically stimulated luminescence (OSL) rock surface dating technique (see review by King et al., 2019) offers completely new opportunities for directly dating the cliff detachment~~transport~~ of coastal boulders. While the application of the more routinely used OSL rock surface burial dating technique (e.g. Simms et al., 2011; Sohbati et al., 2015; Jenkins et al., 2018; Rades et al., 2018) is typically impeded for coastal boulders due to logistical problems with sampling the (inaccessible) light-shielded bottom surfaces of clasts weighing several tons, the OSL rock surface exposure dating (OSL-RSED) technique introduced by Sohbati et al. (2011) can be applied to the light-exposed top surfaces of such clasts. For boulders that were overturned during wave-driven cliff detachment ~~transport~~ and that experienced no subsequent overturning events as well as negligible erosion and shielding of their top surfaces after deposition on the onshore platform, post-transport exposure periods may be estimated based on the time-dependent progression of OSL signal resetting, the so-called bleaching front, into the uppermost millimetres to centimetres of the rock (Sohbati et al., 2012; Freiesleben et al., 2015; Lehmann et al., 2018; Gliganic et al., 2019). ~~OSL-RSED could therefore provide ages for coastal boulders that are not datable by any other technique.~~ OSL-RSED is applicable to a wide spectrum of lithologies, as long as they contain quartz and/or feldspar, and to timescales of decades, centuries up to a few millennia. While it thus cannot be applied to pure limestone boulders, ~~OSL-RSED could therefore~~the approach may ~~therefore~~ provide ages for coastal boulders that are so far not datable by any other technique.

Here, we present the first attempt to ~~application of~~use OSL-RSED to reconstruct storm and/or tsunami frequency patterns from wave-~~emplaced~~ displaced boulders. All analyses were conducted on carbonatic sandstone boulders from the Atlantic coast of Morocco, south of Rabat, that were previously documented by Mhammdi et al. (2008) and Medina et al. (2011). These boulders were selected, because they offer all indispensable prerequisites for the application of OSL-RSED, including a lithology containing sensitive quartz and feldspar (Barton et al., 2009), unambiguous signs of boulder overturning in their taphonomy, and age control at least for some of the boulders. Boulder sites with potentially more appropriate lithologies for OSL-RSED typically lack clear indication of boulder movement and age control, and coastal boulders with better independent chronologies are typically composed of pure limestone that cannot be used for OSL dating. Primarily, this study aims at evaluating the novel OSL-RSED technique for coastal boulders, which was achieved by using artificially exposed rock surfaces for calibration of the bleaching model and by testing its performance against age control deduced from satellite images and eyewitness accounts. The successfully validated model was then applied to boulders of unknown age. While

some of the dated~~se~~ boulders had previously been tentatively attributed to the 1755 Lisbon Tsunami (Mhammdi et al., 2008; Medina et al., 2011), they lack robust chronological data. Besides discussing limitations of the dating approach due to local OSL signal properties and erosion of boulder surfaces exposed after transportation~~post-transport exposed boulder surfaces~~, we also discuss the future potential of this method and the implications of the new relative OSL-RSED boulder ages for the long-term storm and tsunami hazard at the Atlantic coast of Morocco.

2. The OSL rock surface exposure dating model applied to coastal boulders

Conventional OSL dating relies on the accumulation of an energy dose (palaeodose) due to the impact of ionising radiation over time (dose rate) on sand or silt grains shielded from sunlight. The palaeodose is proportional to the burial age of the sediment and can be quantified by measuring the light emission (OSL signal) of quartz or feldspar grains during stimulation with laboratory light. In natural settings, resetting of OSL signals takes place by sunlight exposure during sediment transport, so that buried sediment grains can provide information about the time that passed since the last sunlight exposure (burial age).

The uppermost millimetres to centimetres of rock surfaces exposed to sunlight experience bleaching and accumulation of OSL signals at the same time. However, OSL signal resetting or bleaching is by far the dominant process in rocks with low environmental dose rates and Holocene exposure histories (Sohbati et al., 2012). For coastal boulders with dose rates of less than 1 Gy/ka and ages post-dating the stabilization of Holocene eustatic sea level around its present position about six millennia ago (e.g. Khan et al., 2015), as investigated in this study, OSL signal accumulation can be neglected. The time-dependent evolution of OSL signals in ~~the upper layer of~~ exposed boulder surfaces can therefore be reduced to the term for OSL signal resetting, which following Sohbati et al. (2012) is expressed by

$$L(\mathrm{x}) = L_0 e^{-\overline{\sigma\varphi_0} t_e e^{-\mu x}}, \quad (1)$$

where L_0 is the initial OSL signal intensity prior to exposure, L the remaining OSL signal at depth x (mm) after exposure, t_e (s) the exposure time, $\overline{\sigma\varphi_0}$ (s^{-1}) the effective bleaching rate of the OSL signal at the rock surface (i.e. the product of the photo-ionisation cross section σ, and the light flux at the rock surface φ_0), and μ (mm^{-1}) the light attenuation coefficient of the rock.

Figure 1 illustrates how Equation (1) can be used to estimate the ~~transport age~~timing of wave-driven boulder detachment from the coastal cliff, if this event was associated by overturning of the clast~~s overturned by waves~~. When attached to the cliff, only the (usually bio-eroded) upper surface of a typical boulder in the pre-transport position is exposed to sunlight and experiences OSL signal resetting (Fig. 1a). Its shielded bottom side is only exposed to ionising radiation from radioactive elements in the surrounding rock and cosmic rays that, after a prolonged time, cause OSL signals to be in or close to field saturation (Fig. 1a). When overturned during ~~transport~~cliff detachment, the new upper surface of the boulder in ~~the~~ post-transport position on the cliff platform is suddenly exposed to sunlight and the bleaching front starts to move into the rock (Fig. 1b); boulders with a platy shape may be repeatedly pushed landwards by waves afterwards, while a second overturning is very unlikely. T~~t~~he same is true for the surfaces of quarrying niches that are formed by boulder detachment (Fig. 1b). In both cases, the exposure time can be estimated by fitting Equation (1) to the depth-dependent OSL signals measured in rock samples collected from these surfaces. The shielded bottom side of the boulder in the post-transport position is generally suitable for rock surface burial dating, by making use of the time-dependent dose accumulation in the

previously bleached surface; due to inaccessibility of shielded surfaces for sample collection this was not tried in this study.

3. Study area

3.1 Marine flooding hazard along the Atlantic coast of Morocco

The approximately 3000 km-long Moroccan Atlantic coast is exposed to swell waves, north Atlantic winter storms and rare tsunamis that cause erosion and/or flooding of low-lying areas. The energy of swell waves is strongest along the central section of the Moroccan coast, between Agadir and Rabat, since it is not sheltered by the Canary Islands or the Iberian Peninsula; waves approach from the northwest to west and are significantly stronger during winter (Medina et al., 2011). The influence of Atlantic hurricanes is comparatively small (Fig. A1a) with only two former tropical storms recorded to have made landfall as tropical depressions (core pressure 988-1000 hPa) at the coast of Morocco and the southern Iberian Peninsula between 1851 and 2016 (Fig. 2a). Instead, maximum wave heights are associated with winter storms that typically cross France or the UK (Fig. A1b), but may have tracks as far south as Morocco (Fig. 2a). During recent winter storms within the last century, wave heights of up to 7 m (compared to regular swell heights of 0.5-1.5 m) have been observed at the Rabat coast (Mhammdi et al., 2020), associated with flooding of back-beach areas and waves overtopping the coastal cliff (Fig. A2).

An additional flooding hazard emanates from tsunamis triggered by earthquakes offshore of Portugal, between the Azores triple junction and the Strait of Gibraltar, where the African and Eurasian plates converge at a rate of ~4 mm per year (Zitellini et al., 1999). After earthquakes in 1941, 1969 and 1975, Moroccan tide gauges recorded moderate tsunamis with waves <1 m. Further earthquakes, likely accompanied by tsunamis with impact in Morocco, are listed in historical catalogues (e.g. in 382 CE and 881 CE), but unambiguous reports of flooding only exist for the 1st November 1755 Lisbon Tsunami (Kaabouben et al., 2009). Triggered by a M_w 8.5 earthquake, probably due to the rare event of a combined rupture of different seismic structures (Baptista et al., 2003), the associated tsunami is the only known destructive flooding event at the Moroccan coast. Historical sources from Rabat describe the inundation of streets as far as 2 km inland, wreckage of ships in the harbour, and drowned people and camels (Blanc, 2009). Although numerical models indicate that the wave heights of 15 m mentioned in historical reports from Tanger and Safi are most likely exaggerated and that values of 2.5-5.0 m are more realistic (Fig. 2a; Blanc, 2009; Renou et al., 2011), the effects of the 1755 tsunami on the coastal landscape of Morocco were nevertheless significant (e.g. Ramalho et al., 2018).

3.2 Exploiting geological evidence for hazard assessment – The Rabat boulder fields

While instrumental and historical records demonstrate the flooding hazard at the Moroccan coast due to both storms and tsunamis, all documented events except the 1755 Lisbon Tsunami were restricted to the last decades. This does not allow for robust estimates of long-term tsunami and storm occurrence or of all possible magnitudes of storm surges and tsunami inundation. Most published regional geological tsunami and storm evidence for the pre-instrumental era is restricted to Spain and Portugal (e.g. Dawson et al., 1995; Hindson and Andrade, 1999; Lario et al., 2011; Costa et al., 2011; Feist et al., 2019), but fields of wave-~~emplaced~~ displaced boulders offer records of past storms and/or tsunamis for Morocco (Mhammdi et al., 2008; Medina et al., 2011) that could inform about the regional long-term hazard if robust chronological data were available.

The most prominent boulder fields are reported from a 30 km long NE-SW oriented coastal section between Rabat and Skhirat (Fig. 2a,b), consisting of hundreds of boulders with estimated masses between a few and more than 100 t (Mhammdi et al., 2008; Medina et al., 2011). The geomorphology and geology of this area is characterised by a succession of coast-parallel, Pleistocene calcarenite ridges that are related to sea-level highstands and rest on a Palaeozoic basement (Chakroun et al., 2017). A typical cross section (Fig. 2c,d) is composed of: (i) the intertidal platform with an active coastal cliff; (ii) the youngest lithified calcarenite ridge, formed during MIS 5; (iii) an inter-ridge depression, called Oulja, which may be flooded at high tide (the spring tide range is 2-3 m), and which is covered by recent and/or Holocene beach deposits; and (iv) an older calcarenite ridge, probably formed during MIS 7, including an inactive cliff (Medina et al., 2011; Chakroun et al., 2017; Chahid et al., 2017). Towards Rabat, the younger calcarenite ridge is replaced by a simple sandstone platform (Fig. 2e).

As described by Mhammdi et al. (2008) and Medina et al. (2011), most of the calcarenite boulders were sourced from the active cliff (Fig. 2c). Since detachment is guided by lithological boundaries between the calcarenite and interbedded clay units, most of the boulders have platy shapes; only occasionally were boulders derived from subtidal positions and lifted up to 5 m vertically to the top of the first calcarenite ridge, as indicated by vermetids, or sourced from younger sandstones covering the Oulja. The boulders are deposited as single clasts, clusters, or imbricated stacks that rest on top or at the backward slope of the first calcarenite ridge, in the Oulja, or rarely at the seaward slope of the older calcarenite ridge up to 300 m inland (Fig. 2c). The position and orientation of bio-erosive rock pools formed on the surface of the youngest ridge (i.e. the pre-transport surface of most boulders) offers insights into transport modes. While some boulders moved by sliding only, others were overturned during transport as indicated by down-facing rock pools on the pre-transport surface (Mhammdi et al., 2008; Medina et al., 2011). For some of the larger boulders, sliding movement by storm waves after their initial detachment from the cliff is documented on satellite images (Fig. A3). Movement of smaller boulders with up to 1 m³ (~2.5 t) was frequently observed after recent winter storms such as Hercules/Christina in January 2014 (Mhammdi et al., 2020). At some places along the coast between Rabat and Casablanca even boulders exceeding 10 t have been pushed landward during recent winter storms (Mhammdi et al., 2020).

4. Methods

Boulders sampled for dating were characterized in the field with regard to their position, orientation, dimension and surface taphonomy. Distance from the active cliff and elevation above mean high tide level were measured using a laser range finder. Boulder volume estimates (V) are based on tape measurements of a- (length), b- (width) and c-axes (height) and an empirical correction factor of 0.5 (Engel and May, 2012) using

$$V = (a * b * c) * 0.5, \quad (2)$$

To calculate boulder weights, volumes are multiplied with boulder densities (ρ_B) determined individually for each sample using the Archimedean principle of buoyancy in water following

$$\rho_B = \rho_W * \frac{w_a}{w_a - w_w}, \quad (3)$$

with w_a = weight of the sample in air, w_w = weight of the sample in water and ρ_W = density of sea water (1.02 g/cm³). Surface orientation and inclination of sampled boulders were measured with a compass.

For OSL-RSED, samples of approximately 10 cm³ were collected from selected boulder surfaces using a combination of a battery-driven rock drill, hammer and chisel. Rock samples were wrapped in black plastic bags and brought to the Cologne Luminescence Laboratory (CLL) for further processing under dimmed red-light conditions. First, a circular rock saw was used to cut ~5 cm thick surface slabs, from which cores of ~1 cm diameter and ~4 cm length were extracted using a bench drill (Proxxon Professional) with water cooled diamond core bits. After immersion in resin (Crystalbond 509, the resin was tested to have no OSL emission) and subsequent oven drying to stabilize fragile parts of the sandstone cores, they were cut into ~0.7 mm thick slices using a water-cooled low speed diamond saw (Bühler Isomet 1000) with 0.3 mm blade thickness. Slices were gently crushed with a mortar to obtain polymineralic sand grains that were fixed on aluminium cups using silicon grease in monolayer. Separation of pure quartz and/or potassium feldspar for the grains of each slice, standard practice in conventional OSL dating, was not feasible due to the large number of slices and the small amount of polymineralic grains per slice.

~~For validation of the post-IRSL-BSL protocol~~To guide the selection of a measurement protocol for the polymineralic aliquots used for dating in this study, pure quartz and potassium feldspar extracts in the 150-200 µm grain-size fraction were prepared ~~for~~from the light-shielded parts (i.e. >5 cm below surface) of the 10 cm³ sample blocks of HAR 1-1 and TEM 3-1. Sample preparation followed standard coarse grain procedures including dry sieving, treatment with 10% HCl and 10% H_2O_2, density separation (potassium feldspar<2.58 g/cm³<2.62 g/cm³<quartz<2.68 g/cm³), and 40% HF etching in the case of quartz. Dose recovery experiments with signal resetting in a solar simulator for 24 hours and administering of a ~12 Gy laboratory beta dose, as well as continuous wave fitting of quartz BSL components using the **R** package "Luminescence" version 0.9.0.88 (Kreutzer et al., 2019) were performed for both the pure quartz and the polymineralic fraction. Preheat-plateau tests were performed on the quartz extracts to establish an appropriate measurement temperature. ~~Additional preheat plateau tests and~~Quartz extracts of two samples (HAR 1-1 and TEM 3-1) were also used for palaeodose determinations ~~were conducted on quartz extracts~~ following a conventional SAR protocol according to Murray and Wintle (2003) (Tab. A3). Combined with d~~D~~ose rates ~~are~~ based on high-resolution gamma spectrometry and the conversion factors of Guerin et al. (2011), ~~.~~ c~~C~~onventional OSL ~~burial~~ ages for the formation of the sandstone were calculated from ~~burial doses~~palaeodoses ~~and dose rates~~ using the DRAC software version 1.2 (Durcan et al., 2015).

~~To optimize the information extracted from the polymineralic samples, a~~All luminescence measurements of polymineralic aliquots for OSL-RSED followed a post-IRSL-BSL protocol (e.g. Banerjee et al., 2001). After preheating at 220 °C for 10 s, ~~that~~ the protocol records an infrared stimulated luminescence (IRSL) signal at 50 °C for 160 s, followed by a blue stimulated luminescence (BSL) signal at 125 °C for 40 s (Tab. A2). Measurements were performed on a Risø TL/OSL DA20 reader equipped with an U340 filter for signal detection. All thermal treatments were performed with heating rates of 2 °C/s. In the post-IRSL-BSL protocol, stimulation with infrared LEDs specifically bleached luminescence signals originating from feldspar (feldspar IRSL). This reduced the contribution of feldspar signals to the BSL signal of quartz (quartz BSL), which unlike feldspar is insensitive to infrared stimulation (cf. Bailey, 2010).

~~For validation of the post-IRSL-BSL protocol, pure quartz and potassium feldspar extracts in the 150-200 µm grain-size fraction were prepared for the light-shielded parts (i.e. >5 cm below surface) of the 10 cm³ sample blocks of HAR 1-1 and TEM 3-1. Sample preparation followed standard coarse grain procedures including dry sieving, treatment with 10% HCl and 10% H_2O_2, density separation (potassium feldspar<2.58 g/cm³<2.62 g/cm³<quartz<2.68 g/cm³), and 40% HF etching in the case of quartz. Dose recovery experiments with signal~~

~~resetting in a solar simulator for 24 hours and administering of a ~12 Gy laboratory beta dose, as well as continuous wave fitting of quartz BSL components using the **R** package "Luminescence" version 0.9.0.88 (Kreutzer et al., 2019) were performed for both the pure quartz and the polymineralic fraction. Additional preheat plateau tests and palaeodose determinations were conducted on quartz extracts following a conventional SAR protocol according to Murray and Wintle (2003) (Tab. A3). Dose rates are based on high-resolution gamma spectrometry and the conversion factors of Guerin et al. (2011). Conventional OSL burial ages for the sandstone were calculated from burial doses and dose rates using the DRAC software version 1.2 (Durcan et al., 2015).~~

For OSL-RSED, the natural OSL signals (L_n) and the OSL signals in response to a ~12 Gy test dose (T_n) of the post-IRSL-BSL protocol were measured for the polymineralic grains of all crushed slices to generate plots of OSL signal versus depth below the boulder surface. The depth-dependent L_n/T_n data of each core (mean of two aliquots) were normalized to the core's individual ~~background~~ plateau signal~~level~~ calculated from the average of the deepest 5-10 slices. The normalized data of all cores of a sample were then averaged (arithmetic mean and standard error) to receive a mean signal-depth curve for each rock sample; we only excluded ~~apparent outliers, i.e.~~ cores without any signal-depth trends ~~completely different from all other cores of the sample, were excluded from averaging~~and data points that deviated more than two standard deviations from the mean. The mean signal-depth curves were fitted with Equation (1) using the rock surface exposure dating function in the R package "Luminescence" (Burow, 2019) and the software OriginPro (version 8.5). ~~Shared~~ μ ~~values for each site~~ and ~~shared~~ $\overline{\sigma\varphi_0}$ values shared between several samples ~~for flat calibration surfaces~~ were determined using the "global fit" function that allows the fitting of multiple signal-depth curves at the same time. Post-depositional erosion has recently been shown to exercise a strong effect on the depth of the bleaching front, and thus the apparent age, of exposed rock surfaces (Sohbati et al., 2018; Lehmann et al., 2019a,b; Brown and Moon, 2019). Their potential effects were therefore modelled using the approach of Lehmann et al. (2019a).

5. Results

5.1 Boulders selected for OSL surface exposure dating

Samples for OSL-RSED were collected from nine boulders at four different sites along the Rabat coast in July 2016, including Rabat (RAB), Haroura (HAR), Temara (TEM) and Val d'Or (VAL) (Fig. 2b). Boulders selected for dating were composed of carbonate-cemented sandstone (calcarenite) with clear signs of overturning during ~~transport~~cliff detachment, indicated by down-facing rock pools and/or fresh-looking post-transport surfaces (Fig. 3d). Due to the platy shape of the boulders, repeated overturning on the coastal platform after cliff detachment can be excluded. To ensure comparable ~~pre~~conditions for sunlight exposure, only surfaces without significant shielding by vegetation, other boulders or water, and wherever possible without significant inclination of their top surfaces were sampled. Most sampled boulders, thus, rested in supratidal positions and had relatively smooth post-transport surfaces (RAB 1, HAR 1, HAR 2, TEM 3, VAL 4, VAL 6). However, boulders from the intertidal platform with post-transport rock pools (VAL 1, Fig. 3h) or boulders with higher surface roughness probably due to increased sea spray influence (TEM 2 and RAB 5, Fig. 3g) were also sampled for assessing the effects of post-depositional erosion on dating accuracy. In addition, surfaces of niches in the active cliff, exposed after detachment of the associated boulders, were sampled at Haroura (HAR 3, Fig. 3e) and Temara (TEM 4).

The characteristic features of all sampled boulders – including post-transport position, arrangement, shape, dimension, orientation of the sampled surface and taphonomy of boulder surfaces – are summarized in Table 1.

Satellite images covering the last 50 years (Google Earth images from 2001 to 2019, Corona images from 1966), field observations for very young features, and, in case of VAL 1, the depth of post-depositional rock pools helped to roughly constrain when the boulders and niches were deposited or formed (see Tab. A1 for a summary). Precise age control by observations of local residents confirmed the movement of boulder TEM 3 during winter storm Hercules/Christina in January 2014 (t_e = 2.5 years), and the formation of niche TEM 4 (sampled in September 2018) between the 2016 and 2018 field surveys, most likely during the unnamed winter storm in February 2017 (t_e = 1.5 years) (Fig. A4). Corona satellite images provide minimum ages of 50 years for boulders RAB 1, RAB 5, VAL 1, VAL 4 and HAR 2, since all of them were identified at their present position on images from April 1966 (Fig. A5, A6, A7, A8, A9). However, considering the up to 45 cm deep post-depositional rock pools on the surface of VAL 1 and assuming typical rates of bio-erosion in the range of up to 1 mm/year (Kelletat, 2013), boulder VAL 1 is probably much older than 50 years, at least a few centuries. All other boulders and niches could not be identified on the 1966 satellite images due to their limited resolution. However, these clasts did not change their position between 2001/2004 and 2019 (Fig. A9, A10, A11), equalling minimum ages of 12-15 years (Tab. A1).

5.2 Luminescence properties of the ~~dated~~ target sandstone

Comparative measurements on polymineralic grains and potassium feldspar extracts on sample HAR 1-1 show that post-IRSL-BSL signals from the polymineralic aliquots of all four sites are (i) the dominant emission compared to IRSL signals, and (ii) relatively unaffected by a feldspar signal contribution (Fig. A12). Therefore, OSL-RSED in this study was based on the mainly quartz derived post-IRSL-BSL signal of polymineralic aliquots. Experiments on pure quartz extracts of sample HAR 1-1 revealed adequate OSL properties in terms of rapidly decaying signals dominated by the fast component (Fig. A12a,b), independence of thermal treatment for the selected preheat temperature (Fig. A13), and good reproducibility of laboratory doses (dose recovery ratios of 1.02-1.08). Similarly, suitable OSL properties, i.e. signals dominated by the quartz fast component (Fig. A12c) and successful dose recovery experiments, are also documented for post-IRSL-BSL signals of polymineralic aliquots.

When plotted against their depth below the boulder surface, test dose corrected and normalized mean post-IRSL-BSL signals from the uppermost 15 mm of each sample (note that signal-depth curves of each sample are based on 2 to 5 cores with 2 aliquots per slice) showed a general increase from completely reset signals at the rock surface towards a constant ~~background~~ plateau level deeper in the rock (Fig. 4, Fig. A14, A15). ~~The background levels~~These plateaus reflected a quartz palaeodose of ~40-50 Gy or a~~n~~ rock formation age of ~80-100 ka (measured on HAR 1-1 and TEM 3-1, Tab. A4), which is below the sample-specific saturation level of 50-120 Gy. The robustness of the average post-IRSL-BSL-depth trends used for dating is supported by good reproducibility of signals derived from different aliquots of the same slice (Fig. 4a), and reasonable correlation of different cores from the same sample (Fig. 4b, Fig. A14, A~~S~~15). Where signal-to-noise ratios also allowed feldspar IRSL signals to be analysed (i.e. at TEM and RAB), these showed bleaching fronts that intruded deeper into the rock compared to the post-IRSL-BSL signal (Fig. 4c, Fig. ~~A11~~A14, A15).

5.3 Calibration of the OSL rock surface exposure dating model using artificially exposed surfaces

To estimate boulder ages with OSL-RSED, measured post-IRSL-BSL signal-depth data ~~were~~ must be fitted with the bleaching model described in Equation (1). Besides the exposure time (t_e), the bleaching model contains two further *a priori* unknown parameters: the effective OSL signal bleaching rate at the rock surface ($\overline{\sigma\varphi_0}$), and the

light attenuation in the rock (μ). These vary with geographical location and rock type, respectively, and have to be determined individually for each location and lithology prior to dating. Since determination on the basis of first order principles was not successful in earlier studies (Sohbati et al., 2011~~2~~), for the Rabat site these parameters were obtained empirically by fitting Equation (1) to calibration samples with known exposure ages (e.g. Sohbati et al., 2012; Lehmann et al., 2018).

For this, fresh rock surfaces were exposed during the first field survey in July 2016 and sampled during the second survey in September 2018, equivalent to an exposure time of ~2.15 years. A total of five calibration samples, at least one rock sample from each site, were collected ~~to account for potential site-to-site variability~~ (CAL samples in Tab. 1). Exposures were created directly on the top surfaces of boulders RAB 5, TEM 3 and VAL 4 (Fig. A1~~6~~7b,d), as well as by placing previously unexposed rock samples collected from boulders HAR 1 and VAL 4 on the roof top of a nearby house (Fig. A1~~6~~7a,c). Since the effective luminescence decay rate ($\overline{\sigma\varphi_0}$) is sensitive to the inclination and orientation of the dated rock surfaces (Gliganic et al., 2019), all exposure surfaces except from TEM 3 CAL, which had the same inclination as the associated dating sample, were orientated approximately horizontally.

The first step was the estimation of a rock-specific μ value. Light attenuation in the rock may be influenced by small-scale variations in lithology and therefore μ should have sample~~boulder~~-dependent values (Gliganic et al., 2019). However, individual best-fit μ values that were achieved by fitting Equation (1) to the post-IRSL-BSL signal-depth data of individual samples while treating the product of age and $\overline{\sigma\varphi_0}$ as a single parameter (e.g. Sohbati et al., 2015) revealed huge uncertainties ~~(Tab. 2)~~. Sample-specific best-fit μ values ranged between 0.5 and 3.4 mm^{-1} for the boulder samples in this study (Tab. 2), while literature values for the BSL signal of quartz sandstone and quartzite are in the range of 0.9-1.3 mm^{-1} (cf. Sohbati et al., 2012, Gliganic et al., 2019). This indicates that sample-specific values in this study may not only be imprecise but, due to large measurement uncertainties, may also be incorrect for some samples. Since the estimation of shared μ values for several rock samples can improve the accuracy of the estimate significantly (Lehmann et al., 2018), the use of a shared μ value for all samples was chosen as a reasonable and necessary compromise. The assumption of a common μ value for all boulders targeted in this study is supported by their very similar lithology, since all of the boulders are derived from the same local calcarenite facies. The mutual μ value was obtained by simultaneously fitting Equation (1) to the signal-depth data of all samples (n = 16) except from VAL 4-1 CAL 2 and RAB 5-1 CAL, which revealed extremely scattered data and were therefore excluded from all further analyses (Fig. 5). While μ was defined as a free ~~but~~parameter shared ~~parameter~~between all samples, the product of exposure time and $\overline{\sigma\varphi_0}$ was kept a free parameter with individual values for each sample. The mutual μ value of 1.39±0.15 mm^{-1} (Tab. 2) seems to be much more realistic when compared to the literature values for BSL signal attenuation in quartz sandstone and quartzite of 0.9-1.3 mm^{-1} (cf. Sohbati et al., 2012, Gliganic et al., 2019).

In a ~~first~~ second step, local values for $\overline{\sigma\varphi_0}$ were determined. Since all samples in this study were collected within a radius of less than 20 km, the local light flux should be similar for all surfaces with comparable inclination and orientation. This was supported ~~by~~ when fitting each calibration sample individually with fixed values for μ (1.39 mm^{-1}) and exposure age (2.15 years) (Fig. 5, Tab. 2), reflecting systematic differences of $\overline{\sigma\varphi_0}$ ~~only~~ between the inclined calibration surface of TEM 3-1 CAL (1.4~~23~~x10^{-5} s^{-1}) and the horizontal calibration surfaces of all other calibration samples (2.1~~7~~x10^{-7} to 4.7x10^{-8} s^{-1}). We therefore determined a shared $\overline{\sigma\varphi_0}$ value for ~~all~~ horizontal surfaces by simultaneously fitting ~~the respective~~ calibration samples VAL 4-1 CAL 1 and HAR 1-1 CAL (i.e.

again excluding VAL 4-1 CALal -2 and RAB 5-1 CAL), using $\overline{\sigma\varphi_0}$ (shared) as a free variable, and the mutual μ value of 1.39 mm^{-1} μ (individual best-fit value for each sample) as free variables and an exposure age of 2.15 years as a fixed parameters (Tab. 2). This resulted in shared $\overline{\sigma\varphi_0}$ values of 1.22.6(±2.3)x10^{-6}5 ±5.3x10^{-7} s^{-1} for the inclined surface and 9.23.0(±2.0)x10^{-7}8 ±7.0x10^{-8} s^{-1} for the horizontal surfaces (Fig. 5, Tab. 2).

The second step was the estimation of local values for μ. Light attenuation in the rock may be influenced by small-scale variations in lithology and therefore μ should have boulder-dependent values (Gliganic et al., 2019). However, fitting Equation (1) to the post-IRSL-BSL signal-depth data of individual samples revealed μ values with huge uncertainties (Fig. 5a-5e, Tab. 2). Sample-dependent best-fit μ values ranged between 0.26 and 3.5 mm^{-1} for the boulder samples in this study (Tab. 2), while literature values for the BSL signal of quartz sandstone and quartzite are in the range of 0.9-1.3 mm^{-1} (cf. Sohbati et al., 2012, Gliganic et al., 2019). This indicates that sample-specific values may not only be imprecise but, due to large measurement uncertainties, may also be inadequate for some samples. Since the estimation of shared μ values for several rock samples can improve the accuracy of the estimate significantly (Lehmann et al., 2018), the use of shared μ values for all boulders from an individual site (i.e. RAB, HAR, TEM and VAL) was chosen as a reasonable and necessary compromise. The assumption of very similar μ values for all boulders from one individual site is supported by their very similar lithology, since all of the boulders are derived from the same local calcarenite facies. Site-dependent μ values were obtained by fitting Equation (1) to all samples from a site at the same time, using μ (shared) and exposure time (individual for each sample) as free variables, and the shared $\overline{\sigma\varphi_0}$ value for horizontal surfaces determined in the previous step as a fixed parameter (only for TEM 3-1, TEM 4-1 and TEM 3-1 CAL the $\overline{\sigma\varphi_0}$ value for inclined surfaces was used). Site-averaged μ values vary between 1.04±0.26 mm^{-1} at RAB and 1.54±0.31 mm^{-1} at TEM (Tab. 2), which seem to be much more realistic when compared to the literature values for BSL signal attenuation in quartz sandstone and quartzite of 0.9-1.3 mm^{-1} (cf. Sohbati et al., 2012, Gliganic et al., 2019).

5.4 Model validation and dating of boulders with unknown transport historyages

OSL exposure ages for all non-calibration boulder and niche samples were derived by fitting their post-IRSL-BSL signal-depth profiles with Equation (1) using the site-averagedmutual μ values and the shared $\overline{\sigma\varphi_0}$ value for horizontal surfaces (the value for inclined surfaces was only used for TEM 3-1 and TEM 4-1) as fixed parameters (Tab. 2). Complete incorporation of both μ and $\overline{\sigma\varphi_0}$ uncertainties resulted in relatively large fitting uncertainties (Fig. 6a) that were finally reflected in the error margins of the OSL surface exposure ages. The fitted post-IRSL-BSL signal-depth curves of all dating samples and the associated exposure ages are summarized in Figure 6b and Table 2, respectively. To evaluate the accuracy of model-derived exposure ages, they were compared with minimum transport ages deduced from satellite images, eyewitness observations and the depth of bio-erosive rock pools (Fig. 6c). The OSL surface exposure ages of most samples agree with the control ages, i.e. ages either post-dated the minimum age or showed overlap within their dating uncertainties. However, the exposure ages of samples RAB 1-2, VAL 1-1, VAL 1-2, HAR 1-1 and HAR 2-1 were too young, i.e. they pre-dated the minimum control ages.

5.5 Modelling post-depositional erosion of boulder surfaces

In order to explore whether erosion offers a plausible explanation of the age underestimations recorded for samples RAB 1-2, HAR 1-1, HAR 1-2, VAL 1-1 and VAL 1-2, the potential effect of erosion on the luminescence bleaching profiles was modelled using the analytical numerical approach of Lehmann et al. (2019a). The modelled

sample ages ($t_{exp\ mean}$) and minimum independent ages ($t_{age\ control}$) were used as model inputs, together with the shared values of μ and $\overline{\sigma\varphi_0}$ (Tab. 2). 50 different erosion rates from 0.001 mm/year to 1 mm/year were tested together with 50 different times for the onset of erosion (t_s) ranging from 1 year to the independent sample age (both variables were sampled equidistantly in log space). The misfits between modelled and measured values were determined and paths with normalised misfit >0.99 were retained. The sensitivity of the calculated erosion rates to the independent age was also evaluated by contrasting the results calculated for sample VAL 1-12 for independent ages of 50 years, 450 years and 6000 years, which reflect the minimum exposure age based on satellite images, a plausible estimate of the boulder turning age based on the depth of post-depositional rock pools (assuming bio-erosion of 1 mm/year; cf. Kelletat, 2013) and finally the time when Holocene sea level reached approximately its present position. The calculated erosion rates vary dependent on t_s (Fig. 7), thus to facilitate comparison, erosion rates for t_s ~~of ten years~~equal to the respective expected age (i.e. assuming constant erosion during exposure) are contrasted between samples (Tab. A5). The modelled erosion rates tend to increase with increasing surface age, from 0.025 mm/year assuming an age of 50 years, to 0.0320 mm/year assuming ~~an~~ ages of 450 and ~~years, and to 0.40 mm/year assuming an age of~~ 6000 years in case of sample VAL 1-1. Thus, erosion rate estimates based on minimum control ages should be regarded as minimum values. Minimum erosion rates varied from 0.183 mm/year (HAR~~RAB~~ 1-12) to ~~<~~0.021 mm/year (VAL 1-1), maximum values (based on maximum ages) may be slightly larger as indicated for VAL 1-1 ~~reach 0.32 to 0.40 mm/year (VAL 1-1 and VAL 1-2)~~. In agreement with expectation, the model did not identify any significant erosion (i.e. erosion rates <0.01 mm/year) for samples that do not underestimate the minimum control ages.

6. Discussion

6.1 Performance of OSL surface exposure dating on ~~coastal sandstone~~ calcarenite boulders

The OSL surface exposure ages derived for boulders and niches from the Rabat coast show two striking characteristics: (1) All exposure ages are associated with relatively large dating uncertainties compared to previous applications of OSL-RSED (e.g. Sohbati et al., 2012; Lehmann et al., 2018); and (2) five of the 13 dated boulder samples yield OSL exposure ages that underestimate minimum ages deduced from satellite imagery and rock-pool depth, even when their uncertainties are considered (Fig. 6c).

The low dating precision ~~achieved~~ observed in this study is mainly the result of the boulder source rock, a late Pleistocene calcarenite. All rock samples dated in this study display strongly scattered post-IRSL-BSL signal-depth data (e.g. Fig. 4 and Fig. 5) that entail large fitting uncertainties, imprecisely constrained μ and $\overline{\sigma\varphi_0}$ parameters and, eventually, large dating uncertainties. OSL signal scatter is primarily due to dim post-IRSL-BSL signals with not more than a few hundred photon counts in the analysed signal interval. Since pure quartz extracts of the same samples proved to be rather sensitive (Fig. A12), dim post-IRSL-BSL signals must be the result of low percentages of quartz on the carbonate-rich polymineralic aliquots used for dating. Additional signal scatter for our samples ~~is~~ may be introduced by spatial variations of ~~t~~light penetration that is caused by heterogeneities in the rock mineralogy (Meyer et al., 2018)~~.~~ ~~he post-IRSL-BSL signal accumulated prior to exposure (L_0). Since post-IRSL-BSL signals in the relatively young source rocks of the boulders (i.e. 40-50 Gy and 80-100 ka) are not in field saturation, they depend on mineralogy-induced dose-rate differences within the rock. Thirdly, a small contamination of post-IRSL-BSL signals by feldspar emissions remains in all dated samples. If the amount of feldspar varies from aliquot to aliquot, varying contributions of feldspar emissions to the post-IRSL-BSL signals~~

from polymineralic aliquots will introduce additional scatter. While OSL exposure ages of rocks with more suitable luminescence properties are also affected by fitting uncertainties due to mineralogical heterogeneities (Meyer et al., 2018) and core-to-core variations of OSL signal resetting (Sellwood et al., 2019)., Pprevious studies demonstrated that lithologies with brighter quartz signals in polymineralic samples (e.g. quartzite or quartz-dominated sandstone) or stronger feldspar signals to avoid using quartz OSL for dating (e.g. granite or gneiss) can provide much higher dating precision than achieved for the Rabat boulders (Sohbati et al., 2012; Freiesleben et al., 2015; Lehmann et al., 2018; Gliganic et al., 2019).

Although large post-IRSL-BSL signal scatter may also affect dating accuracy, since it prevents using individual μ values for each sample as suggested e.g. by Gliganic et al. (2019), the unambiguous disagreement between exposure ages and age control for five of the boulder samples (Fig. 6c) is interpreted to result from inadequate unreliable $\overline{\sigma\varphi_0}$ values and post-depositional erosion. In the constrained geographical area visited in this study, $\overline{\sigma\varphi_0}$ should be comparable for all boulder surfaces as long as they share the same aspect and inclination (e.g. Sohbati et al., 2018). However, if calibration and dating samples do not share surface inclination and aspect, the use of a shared $\overline{\sigma\varphi_0}$ value is inappropriate, as observed in controlled bleaching experiments (Gliganic et al., 2019) and indicated by the systematic differences of $\overline{\sigma\varphi_0}$ between calibration samples with inclined and flat surfaces in this study. The clearly too young OSL exposure ages of samples HAR 2-1 and RAB 1-2, i.e. 2517±68 and 1112±3 years, although these both boulders were overturned at least 50 years ago (Fig. 6c), could both reflect the mismatch between their inclined surfaces and fitting with a $\overline{\sigma\varphi_0}$ that was determined on flat calibration surfaces. Future boulder dating studies should ensure calibration samples with comparable inclination and orientation to the dating samples.

Besides inadequate model calibration, OSL rock surface exposure ages become inaccurate when their OSL signal-depth curves are affected by environmental factors beyond thedifferent than exposure time. Since OSL-RSED is restricted to the uppermost few mm or cm of rock surfaces, the position and shape of the bleaching front is very susceptible to erosion (Sohbati et al., 2018; Lehmann et al., 2019a,b; Brown and Moon, 2019). For soft sandstone boulders in the coastal zone as dated here, the combination of sea-spray and rain-induced weathering and strong winds is likely to cause erosion of grains at the exposed post-transport surfaces (e.g. Mottershead, 1989). By yielding erosion rates from 0.026 to 0.1820 mm/year, inversion of the rock surface-exposure data for boulder samples that clearly underestimate age control (i.e. RAB 1-2, HAR 1-1, HAR 1-2, VAL 1-1 and VAL 1-2) supports the assumption of significant erosion for some of the boulders dated in this study (Fig. 7).

The erosion processes of interest in this study are affecting the surface of the boulders at the spatial scale of the individual mineral grains and timescales of centuries to millennia. Empirical approaches such as micro-erosion meters (Stephenson and Finlayson, 2009) and remote sensing methods (Moses et al., 2014), allow accurate erosion rate quantification but only on sub-decadal timescales. On the other hand, terrestrial cosmogenic nuclide concentrations provide erosion rate estimates from exposed bedrock (Small et al., 1997; Portenga and Bierman, 2011) but only on timescales of > 10^4-10^6 years and over spatial scales of several decimetres to several meters. Besides being an emerging method and still in development, the OSL-RSED method allows to quantify surface erosion stories according to linear, non-linear and stochastic temporal functions at the sub-centimetreic scale and over timescales of centuries to millennia (Sohbati et al., 2018; Lehmann et al., 2019a,b; Brown and Moon, 2019). The impact of erosion inferred from luminescence signal-depth data in this study agrees with expectations based on geomorphological evidence for boulders with post-transport surfaces covered by bio-erosive rock pools, such as boulder VAL 1. Since the lower part of this boulders is lying in the intertidal zone, modelled erosion rates of

0.02 to 0.07 mm/year can be explained by weathering due to ~~it is regularly covered by~~ sea spray and overtopping waves. ~~Surfaces between bio-erosive rock pools, which can form with erosion rates of up to 1 mm/year (e.g. Kelletat, 2013), were sampled in the case of VAL 1-1 and VAL 1-2. For these samples relatively large modelled erosion rates of 0.20 mm/year, when assuming an age of ~450 years based on rock pool depth and bio-erosion rates of 1 mm/year (Fig. 7a), may therefore be realistic.~~ These data also illustrate the spatial heterogeneity in erosion rates for some of the coastal boulders sampled and the importance of careful sample location selection. Comparable erosion rates of 0.04-0.06 mm/year were inferred ~~Erosion rates are assumed to be much lower~~ for boulders in supratidal positions despite their apparently smooth surfaces (HAR 2-1. RAB 1-2)~~, as indicated by much smoother post-transport surfaces (see Tab. 1)~~. Thus, o~~O~~ur data suggest that some influence of erosion cannot unambiguously be ruled out even for calcarenite boulders with apparently smooth surfaces, and all OSL-RSED ages for boulders in this study should be interpreted with caution. While these erosion rates are based on the assumption of constant erosion, the comparatively large~~low~~ erosion rate of 0.18~~06~~ mm/year for the smooth and fresh-looking surface HAR 1-1 may indicate accelerated erosion in the first few years after exposure of fresh boulder surfaces.~~, consistent with its flat and apparently smooth post-transport surface (Fig. 7b)~~. ~~Our data suggest that some influence of erosion cannot unambiguously be ruled out even for calcarenite boulders with apparently smooth surfaces, and all OSL-RSED ages for boulders in this study should be interpreted with caution.~~

Other environmental factors that might affect OSL exposure ages are assumed to be negligible for all dated boulders. The post-transport surfaces of all boulders are bare of vegetation and not shielded by topography or houses. The surfaces of boulders in the intertidal zone (i.e. VAL 1) may be overtopped by waves during stronger storms (particularly contemporaneous with high-tide conditions), but periods with submersion are insignificantly short compared to the total exposure time. Likewise, the exposure duration of the calibration surfaces, i.e. another important parameter for model calibration, had no negative effect on dating accuracy. The exposure time of ~2 years used in this study was more than sufficient to generate pronounced bleaching fronts in all calcarenite samples. Although model calibration generally benefits from calibration samples with long, and in the best case several different, exposure durations, even shorter exposure intervals than 2 years would have sufficed. In boulder samples with bright IRSL signals, these were even better bleached than the associated post-IRSL-BSL signals (Fig. 4c), potentially because longer wavelengths that feldspar signals are sensitive to are less attenuated by the rock than the shorter wavelengths (Ou et al., 2018) that bleach quartz signals (Wallinga, 2002). Thus, the application of IRSL instead of post-IRSL-BSL signals may reduce the time required for calibration to durations as short as a few months (Freiesleben et al., 2015; Ou et al., 2018). While IRSL signals were not used in this study due to insufficiently bright signals for most samples, in retrospect their use might be advantageous to post-IRSL-BSL signals at least for some of the investigated boulders.~~the application of IRSL instead of post-IRSL-BSL signals may reduce the time required for calibration to durations as short as a few months (Freiesleben et al., 2015; Ou et al., 2018).~~

6.2 New information on storm and tsunami hazard at the Atlantic coast of Morocco

Knowing the chronology of boulder transport can help to better assess the local flooding hazard at the Rabat coast. Energetic waves during storms and tsunamis will generally exacerbate the effects of coastal flooding in the course of climate-induced sea-level rise (Nicholls et al., 2018). It is therefore of paramount interest whether coastal inundation strong enough to lift boulders at the Rabat coast only occurred during the very rare tsunami events, such as the 1755 Lisbon Tsunami, or also during much more frequent winter storms. While the discrimination

between storm and tsunami transport based on boulder features is hardly possible, with the exception of extreme cases that disregard storm transport due to exceptional boulder masses or elevations (Lau and Autret, 2020 and references therein), chronological patterns of boulder detachment may provide useful information for the recognition of storm and tsunami boulders.

Comparison with satellite images showed that apparent OSL-RSED ages ~~are~~ definitely ~~inaccurate~~ do not reflect the timing of cliff detachment for boulders affected by severe post-depositional erosion (VAL 1-1 and VAL 1-2, squares in Fig. 6c) and for boulder samples with significantly inclined surfaces (HAR 2-1 and RAB 1-2, stars in Fig. 6c); the associated OSL exposure ages cannot be considered for any further interpretation. All other boulder samples, including those with apparently smooth surfaces, were likely affected to some extent by erosion as well. Slight age underestimation, thus, cannot be excluded and their exposure ages should be interpreted carefully. We nevertheless are confident that the latter provide valuable relative chronological information for ~~boulder transport~~the cliff detachment of boulders that is shown in Figure 8a and allows differentiation between boulder ages.

The reliability of this relative chronology is supported by correlation between OSL exposure ages and the surface taphonomy of the associated boulders and niches (Fig. 8a, b). Exposure ages younger than ~10 years were achieved for boulders and niches with smooth surfaces and fresh fractures, i.e. taphonomy classes 4 and 5 (TEM 4, TEM 3, HAR 1; Fig. 8b1). Boulders with exposure ages between ~10 and ~100 years are characterised by smooth surfaces with very scarce lichen or algae cover, i.e. taphonomy classes 3 and 4 (HAR 3, ~~RAB 1,~~ VAL 4, VAL 6, TEM 2; Fig. 8b2). Finally, boulders with exposure ages older than ~100 years are characterised by weathered fractures and rougher surfaces, i.e. taphonomy classes 2 and 3 (~~VAL 4~~RAB 1, RAB 5; Fig. 8b3,b4). According to the chronology presented here, with OSL exposure ages of 30-250 years (VAL 4) and~~,~~ 60-490 ~~152±52~~ years (RAB 1~~VAL 4~~) ~~and 360–4100 577±247 years (RAB 5) and rather rough/weathered rock surfaces~~, ~~these~~ only two boulders ~~are the only clasts that~~ may have been moved by the 1755 Lisbon Tsunami. However, with masses of 16-37~~24~~ t and positions on the intertidal platform (~~RAB 5,~~ RAB 1) or on top of cliffs 3-4 m above sea level (VAL 4), they do not systematically differ from the other dated boulders in terms of wave power required for transportation.

Although the relative chronology does not unambiguously allow for correlating individual boulders with specific historical storms or tsunamis, two important conclusions with regard to the local flooding hazard can be drawn from the dataset. Firstly, the relative chronology in Figure 8a implies that most boulders at the Rabat coast were detached from the cliff and overturned by storm waves. The large spread of OSL exposure ages between a few years and several centuries indicates that numerous transport events were responsible for the formation of the dated boulders. Since the 1755 Lisbon Tsunami was the only tsunami with significant flooding at the Moroccan Atlantic coast during the last 1000 years (Kaabouben et al., 2009), boulder transport dominated by tsunamis is assumed to have resulted in more significant clustering of ages around ~260 years ago.

Secondly, correlation of exposure ages and masses of the associated boulders shows that storm waves were capable of lifting much larger boulders than observed during recent winter storms. At the Rabat coast, observations from the last decade are restricted to the lifting of smaller boulders (Mhammdi et al., 2020), while boulders larger than ~5 t were only observed to move by sliding (Fig. A3). However, boulders with OSL exposure ages that clearly postdate the 1755 Lisbon Tsunami and therefore must have been lifted by storms reach up to 21-24~~1~~38 t (VAL 6, RAB 5~~1~~). These storm boulders yield comparable ~~or even larger~~ masses ~~than~~ as boulders that, based on their exposure ages, might have been transported and overturned during the 1755 Lisbon Tsunami (i.e. VAL 4 and~~,~~ RAB 1 ~~and RAB 5~~ with masses of 16-~~24~~ 37 t). Of course, we cannot exclude that the largest boulders at the Rabat

coast, such as VAL 1 with ~65 t that could not be dated with OSL-RSED due to strong erosion of its~~their~~ post-transport surface in the intertidal zone, can exclusively be overturned by tsunamis. Nevertheless, in agreement with hydrodynamic experiments (Cox et al., 2019), ~~and~~ observations after recent tropical cyclones or winter storms (e.g. May et al., 2015; Cox et al., 2018), and other boulder studies from the North Atlantic (e.g. Oliveira et al., 2020), our results support the perception that storm waves significantly contribute to boulder quarrying along cliffs and may be considered ~~an~~ the most important driver for the evolution of wave-emplaced coarse-clast deposits in storm-prone areas worldwide, including boulders with masses of several tens of tons that occasionally have ~~previously~~ been associated with tsunamis previously. It is, therefore, likely that also most other boulders documented along the Atlantic coasts of Morocco ~~(Mhammdi et al., 2008; Medina et al., 2011),~~ and the Iberian Peninsula ~~(Whelan and Kelletat, 2005; Scheffers and Kelletat, 2005; Costa et al., 2011)~~, for some of which ~~have tentatively been related to the~~ the 1755 Lisbon Tsunami and potential predecessors have tentatively been discussed as an alternative explanation to storm waves (Whelan and Kelletat, 2005; Scheffers and Kelletat, 2005; Mhammdi et al., 2008; Medina et al., 2011), ~~previously but mainly lack sound chronological data,~~ in fact represent storm boulders. Interpretation of tsunami boulders at the storm-prone coast of the North Atlantic should be restricted to the very rare cases, where chronological information is precise enough to relate them to a specific event such as the 1755 Lisbon tsunami (e.g. Costa et al., 2011; Oliveira et al., 2020).

7. Conclusions

OSL rock surface exposure dating was for the first time ~~applied to~~tested on coastal boulders overturned during wave transport to evaluate its reliability as a dating approach in this setting. Successful calibration of the bleaching model using surfaces exposed for ~2 years and evaluation of OSL exposure ages against satellite images indicate the potential of the approach for boulders with limited post-depositional erosion and with surface inclination in agreement with that of the calibration samples. Although fitting uncertainties as a consequence of low amounts of quartz and potassium feldspar in the source rock introduced relatively large dating uncertainties, and although a bias due to post-depositional erosion cannot be excluded even for boulders with smooth surfaces, OSL rock surface exposure dating provides a relative chronology for boulders that could not be dated with any other approach so far. This relative chronology indicates a large variability of boulder ages, most of them different from the only tsunami event at the Rabat coast within the last 2000 years. Thus, OSL exposure ages suggest that even boulders weighing ~~~>40~~ 24 t were moved and overturned by storm waves. This supports the conclusion of previous studies that storms rather than tsunamis can be the most important driver for the formation of coastal boulder deposits in general.

While OSL-RSED offered important relative chronological information for the Rabat coastal boulders but could not provide absolute ages, the approach ~~offers~~ may be a powerful tool for dating boulder deposits with more favourable lithologies. Magmatic rocks, such as granites, are not only significantly less susceptible to erosion, typically they also allow measurement of the luminescence signal of potassium feldspar. Different from the quartz signals of the calcarenite used in this study, IRSL signals of potassium feldspar measured on polymineralic aliquots do not suffer from contamination by other minerals and are typically much brighter than those of quartz. Such lithological properties promise to reduce the uncertainties and inaccuracies related to OSL surface exposure dating of coastal boulders in this study significantly. While OSL-RSED will not be able to date boulder sites with pure

limestone lithologies, our result demonstrate its potential for providing unique chronological information for non-carbonate boulders that today cannot be dated by any other technique.

Author contributions

D.B. and S.M. conceived the study and obtained funding. D.B., S.M., N.M. and G.K. conducted fieldwork. N.M. provided site information and eyewitness accounts. D.B., S.M., D.W. and A.Z. established the equipment for sample preparation at the CLL. D.B. conducted the measurements and evaluated the data. C.B. provided the R-scripts for data analyses and helped with data fitting. S.M, G.K and B.L. helped with analysing and interpreting the data. H.B. along with all other authors commented on the manuscript at all stages.

Data availability

The complete dataset of L_x/T_x values of all samples that were used for the fitting of luminescence depth data in this study are available on PANGEA (https://doi.org/10.1594/PANGAEA.919187).

Competing interests

"The authors declare that they have no conflict of interest."

Acknowledgements

This study was funded by the Deutsche Forschungsgemeinschaft (DFG, German Research Foundation, GZ: BR 5023/3-1 and MA 5768/2-1). The authors are grateful to M. Malika Ait and A. Chiguer for their support during the first field survey in Morocco in July 2016. We would also like to thank the Moroccan Association of Geosciences in the person of its President, Prof. Medina Fida for its support.

References

Araoka, D., Yokoyama, Y., Suzuki, A., Goto K., Miyagi, K., Miyazawa, K., Matsuzaki, H. and Kawahata H.: Tsunami recurrence revealed by Porites coral boulders in the southern Ryukyu Islands, Japan, Geology, 41, 919–922, doi:10.1130/G34415.1, 2013.

Bailey, R.M.: Direct measurement of the fast component of quartz optically stimulated luminescence and implications for the accuracy of optical dating, Quaternary Geochronology, 5, 559-568, 2010.

Banerjee, D., Murray, A.S., Botter-Jensen, L. and Lang, A.: Equivalent dose estimation using a single aliquot of polymineral fine grains, Radiation Measurements, 33, 73-94, 2001.

Baptista, M.A., Miranda, J.M., Chierici, F., and Zitellini, N.: New study of the 1755 earthquake source based on multi-channel seismic data and tsunami modelling, Natural Hazards and Earth System Sciences, 3, 333-340, 2003.

Barton, R.N.E., Bouzouggar, A., Collcutt, S.N., Schwenninger, J.-L. and Clark-Balzan, L.: OSL dating of the Aterian levels at Dar es-Soltan I (Rabat, Morocco) and implications for the dispersal of modern Homo sapiens, Quaternary Science Reviews, 28, 1914-1931, 2009.

Blanc, P.L.: Earthquakes and tsunami in November 1755 in Morocco: a different reading of contemporaneous documentary sources, Natural Hazards and Earth System Sciences, 9, 725-738, 2009.

Brown, N.D. and Moon, S.: Revisiting erosion rate estimates from luminescence profiles in exposed bedrock surfaces using stochastic erosion simulations, Earth and Planetary Science Letters, 528, 115842, 2019.

Burow, C.: fit_SurfaceExposure(): Nonlinear Least Squares Fit for OSL surface exposure data. Function version 0.1.0. In: Kreutzer, S., Burow, C., Dietze, M., Fuchs, M.C., Schmidt, C., Fischer, M., Friedrich, J.: Luminescence: Comprehensive Luminescence Dating Data Analysis, R package version 0.9.0.87, https://CRAN.R-project.org/package=Luminescence, 2019.

Chahid, D., Boudad, L., Lenoble, A., Lamothe, M., Chakroun, A., Falguères, C. and Nespoulet, R.: Les paléo-rivages des formations littorales atlantiques du Pléistocène moyen—supérieur de Rabat-Témara (Maroc), L'Anthropologie, 121, 122–132, 2017.

Chakroun, A., Chahid, D., Boudad, L., Campmas, E., Lenoble, A., Nespoulet, R. and El Hajraoui, M.A.: The Pleistocene of Rabat (Morocco): Mollusks, Coastal Environments and Human Behavior, African Archaeological Reviews, 34, 493-510, 2017.

Costa, P., Andrade, C., Freitas, M., Oliveira, M., da Silva, C.M., Omira, R., Taborda, R., Baptista, M.A. and Dawson, A.G.: Boulder deposition during major tsunami events, Earth Surface Processes and Landforms, 36, 2054-2068, 2011.

Cox, R., O'Boyle, L. and Cytrynbaum, J.: Imbricated coastal boulder deposits are formed by storm waves, and can preserve long-term storminess record, Scientific Reports, 9, 10784, doi:10.1038/s41598-019-47254-w5, 2019.

Cox, R., Jahn, K.L., Watkins, O.G. and Cox, P.: Extraordinary boulder transport by storm waves (west of Ireland, winter 2013–2014), and criteria for analysing coastal boulder deposits, Earth-Science-Reviews, 177, 623-636, 2018.

Dawson, A.G., Hindson, R., Andrade, C., Freitas, C., Parish, R. and Bateman, M.: Tsunami sedimentation associated with the Lisbon earthquake of 1 November AD 1755: Boca do Rio, Algarve, Portugal, The Holocene 5, 209-215, 1995.

Durcan, J.A., King, G.E. and Duller, G.A.T.: DRAC: Dose rate and age calculator for trapped charge dating, Quaternary Geochronology, 28, 54-61, 2015.

Engel, M. and May, S.M.: Bonaire's boulder fields revisited: evidence for Holocene tsunami impact on the Leeward Antilles, Quaternary Science Reviews, 54, 126-141, 2012.

Feist, L., Frank, S., Bellanova, P., Laermanns, H., Cämmerer, C., Mathes-Schmidt, M., Biermanns, P., Brill, D., Costa, P., Teichner, F., Brückner, H., Schwarzbauer, J. and Reicherter, K.: The sedimentological and environmental footprint of extreme wave events in Boca do Rio, Algarve coast, Portugal, Sedimentary Geology, 389, 147-160, 2019.

Freiesleben, T., Sohbati, R., Murray, A., Jain, M., al Khasawneh, S., Hvidt, S. and Jakobsen, B.: Mathematical model quantifies multiple daylight exposure and burial events for rock surfaces using luminescence dating, Radiation Measurements, 81, 16-22, 2015.

Gliganic, L.A., Meyer, M., Sohbati, R., Jain, M. and Barrett, S.: OSL surface exposure dating of a lithic quarry in Tibet: Laboratory validation and application, Quaternary Geochronology, 49, 199-204, 2019.

Guerin, G., Mercier, N. and Adamiec, G.: Dose-rate conversion factors: update, Ancient TL, 29, 5-8, 2011.

Hindson, R.A. and Andrade, C.: Sedimentation and hydrodynamic processes associated with the tsunami generated by the 1755 Lisbon earthquake, Quaternary International, 56, 27-38, 1999.

Jenkins, G.T.H, Duller, G.A.T., Roberts, H.M., Chiverrell, R.C. and Glasser, N.F.: A new approach for luminescence dating glaciofluvial deposits – High precision optical dating of cobbles, Quaternary Science Reviews, 192, 263-273, 2018.

Kaabouben, F., Baptista, M.A., Iben Brahim, A., El Mouraouah, A. and Toto, A.: On the moroccan tsunami catalogue, Natural Hazards and Earth System Sciences, 9, 1227-1236, 2009.

Kelletat, D.: Physische Geographie der Meere und Küsten. Eine Einführung, 3rd edition, Borntraeger, pp. 290, 2013.

Khan, N.S., Ashe, E., Shaw, T., Vacchi, M., Walker, J., Peltier, W.R., Kopp, R.E. and Horton, B.P.: Holocene relative sea-level changes from near-, intermediate- and far-field locations, Current Climate Change, 1, 247-262, 2015.

King, G.E., Valla, P.G. and Lehmann, B.: Rock surface burial and exposure dating. In: Bateman, M. (edt.), Handbook of Luminescence Dating, 350-372, 2019.

Kreutzer, S., Burow, C., Dietze, M., Fuchs, M.C., Schmidt, C., Fischer, M. and Friedrich, J.: Luminescence: Comprehensive Luminescence Dating Data Analysis, R package version 0.9.0.87, https://CRAN.R-project.org/package=Luminescence, 2019.

Lario, J., Zazo, C., Goy, J.L., Silva, P.G., Bardaji, T., Cabero, A. and Dabrio, C.J.: Holocene palaeotsunami catalogue of SW Iberia, Quaternary International, 242, 196-200, 2011.

Lehmann, B., Valla, P.G., King, G.E. and Herman, F.: Investigation of OSL surface exposure dating to reconstruct post-LIA glacier fluctuations in the French Alps (Mer de Glace, Mont Blanc massif), Quaternary Geochronology, 44, 63-74, 2018.

Lehmann, B., Herman, F., Valla, P.G., King, G.E. and Biswas, R.H.: Evaluating post-glacial bedrock erosion and surface exposure duration by coupling in situ optically stimulated luminescence and ^{10}Be dating, Earth Surface Dynamics, 7, 633-662, 2019.

Lehmann, B., Herman, F., Valla, P.G., King, G.E., Biswas, R.H., Ivy-Ochs, S., Steinemann, O. and Christl, M.: Postglacial erosion of bedrock surfaces and deglaciation timing: New insights from the Mont Blanc massif (western Alps), Geology, 48, 139-144, 2019.

May, S.M., Engel, M., Brill, D., Cuadra, C., Lagmay, A.M.F., Santiago, J., Suarez, J.K., Reyes, M. and Brückner, H.: Block and boulder transport in Eastern Samar (Philippines) during Supertyphoon Haiyan, Earth Surface Dynamics, 3, 543-558, 2015.

Medina, F., Mhammdi, N., Chiguer, A., Akil, M. and Jaaidi, E.B.: The Rabat and Larache boulder fields; new examples of high-energy deposits related to storms and tsunami waves in north-western Morocco, Natural Hazards, 59, 725-747, 2011.

Meyer, M.C., Gliganic, L.A., Jain, M., Sohbati, R. and Schmidmair, D.: Lithological controls on light penetration into rock surfaces – Implications for OSL and IRSL surface exposure dating, Radiation Measurements, 120, 298-304, 2018.

Mhammdi, N., Medina, F., Kelletat, D., Ahmamou, M. and Aloussi, L.: Large boulders along the Rabat coast (Morocco); possible emplacement by the November 1st, 1755 A.D. tsunami, Science of Tsunami Hazards, 27, 17-30, 2008.

Mhammdi, N., Medina, F., Belkhayat, Z., El Aoula, R., Geawahri, M. and Chiguer, A.: Marine storms along the Moroccan Atlantic coast: An underrated natural hazard? Journal of African Earth Sciences, 163, 103730, doi:10.1016/j.jafrearsci.2019.103730, 2020.

Moses, C., Robinson, D., and Barlow, J.: Methods for measuring rock surface weathering and erosion: A critical review. Earth-Science Reviews, 135, 141-161, 2014.

Mottershead, D.: Rates and patterns of bedrock denudation by coastal salt spray weathering: A seven-year record, Earth Surface Processes and Landforms, 14, 383-398, 1989.

Murray, A.S. and Wintle, A.G.: The single aliquot regenerative dose protocol: potential for improvements in reliability, Radiation Measurements, 37, 377-381, 2003.

Nandasena, N.A.K., Paris, R. and Tanaka, N.: Reassessment of hydrodynamic equations: Minimum flow velocity to initiate boulder transport by high energy events (storms, tsunamis), Marine Geology, 281, 70-84, 2011.

Nicholls, R.J., Brown, S., Goodwin, P., Wahl, T., Lowe, J., Solan, M., Godbold, J.A., Haigh, I.D., Lincke, D., Hinkel, J., Wolff, C. and Merkens, J.: Stabilization of global temperature at 1.5 °C and 2.0 °C: implications for coastal areas, Philosophical Transactions of the Royal Society A, 376, doi:10.1098/rsta.2016.0448, 2018.

NOAA: Historical Hurricane Tracks, https://coast.noaa.gov/hurricanes/ (last access September 2019), 2019.

Oliveira, M.A., Llop, E., Andrade, C., Branquinho, C., Goble, R., Queiroz, S., Freitas, M.C. and Pinho, P.: Estimating the age and mechanism of boulder transport related with extreme waves using lichenometry, Progress in Physical Geography, https://doi.org/10.1177/0309133320927629, 2020.

Ou, X.J., Roberts, H.M., Duller, G.A.T., Dunn, M.D. and Perkins, W.T.: Attenuation of light in different rock types and implications for rock surface luminescence dating, Radiation Measurements, 120, 305-311, 2018.

Paris, R., Naylor, L.A. and Stephenson, W.: Boulders as a signature of storms on rock coasts, Marine Geology, 283, 1-11, 2011.

Portenga, E.W. and Bierman, P.R.: Understanding Earth's eroding surface with ^{10}Be. GSA Today, 21(8), 4-10, 2011.

Rades, E., Sohbati, R., Lüthgens, C., Jain, M. and Murray, A.S.: First luminescence-depth profiles from boulders from moraine deposits: Insights into glaciation chronology and transport dynamics in Malta valley, Austria, Radiation Measurements, 120, 281-289, 2018.

Ramalho, R., Winckler, G., Madeira, J., Helfrich, G., Hipolito, A., Quartau, R., Adena, K. and Schaefer, J.M.: Hazard potential of volcanic flank collapses raised by new megatsunami evidence, Science Advances, 1, doi:10.1126/sciadv.1500456, 2015.

Ramalho, R., Omira, R., El Moussaoui, S., Baptista, M.A. and Zaghloul, M.N.: Tsunami-induced morphological change – A model-based impact assessment of the 1755 tsunami in NE Atlantic from the Morocco coast, Geomorphology, 319, 78-91, 2018.

Reading University: Extratropical Cyclone Atlas, http://www.met.rdg.ac.uk/~storms/cgi-bin/storms/storms.cgi, last access: September 2019, 2019.

Renou, C., Lesne, O., Mangin, A., Rouffi, F., Atillah, A., El Hadani, D. and Moudni, H.: Tsunami hazard assessment in the coastal area of Rabat and Sale, Morocco, Natural Hazards and Earth System Sciences, 11, 2181-2191, 2011.

Rixhon, G., May, S. M., Engel, M., Mechernich, S., Schroeder-Ritzrau, A., Frank, N., Fohlmeister, J., Boulvain, F., Dunai, T. and Brückner, H.: Multiple dating approach (^{14}C, ^{230}Th/U and ^{36}Cl) of tsunami-transported reef-top boulders on Bonaire (Leeward Antilles) – current achievements and challenges, Marine Geology, 396, 100–113, doi:10.1016/j.margeo.2017.03.007, 2017.

Sato, T., Nakamura, N., Goto, K., Kumagai, Y., Nagahama, H. and Minoura, K.: Paleomagnetism reveals the emplacement age of tsunamigenic coral boulders on Ishigaki Island, Japan, Geology, 42, 603–606, doi:10.1130/G35366.1, 2014.

Scheffers, A. and Kelletat, D.: Tsunami relics on the coastal landscape west of Lisbon, Portugal, Science of Tsunami Hazards, 23, 3-16, 2005.

Sellwood, E.L., Guralnik, B., Kook, M., Prasad, A.K., Sohbati, R., Hippe, K., Wallinga, J. and Jain, M.: Optical bleaching front in bedrock revealed by spatially-resolved infrared photoluminescence, Scientific Reports, 9, 2611, doi:10.1038/s41598-019-38815-0, 2019.

Simms, A.R., DeWitt, R., Kouremenos, P. and Drewry, A.M.: A new approach to reconstructing sea levels in Antarctica using optically stimulated luminescence of cobble surfaces, Quaternary Geochronology, 6, 50-60, 2011.

Small, E.E., Anderson, R.S., Repka, J. and Finkel, R.: Erosion rates of alpine bedrock summit surfaces deduced from in situ ^{10}Be and ^{26}Al. Earth and Planetary Science Letters, 150, 413-425.

Sohbati, R., Murray, A.S., Jain, M., Buylaert, J.P. and Thomsen, K.: Investigating the resetting of OSL signals in rock surfaces, Geochronometria, 38, 249-258, 2011.

Sohbati, R., Murray, A.S., Chapot, M.S., Jain, M. and Pederson, J.: Optically stimulated luminescence (OSL) as a chronometer for surface exposure dating, Journal of Geophysical Research, 117, 1-7, 2012.

Sohbati, R., Murray, A.S., Porat, N., Jain, M. and Avner, U.: Age of a prehistoric “Rodedian” cult site constrained by sediment and rock surface luminescence dating techniques, Quaternary Geochronology, 30, 90-99, 2015.

Sohbati, R., Liu, J., Jain, M., Murray, A.S., Egholm, D., Paris, R. and Guralnik, B.: Centennial- to millennial-scale hard rock erosion rates deduced from luminescence-depth profiles, Earth and Planetary Science Letters, 493, 218-230, 2018.

Stephenson, W.J. and Finlayson, B.L.: Measuring erosion with the micro-erosion meter—Contributions to understanding landform evolution. Earth-Science Reviews, 95, 53-62, 2009.

Wallinga, J.: Optically stimulated luminescence dating of fluvial deposits: a review, Boreas, 31, 303-322, 2002.

Whelan, F. and Kelletat, D.: Boulder deposits on the southern Spanish Atlantic Coast: Possible evidence for the 1755 AD Lisbon Tsunami? Science of Tsunami Hazards, 23, 25-38, 2005.

Yu, K.F., Zhao, J.X., Shi, Q. and Meng, Q.S.: Reconstruction of storm/tsunami records over the last 4000 years using transported coral blocks and lagoon sediments in the southern South China Sea, Quaternary International, 195, 128-137, 2009.

Zhao, J.X., Neil, D., Feng, Y.X., Yu, K.F. and Pandolfi, J.M.: High-precision U-series dating of very young cyclone-transported coral reef blocks from Heron and Wistari reefs, southern Great Barrier Reef, Australia, Quaternary International, 195, 122-127, 2009.

Zitellini, N., Chierici, F., Sartori, R. and Torelli, L.: The tectonic source of the 1755 Lisbon earthquake and tsunami, Annals of Geophysics, 42, 49-55, 1999.

Figures and tables

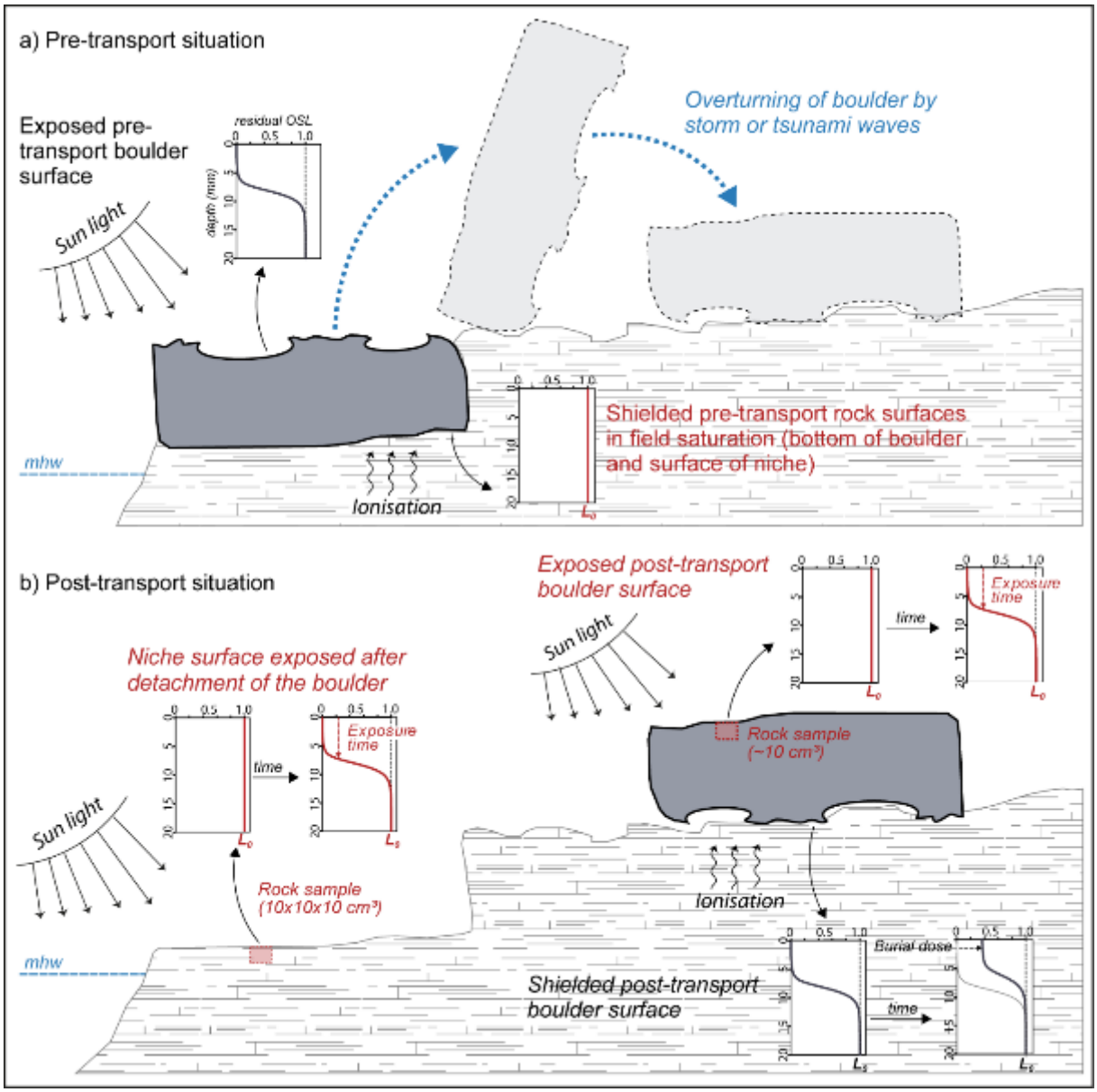

Fig. 1. Schematic model of OSL rock surface exposure dating applied to coastal boulders.

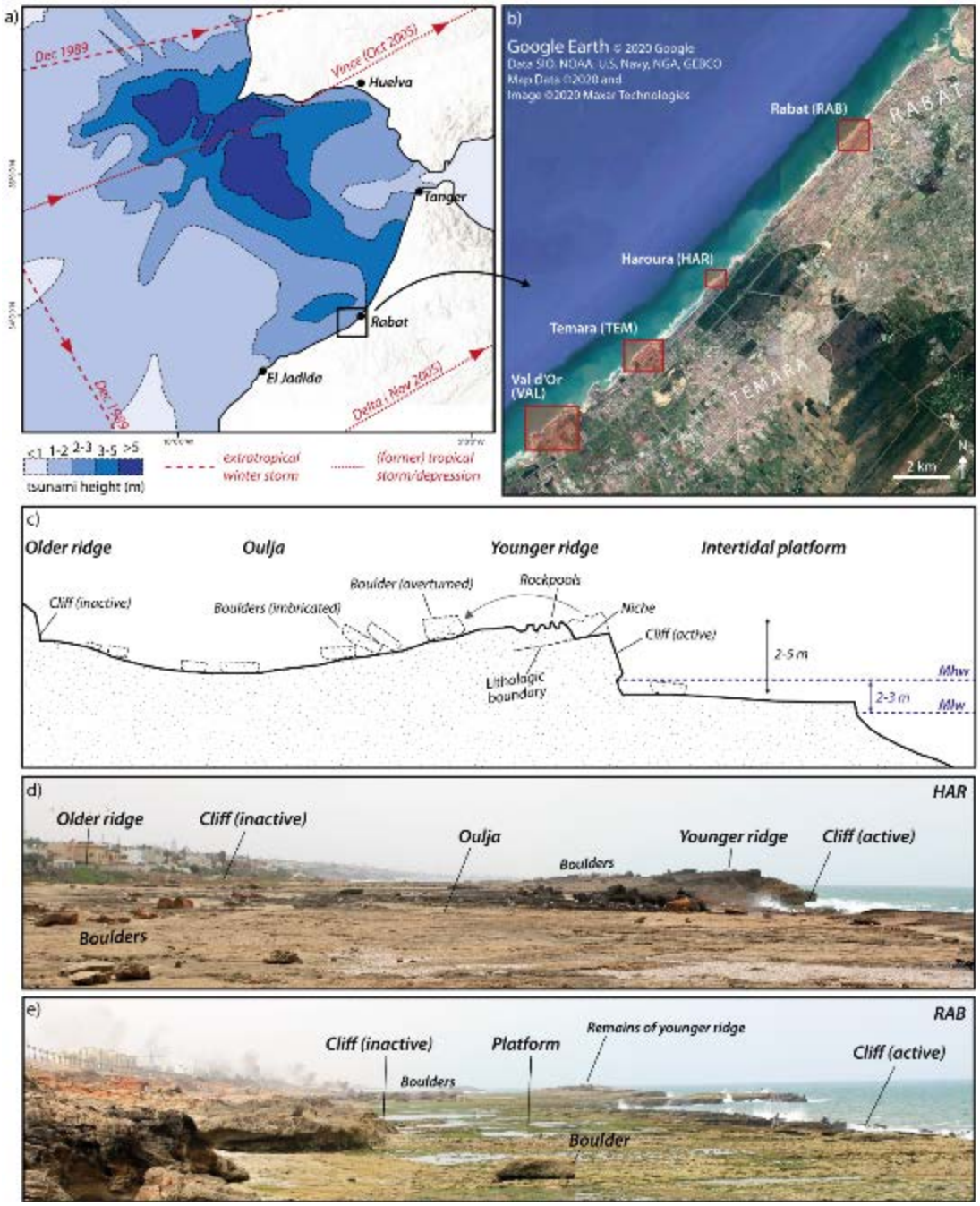

Fig. 2: Flooding hazard and geomorphological setting of the Rabat coast. a) Exposure of the Moroccan Atlantic coast to tsunamis and storms, including modelled wave heights for the 1755 Lisbon tsunami (Renou et al., 2009), tracks of former tropical storms crossing the area between 1851 and 2016 (NOAA, 2019), and extratropical winter storms in the period 1989-2009 (Reading University, 2019). b) The Rabat coast with the four study sites (based on Google Earth images). c) Schematic geomorphological cross section through the Rabat coast at Haroura (HAR, modified from Mhammdi et al., 2008). d) The coastal platform at Haroura as shown in c) (view towards Southwest). e) The coastal platform at Rabat (RAB, view towards Southwest). ©

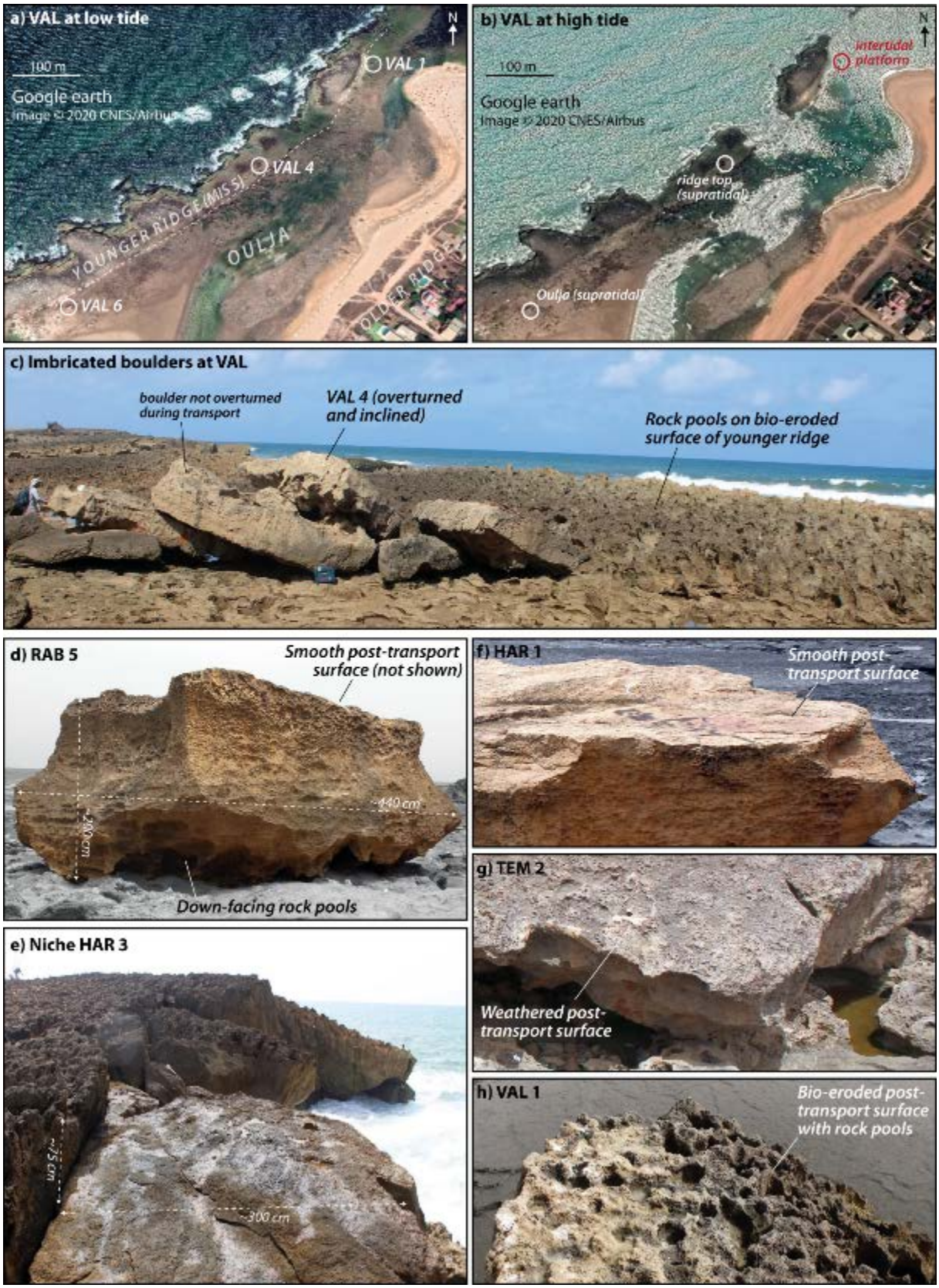

1530

Fig. 3: Coastal boulders at the Rabat coast. Satellite images of Val d'Or taken at low tide (a) and high tide (b) illustrate different boulder settings on top of the younger ridge, within the Oulja and on the intertidal platform (Google Earth images from July 2018 and February 2016). c) Boulder VAL 4 as part of a stack of imbricated boulders in ridge top position. d) Down-facing rock pools of the former cliff surface at the bottom surface of RAB 5. e) Niche HAR 3 formed
1535 **by detachment of the associated boulder. (f-h) Surface roughness of the sampled boulders varies from smooth (HAR 1), over slightly weathered (TEM 2), to rock-pool covered (VAL 1).**

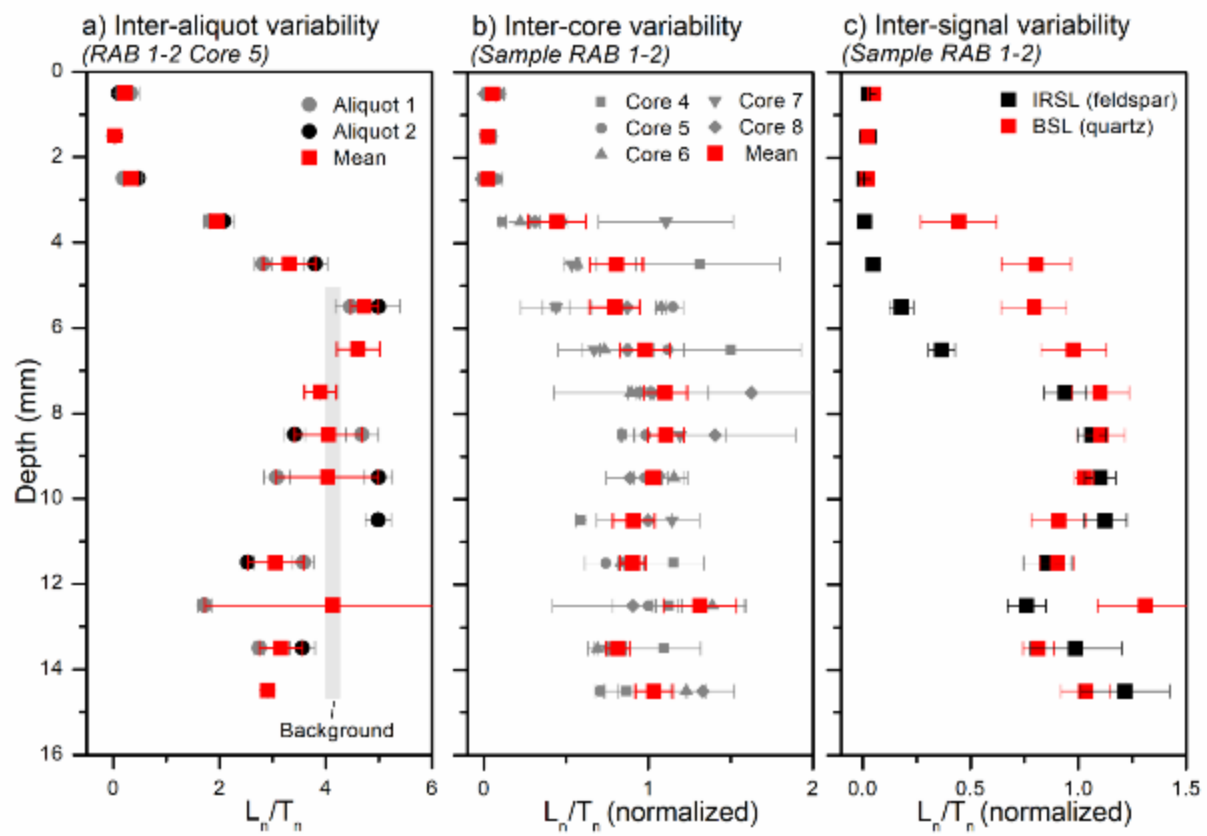

Fig. 4: Exemplary OSL signal-depth data for boulders from the Rabat coast (RAB 1-2). a) Inter-aliquot variations of post-IRSL-BSL signals in core 5 of sample RAB 1-2. b) Variability of post-IRSL-BSL signals from different cores of the sample. c) Comparison of quartz post-IRSL-BSL and feldspar IRSL signals measured in the same post-IRSL-BSL protocol (mean values based on 5 cores each).

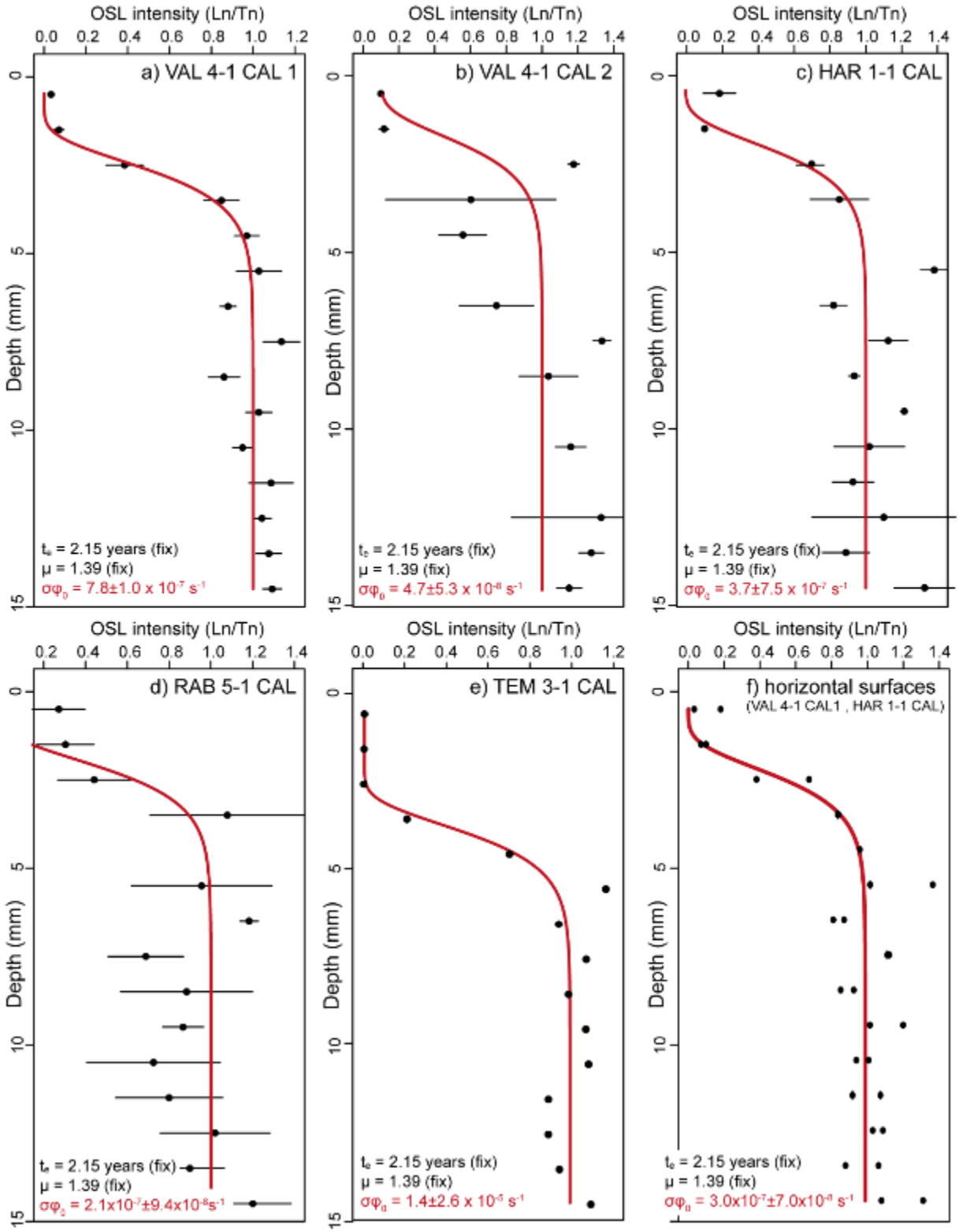

Fig. 5: Fitting post-IRSL-BSL signal-depth data of calibration samples. Individual fitting of the five calibration samples (a-e), and joint fitting of ~~all~~ calibration samples VAL 4-1 CAL 1 and HAR 1-1 CAL (VAL 4-1 CAL 2 and RAB 5-1 CAL are excluded due to the poor quality of their signal-depth data) to estimate a mutual $\overline{\sigma\varphi_0}$ value ~~with horizontal surfaces using shared μ values for each site and a shared $\overline{\sigma\varphi_0}$~~ for all samples with flat surfaces (f). Fixed parameters are shown in black, calculated parameters in red (lower left corner of a-f).

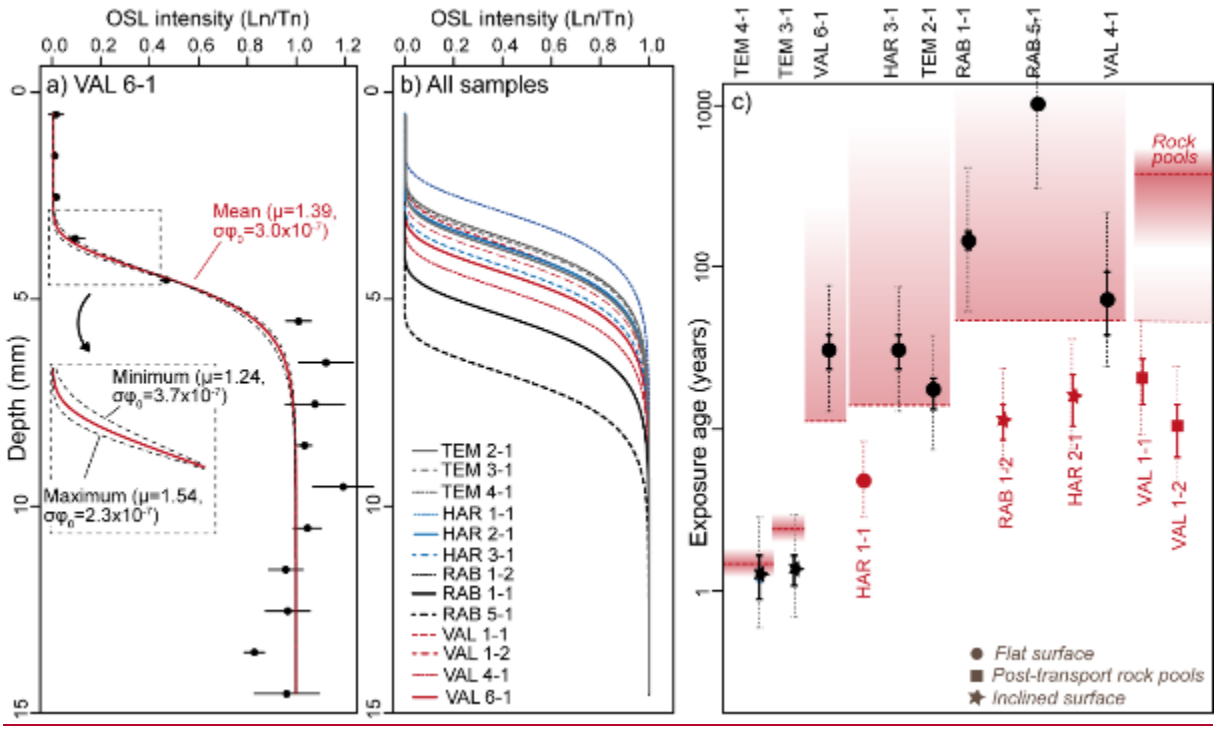

Fig. 6: Fitting of post-IRSL-BSL signal-depth data and comparison of OSL exposure ages with age control. a) Fitting of sample VAL 6-1 with fixed μ (mutual value for all calcarenite samples in this study) and $\overline{\sigma\varphi_0}$ (mutual value for horizontal suurfaces. Fitting uncertainties due to the uncertainties of μ and $\overline{\sigma\varphi_0}$ are highlighted in the close up. b) Model fits for all ~~dated~~ targeted samples (based on ~~mean~~ mutual values for μ and $\overline{\sigma\varphi_0}$). c) Comparison of modelled exposure ages (symbols with error bars) and age control from satellite images, eyewitness observations and depth of post-transport rock pools (indicated by red shaded areas). Exposure ages in agreement with control ages are shown in black, those too young for the control ages in red.

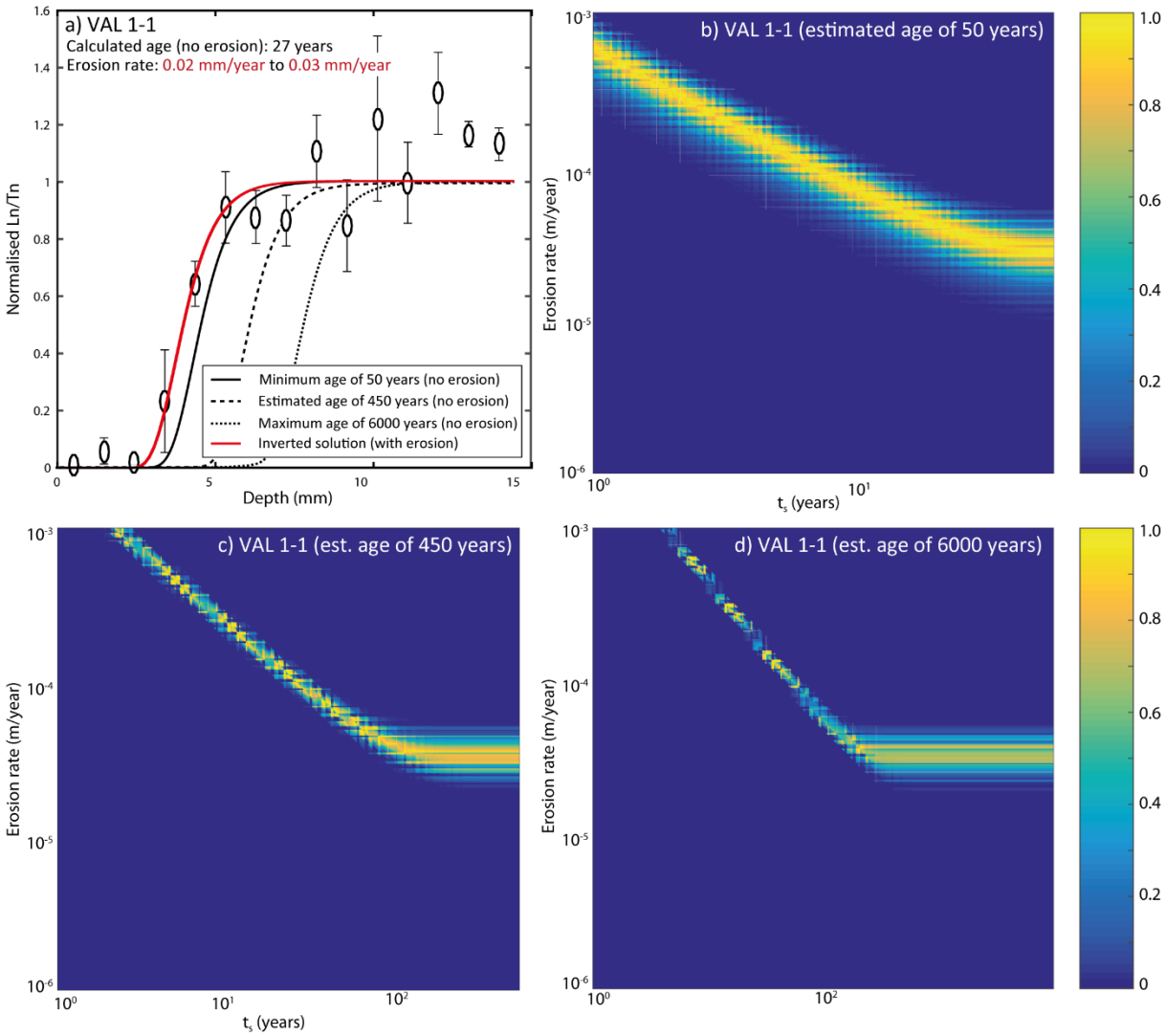

Fig. 7: Inverse modelling of post-deposition erosion rates using the approach of Lehmann et al. (2019a). The effect of erosion on the OSL signal-depth profiles of samples VAL 1-12 ~~(a, b) and HAR 1-1 (c, d)~~ was evaluated using the shared μ and $\overline{\sigma\varphi_0}$ from Table 2 as model input (a). ~~In case of VAL 1-2 e~~Erosion rates were estimated for assumed exposure ages equal to the minimum age (50 years, b), a realistic age estimate based on rock-pool depth (450 years, c), and the maximum age (6000 years, d). ~~For HAR 1-1 only the minimum age of 15 years was used.~~ Since ~~e~~Erosion rates are sensitive to changes of t_s ~~(b, d),~~. ~~t~~The erosion rates reported in a) ~~and c)~~ are based on t_s values ~~of 10~~equal to the assumed exposure time (i.e. constant erosion rates during exposure).

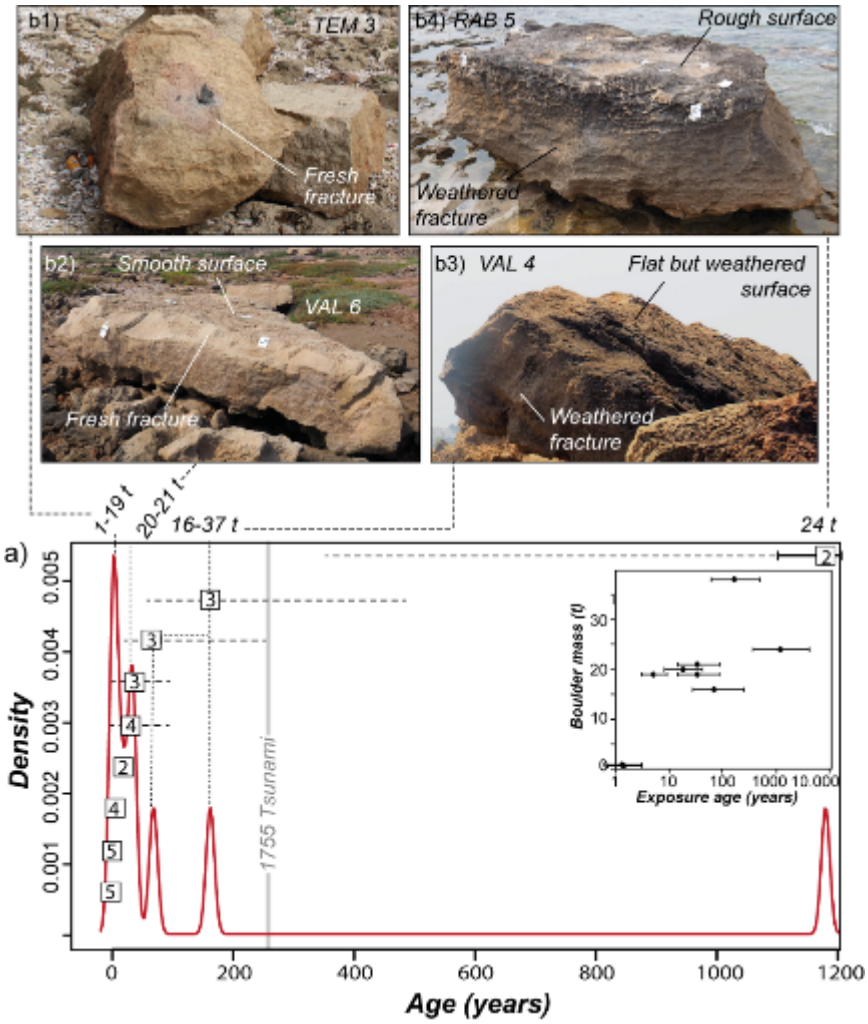

Fig. 8: Relative chronology of boulder transport. a) Exposure ages of all boulders that do not clearly underestimate the control ages presented as KDE plot (dotted error bars with consideration of μ and $\overline{\sigma\varphi_0}$ uncertainties). The numbers in squares refer to the taphonomy classes described in the text and the caption of Table 1. Inset: Correlation between boulder mass and OSL rock surface exposure ages. b) Photographs documenting the taphonomy of boulders with different OSL rock surface exposure ages. Each photograph is correlated with a KDE peak in a) and ~~a~~ associated boulder masses by dashed lines.

Boulder	Depositional setting			Boulder dimension				Samled surface		Sample	
	Lat/Long (°)	*Position*	*Group*	*Shape*	*Vol. (m^3)*	*Density (g/m^3)*	*Mass (t)*	*Orien-tation*	*Tapho-nomy*	*Dating*	*Calibration*
RAB 1	34.007964 -6.869395	Supratidal platform 2.7 m asl, 40 m from cliff	Single	Irregular	15.3	2.45	37.5	0° 25° SE	3	RAB 1-1 RAB 1-2	-
RAB 5	33.999778 -6.877759	Intertidal platform (surface above tides)	Single	Cubic	9.8	2.4	23.5	0°	2	RAB 5-1	RAB 5-1 CAL
HAR 1	33.953904 -6.927609	Oulja 2 m asl, 35 m from cliff	Single	Platy	8.2	2.3	18.9	0°	4	HAR 1-1	HAR 1-1 CAL**
HAR 2	33.953525 -6.928669	Top of younger ridge 4.5 m asl, 16 m from cliff	Imbricated	Platy	3.6	2.4	8.6	25° NW	4	HAR 2-1	-
HAR 3*	33.954182 -6.927901	Niche in active cliff (intertidal)	-	Platy	-	-	-	0°	3	HAR 3-1	-
TEM 2	33.927066 -6.961859	Top of younger ridge 4.2 m asl, 35 m from cliff	Single	Platy	8.3	2.4	19.9	0°	2	TEM 2-1	-
TEM 3	33.926842 -6.961915	Top of younger ridge 4.5 m asl, 38 m from cliff	Single	Irregular	0.3	2.4	0.7	25° W	5	TEM 3-1	TEM 3-1 CAL
TEM 4*	33.927949 -6.960674	Niche in active cliff (supratidal)	-	Platy	-	-	-	25° W	5	TEM 4-1	-
VAL 1	33.909435 -6.989803	Intertidal platform (surface above tides)	Single	Cubic	26.2	2.25	59.0	10° SE	1	VAL 1-1 VAL 1-2	-
VAL 4	33.907733 -6.991505	Top of younger ridge 3 m asl, 25 m from cliff	Imbricated	Platy	7.3	2.2	16.1	0°	3	VAL 4-1	VAL 4-1 CAL1 VAL 4-1 CAL2**
VAL 6	33.906084 -6.993316	Oulja 2.5 m asl, 80 m from cliff	Single	Platy	8.9	2.3	20.5	0°	4	VAL 6-1	-

Tab. 1: Characteristics of dated boulders. Lat/Long = Latitude/Longitude, * = niche at coastal cliff, ** = calibration sample on nearby roof top, taphonomy classes 1 to 5 with 1 – post-transport rock pools, 2 – rough post-transport surface covered with lichens/algae, 3 – smooth post-transport surface with scarce lichen/algae cover, 4 – smooth post-transport surface without/hardly any lichens/algae and fresh fractures, and 5 – fresh post-transport surfaces and fractures.

Sample	Cat.	Indiv. μ (mm^{-1})	Shared μ (mm^{-1})	Indiv. $\sigma\varphi_0$ (s^{-1})	Shared $\sigma\varphi_0$ (s^{-1})	t_{exp} mean (yrs)	t_{exp} Min-Max (yrs)	$t_{age\ control}$ (yrs)
RAB 5-1 CAL	Calibration	0.73±0.35	"	$2.1x10^{-7}±9.4x10^{-8}$	"	**2.15 (fix)**	"	2.15
VAL 4-1 CAL II		0.76±0.53	"	$4.7x10^{-8}±5.3x10^{-8}$	"	**2.15 (fix)**	"	2.15
HAR 1-1 CAL		1.65±0.55		$3.7x10^{-7}±7.5x10^{-7}$		**2.15 (fix)**	"	2.15
VAL 4-1 CAL I		1.62±0.50		$7.8x10^{-7}±1.0x10^{-6}$	**$3.0x10^{-7}±7.0x10^{-8}$**	**2.15 (fix)**	"	2.15
TEM 3-1 CAL		1.83±0.47		$1.4x10^{-5}±2.6x10^{-5}$	**$2.6x10^{-6}±5.3x10^{-7}$**	**2.15 (fix)**	"	2.15
RAB 1-1	Dating	2.71±3.99	**1.39±0.15 (fix)**	"	**$3.0x10^{-7}±7.0x10^{-8}$ (fix)**	**162±21**	60-486	>50
RAB 1-2		1.17±0.39		"	**$3.0x10^{-7}±7.0x10^{-8}$ (fix)**	**12±3**	6-26	>50
RAB 5-1		0.51±0.18		"	**$3.0x10^{-7}±7.0x10^{-8}$ (fix)**	**1180±158**	360-4110	>50
HAR 1-1		1.97±0.35		"	**$3.0x10^{-7}±7.0x10^{-8}$ (fix)**	**4.8±0.2**	3-9	>15
HAR 2-1		1.16±0.53		"	**$3.0x10^{-7}±7.0x10^{-8}$ (fix)**	**17±6**	8-40	>50
HAR 3-1		1.03±0.27		"	**$3.0x10^{-7}±7.0x10^{-8}$ (fix)**	**33±8**	14-85	>15
TEM 2-1		1.02±0.24		"	**$3.0x10^{-7}±7.0x10^{-8}$ (fix)**	**18±4**	8-42	>15
TEM 3-1		2.17±0.99		"	**$2.6x10^{-6}±5.3x10^{-7}$ (fix)**	**1.4±0.3**	0.7-3.1	~2.5
TEM 4-1		0.79±0.24		"	**$2.6x10^{-6}±5.3x10^{-7}$ (fix)**	**1.3±0.4**	0.6-3	~1.5
VAL 1-1		1.10±0.40		"	**$3.0x10^{-7}±7.0x10^{-8}$ (fix)**	**22±7**	10-52	>50 ~450
VAL 1-2		1.01±0.38		"	**$3.0x10^{-7}±7.0x10^{-8}$ (fix)**	**11±4**	5-27	>50 ~450
VAL 4-1		0.87±0.31		"	**$3.0x10^{-7}±7.0x10^{-8}$ (fix)**	**68±24**	27-250	>50
VAL 6-1		3.43±3.77		"	**$3.0x10^{-7}±7.0x10^{-8}$ (fix)**	**33±8**	14-87	>12

Tab. 2: Summary of model parameters for all calibration and dating samples. Bold numbers indicate values that were ~~calculated by the model~~eventually used for calibration and dating. Cat. = sample category, Indiv. = individual, t_{exp} mean = exposure ages based on fixed μ and $\overline{\sigma\varphi_0}$ values without their uncertainties, t_{exp} Min-Max = exposure age range with consideration of μ and $\overline{\sigma\varphi_0}$ uncertainties.

Appendices

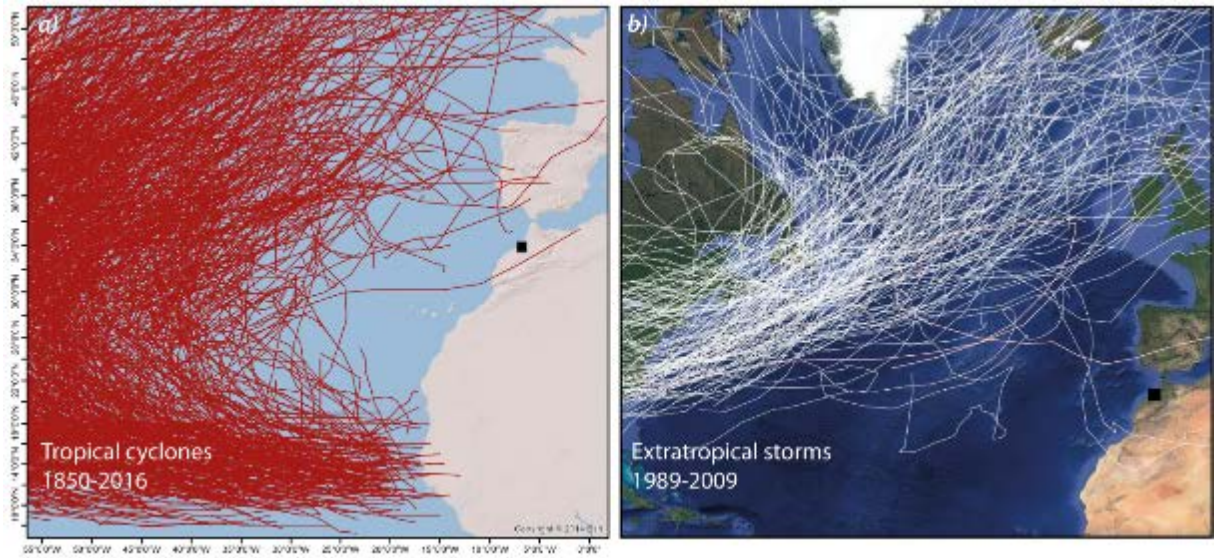

Fig. A1: Storm hazard at the Rabat coast. a) Tracks of historical (1850-2016) tropical storms in the North Atlantic (NOAA, 2019); even aged tropical cyclones (tropical depressions) rarely strike the coastlines of the eastern Atlantic as far south as Spain or Morocco. b) Tracks of the 200 strongest extratropical storms in the North Atlantic 1989-2009 (Atlas of extratropical storms, University of Reading, 2019); most winter storms cross northern Europe, storm tracks as far south as Spain or Morocco are very rare.

Fig. A2: Storm waves and coastal flooding at Haroura. a) During normal wave conditions, all sampled boulders are located above tide level. b) Flooding of the Oulja and local wave overwash reaching up to 50 m landward of the shoreline during a winter storm in December 2018. Both scenes are based on Google Earth images.

Fig. A3: Storm transport of boulders recorded on satellite images (Google Earth). a) Positions of boulders VAL 6 and 7 in June 2010. b) Positions of the same boulders in February 2014. While VAL 6 remains stable, pushed by storm waves VAL 7 has moved for about 15 m perpendicular to the shoreline. c) After relocation in February 2014, both boulders remained in stable positions until July 2018. All scenes are based on Google Earth images.

Boulder/Niche	*Corona 1966*	*Google Earth*	*Observation*	*Age (years)*
RAB 1	at present position or slightly seaward but already overturned	at present pos. in 2001	-	>50
RAB 5	at present position	at present pos. in 2001	-	>50
HAR 1	-	at present pos. in 2001	-	>15
HAR 2	at present position, a-axis slightly turned	at present pos. in 2001	-	>50
HAR 3	-	at present pos. in 2001	-	>15
TEM 2	-	at present pos. in 2001	-	>15
TEM 3	-	-	deposited in Feb 2014	~2.5
TEM 4	-	-	formed between Jul 2016 and Sept 2018	~1.5
VAL 1	at present position	at present pos. in 2004	Up to 45 cm deep post-transport rock pools	>50 ~450*
VAL 4	at present position	at present pos. in 2004	-	>50
VAL 6	-	at present pos. in 2004	-	>12

Tab. A1: Summary of age control for boulder movement and niche formation in the form of satellite images and own observations. pos. = position, - = no clear evidence. *Minimum age estimate based on the depth of post-depositional rock pools and empirical rates of bio-erosion in the order of 1 mm/year (Kelletat, 2013).

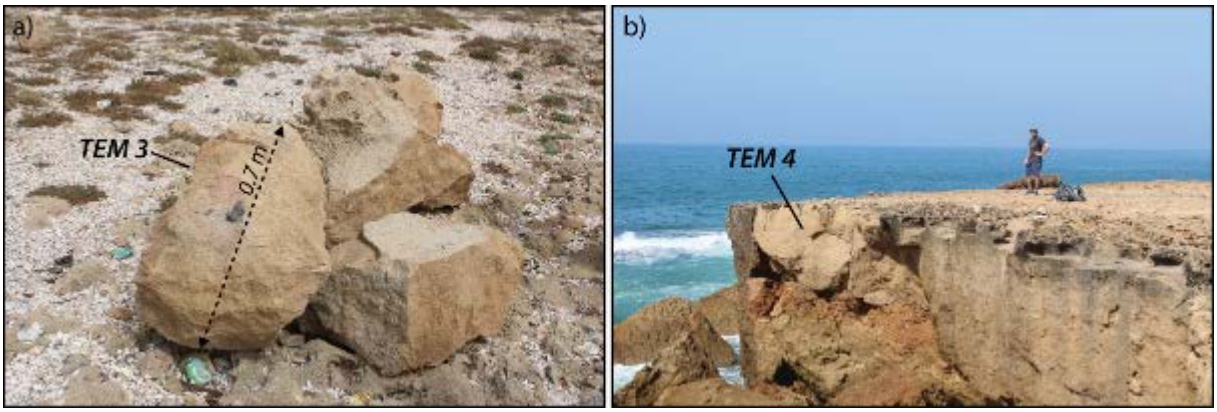

Fig. A4: Boulder TEM 3 (a) was transported to its onshore location during winter storm Hercules/Christina in February 2014 as reported by local residents. Niche TEM 4 was formed between the field surveys in Juli 2016 and September 2018, most likely by a winter storm in 2017.

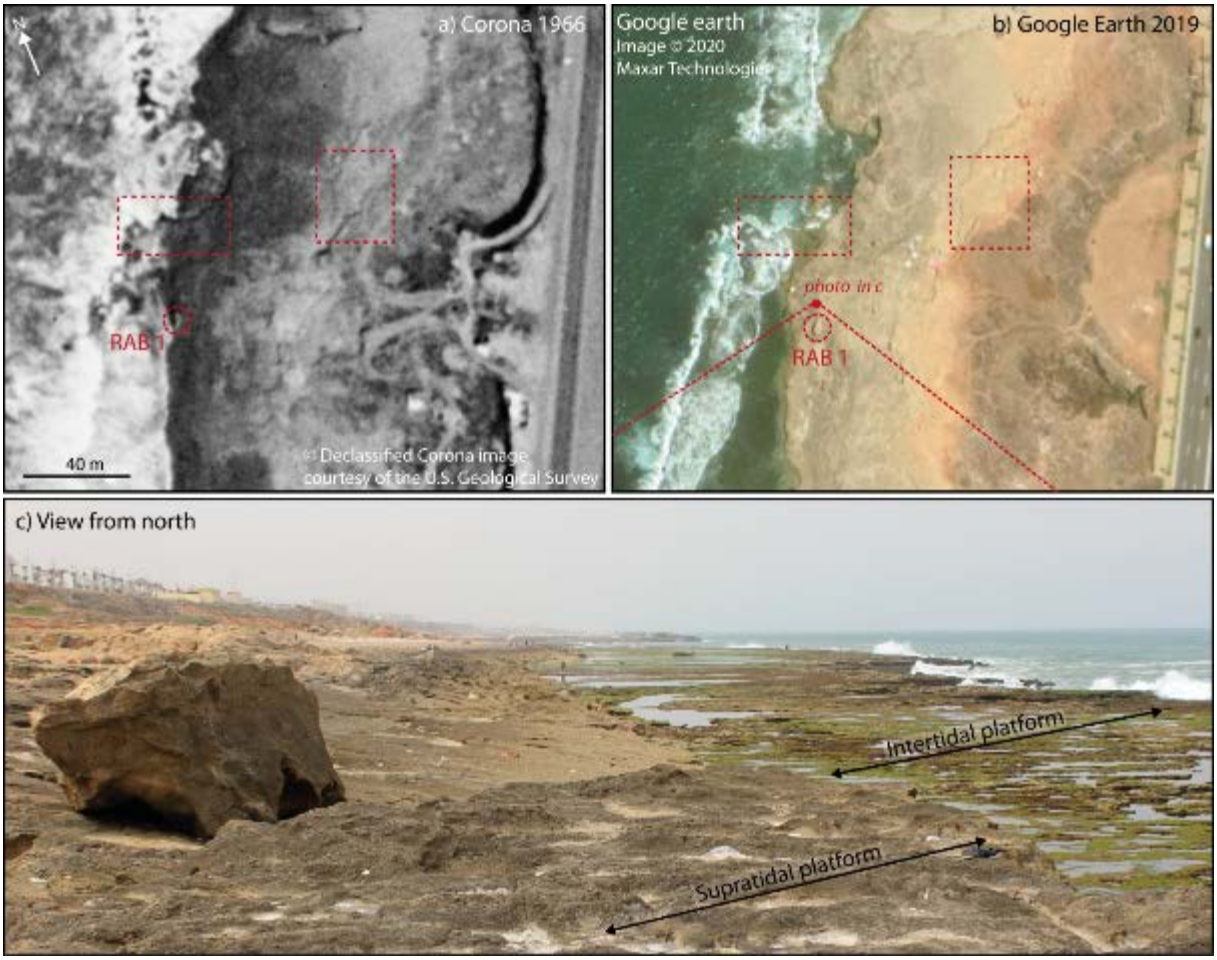

Fig. A5: Boulder RAB 1. a) RAB 1 (red circle) can be located on the 1966 Corona satellite image. Compared to its present position on the 2019 Google Earth image (b) it might have been pushed a few meters landward but there is no indication of overturning (red rectangles mark features clearly identified on both images for better orientation). c) View towards south with boulder RAB 1 lying on the slope of the supratidal platform (photography July 2016).

Fig. A6: Boulder RAB 5. a) RAB 5 (white/red circle) can be located on the 1966 Corona satellite image. It has not changed compared to its present position on the 2019 Google Earth image (b).

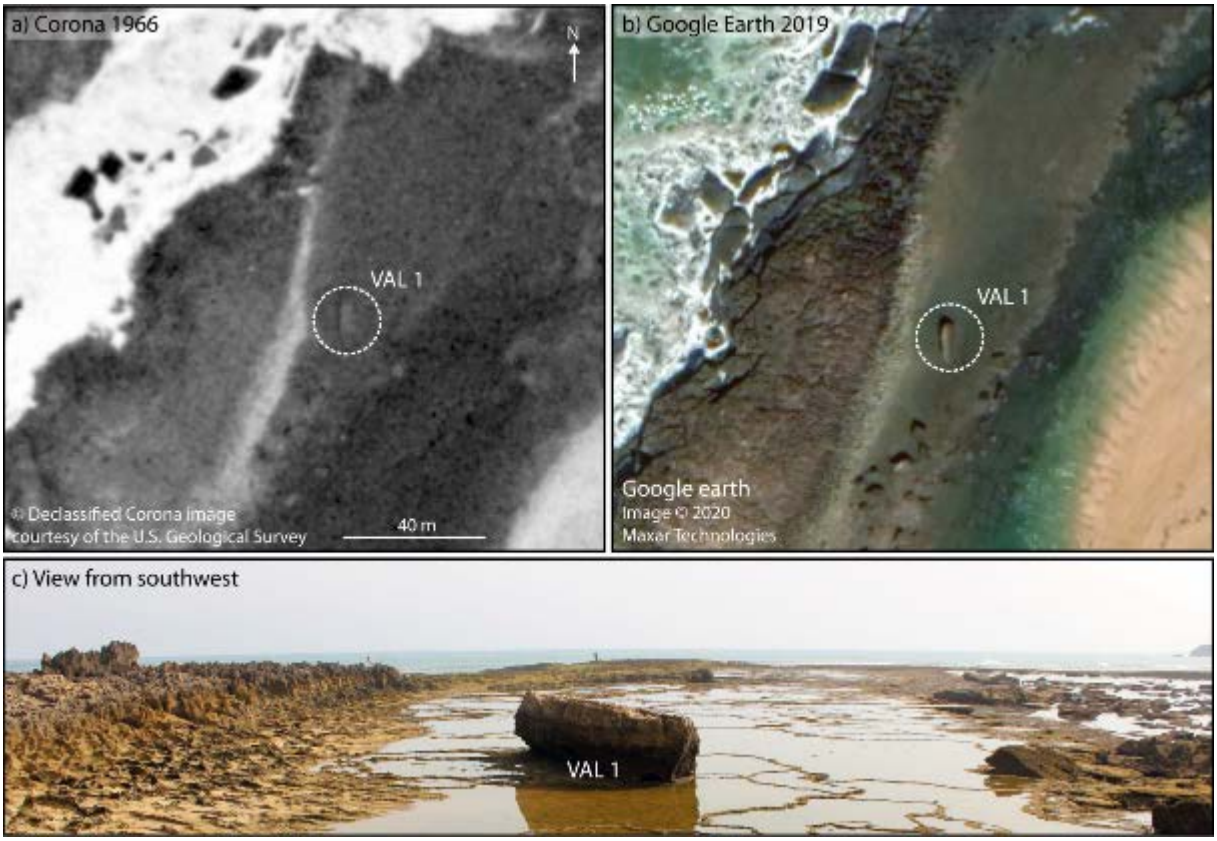

Fig. A7: Boulder VAL 1. a) VAL 1 (white circle) can be located on the 1966 Corona satellite image. It has not changed compared to its present position on the 2019 Google Earth image (b). c) View towards northeast with boulder VAL 1 lying on the intertidal platform behind the youngest ridge (photography July 2016).

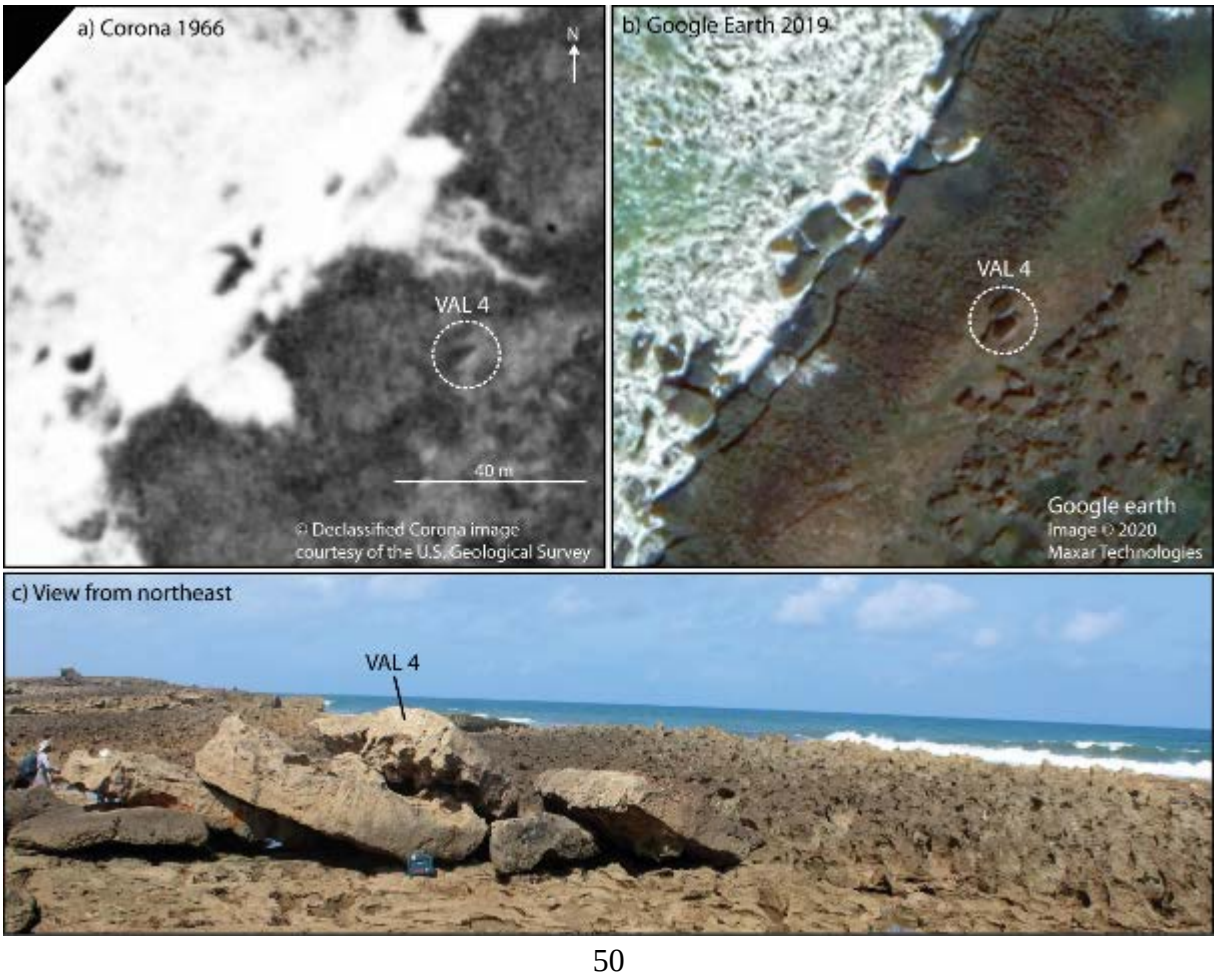

Fig. A8: Boulder VAL 4. a) VAL 4 (white circle) can be located on the 1966 Corona satellite image. It has not changed compared to its present position on the 2019 Google Earth image (b). c) View towards southwest with boulder VAL 4 lying on the youngest ridge (photography July 2016).

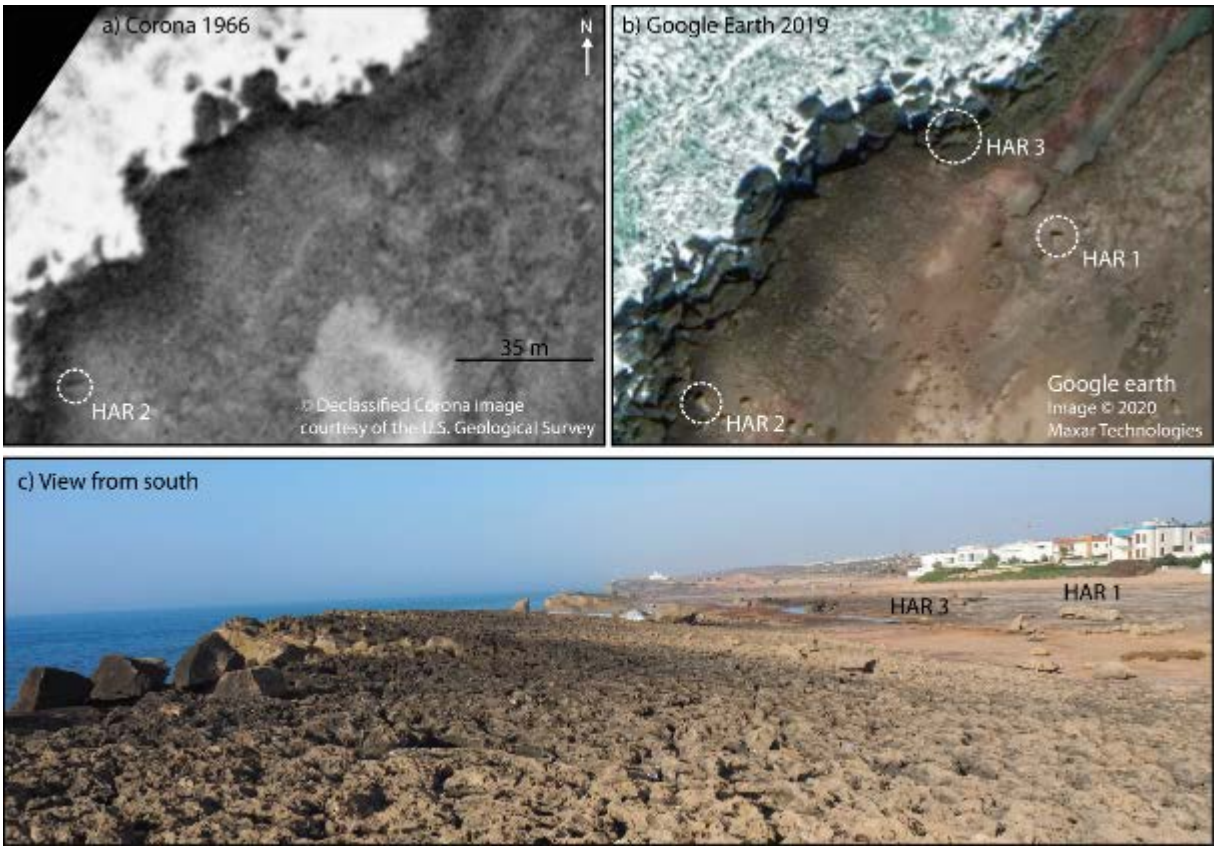

Fig. A9: Boulders at site HAR. a) Boulder HAR 2 (white circle) can be located on the 1966 Corona satellite image. It slightly rotated along its a-axis, but has not changed its position compared to the 2019 Google Earth image (b). Boulder HAR 1 and niche HAR 3 cannot be identified on the 1966 image; this may be due to poor quality of the image or since they were formed afterwards. c) View towards the north with boulder HAR 1 lying in the depression behind the youngest ridge (photography September 2018).

Fig. A10: Boulder TEM 2 at Temara. a) Boulder TEM 2 (white circle) can be located on 2001 Google Earth satellite images. It has not changed compared to its present position on the 2019 Google Earth image (b). It cannot be identified on the 1966 image; this may be due to poor quality of the image, or since it was deposited afterwards. c) View towards south with boulder TEM 2 lying on the supratidal clifftop platform formed by the youngest ridge (photography Juli 2016).

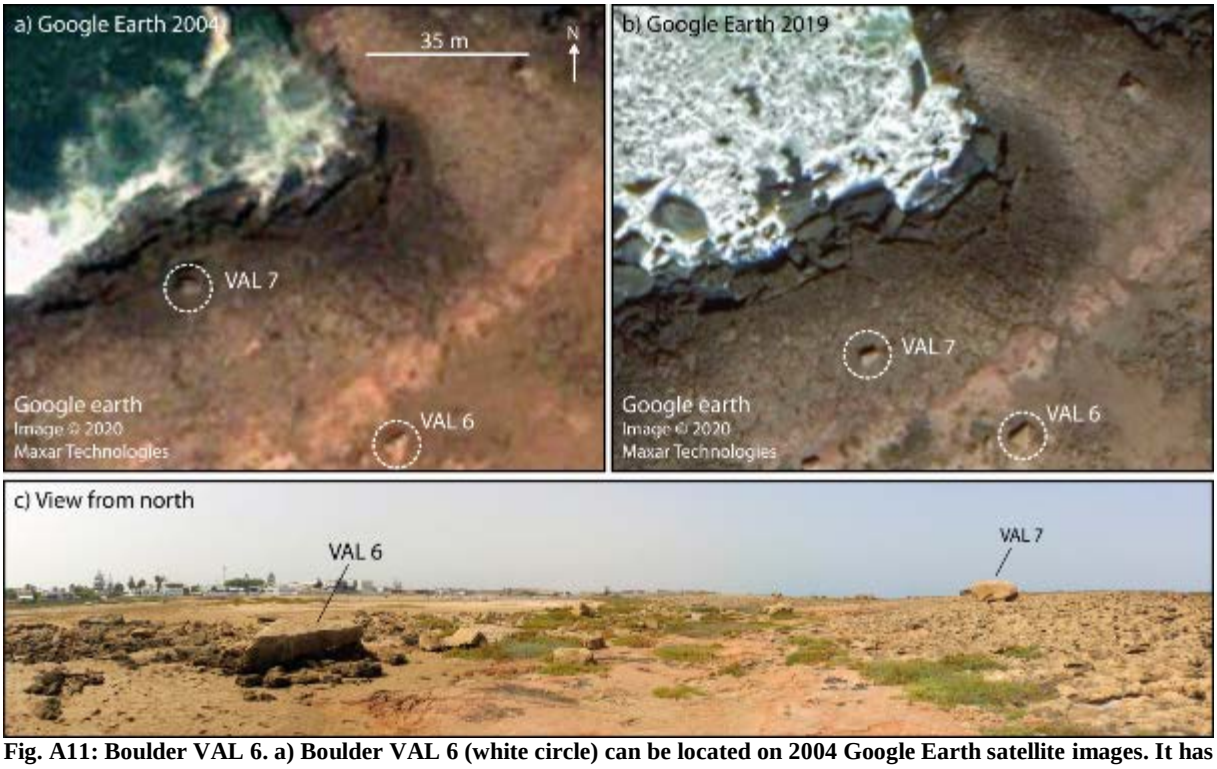

Fig. A11: Boulder VAL 6. a) Boulder VAL 6 (white circle) can be located on 2004 Google Earth satellite images. It has not changed compared to its present position on the 2019 Google Earth image (b). It cannot be identified on the 1966 Corona image; this may be due to poor quality of the image, or since it was deposited afterwards. c) View towards south with boulder VAL 6 lying in the depression behind the youngest ridge (photography Juli 2016).

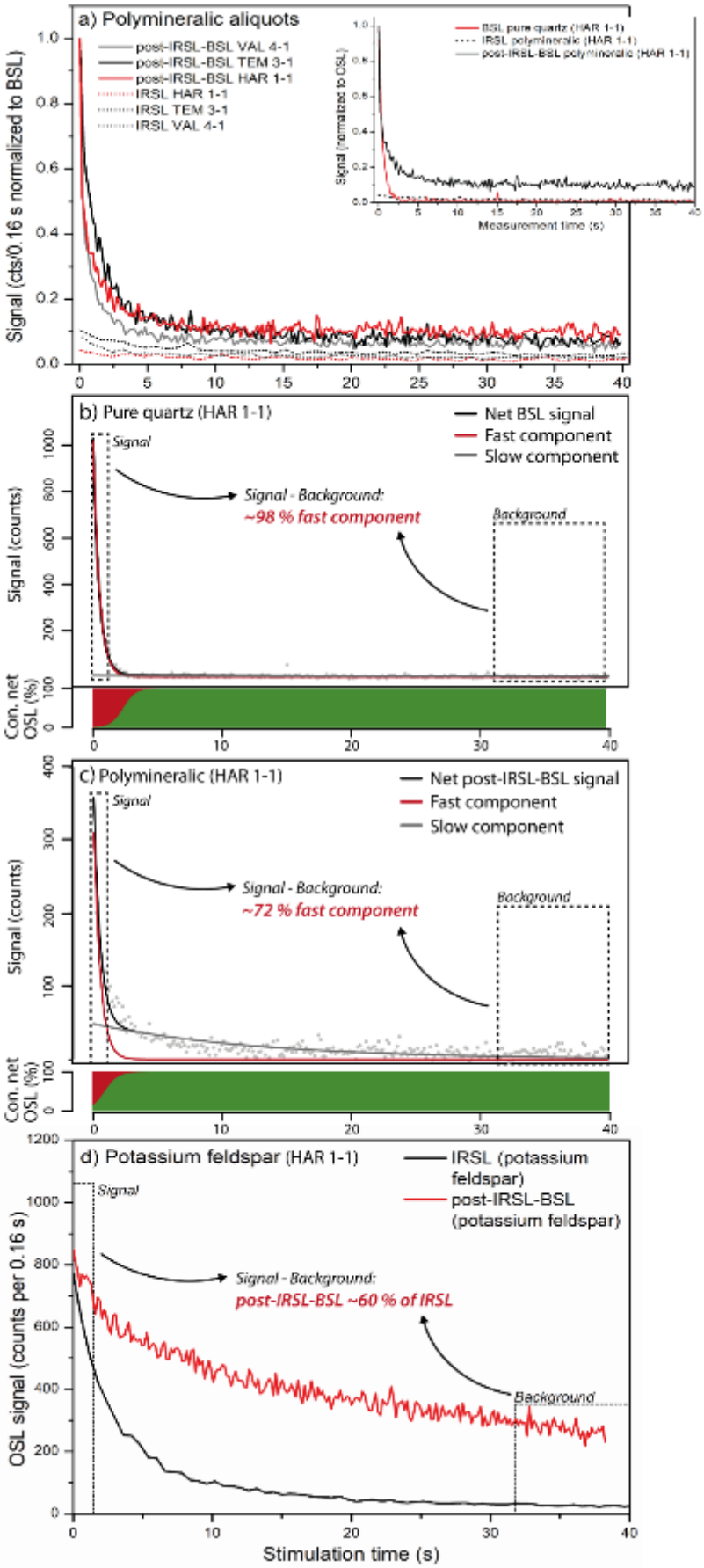

Fig. A12: Luminescence signal properties in the dated sandstone. a) Decay curves of post-IRSL-BSL and IRSL signals of polymineralic aliquots. The post-IRSL-BSL signals are significantly more intensive than the associated IRSL signals

(intensities sum up to only 12-24 % of those of the associated post-IRSL-BSL signals). Inset: Comparison of post-IRSL-BSL and IRSL decay curves of polymineralic aliquots and a pure quartz extract of sample HAR 1-1. b) Quartz BSL signal components achieved by fitting the BSL decay curve of pure quartz of HAR 1-1. The signal in the selected integration limits is dominated by a stable and easily bleachable fast component (σ = 2.4-2.5x10-17, cf. Jain et al., 2003), accounting for 98 % of the analysed net signal. c) Although less pronounced, post-IRSL-BSL signals of polymineralic samples are still dominated by the fast component (σ = 2.4-2.5x10-17, 72% of net signal). d) Comparison of IRSL and post-IRSL-BSL signals measured on potassium feldspar extracts of HAR 1-1. The counts of the background-corrected post-IRSL-BSL signal equal ~60 % of the background-corrected IRSL signal. This indicates that post-IRSL-BSL signals on our polymineralic aliquots are relatively unaffected by a feldspar signal contribution: IRSL signals amount to 12-24 % of the post-IRSL-BSL signals n polymineralic aliquots; 60 % of this IRSL emission still contributes to the post-IRSL-BSL signals, which equals 7.5-15 % of the net post-IRSL-BSL signal in polymineralic aliquots.

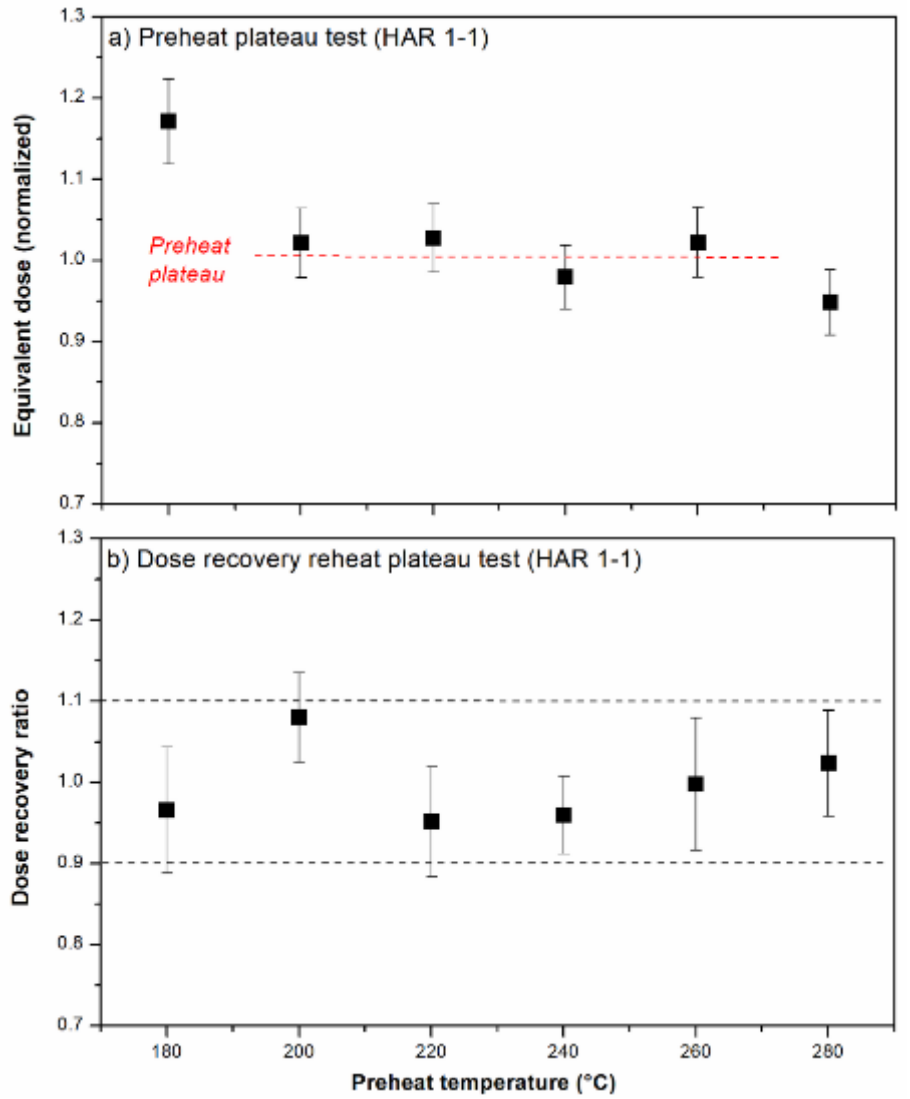

Fig. A13: Preheat plateau test (a) and dose recovery preheat plateau test with laboratory doses of ~5 Gy (b) performed on quartz extracts of sample HAR 1-1. Both experiments indicate a preheat plateau for temperatures between 200 and 260 °C.

Step	Treatment	Signal
1	Preheat (220 °C for 10 s)	
2	IR LEDs (1650 s @ 50 °C)	L_n (IRSL)
3	Blue LEDs (40 s @ 125 °C)	L_n (post-IRSL-BSL)
4	Test dose (~12 Gy)	
5	Preheat (220 °C for 10 s)	
6	IR LEDs (1650 s @ 50 °C)	T_n (IRSL)
7	Blue LEDs (40 s @ 125 °C)	T_n (post-IRSL-BSL)

Tab. A2: Double SAR protocol used for measurement of Ln/Tn data from polymineralic aliquots of crushed slices.

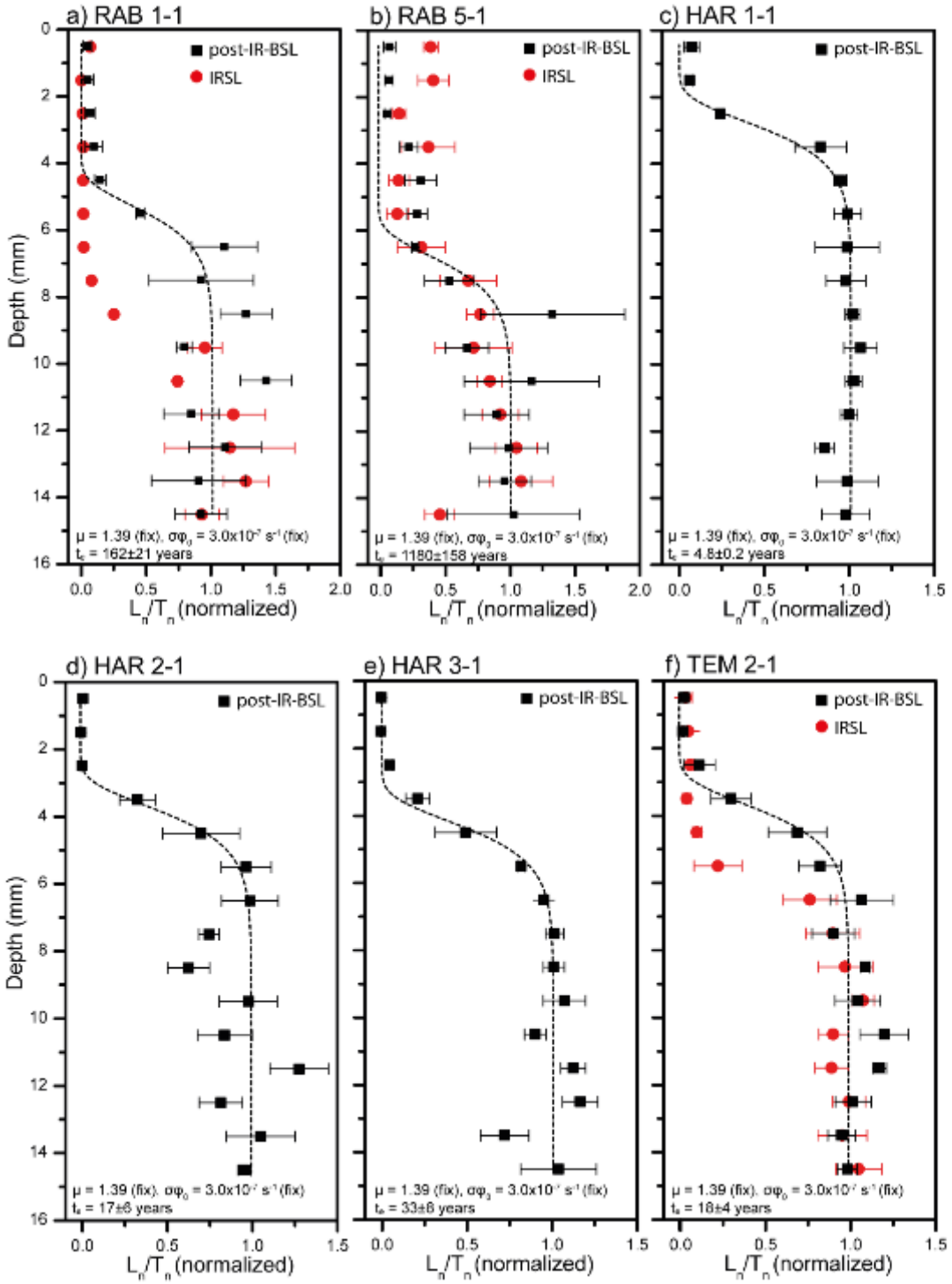

Fig. A14: Fitted p~~P~~ost-IRSL-BSL signal-depth curves for ~~all cores of~~ boulder samples RAB 1-1, RAB 5-1, HAR 1-1, HAR 2-1, HAR 3-1 and TEM 2-1. ~~Black squares = cores included in calculation of mean signal-depth curves, grey circles = cores excluded from calculation of mean signal-depth curves, red squares =~~ All data points represent mean values plus standard error of 3-5 cores. For samples with sensitive IRSL signals, these were plotted for comparison.

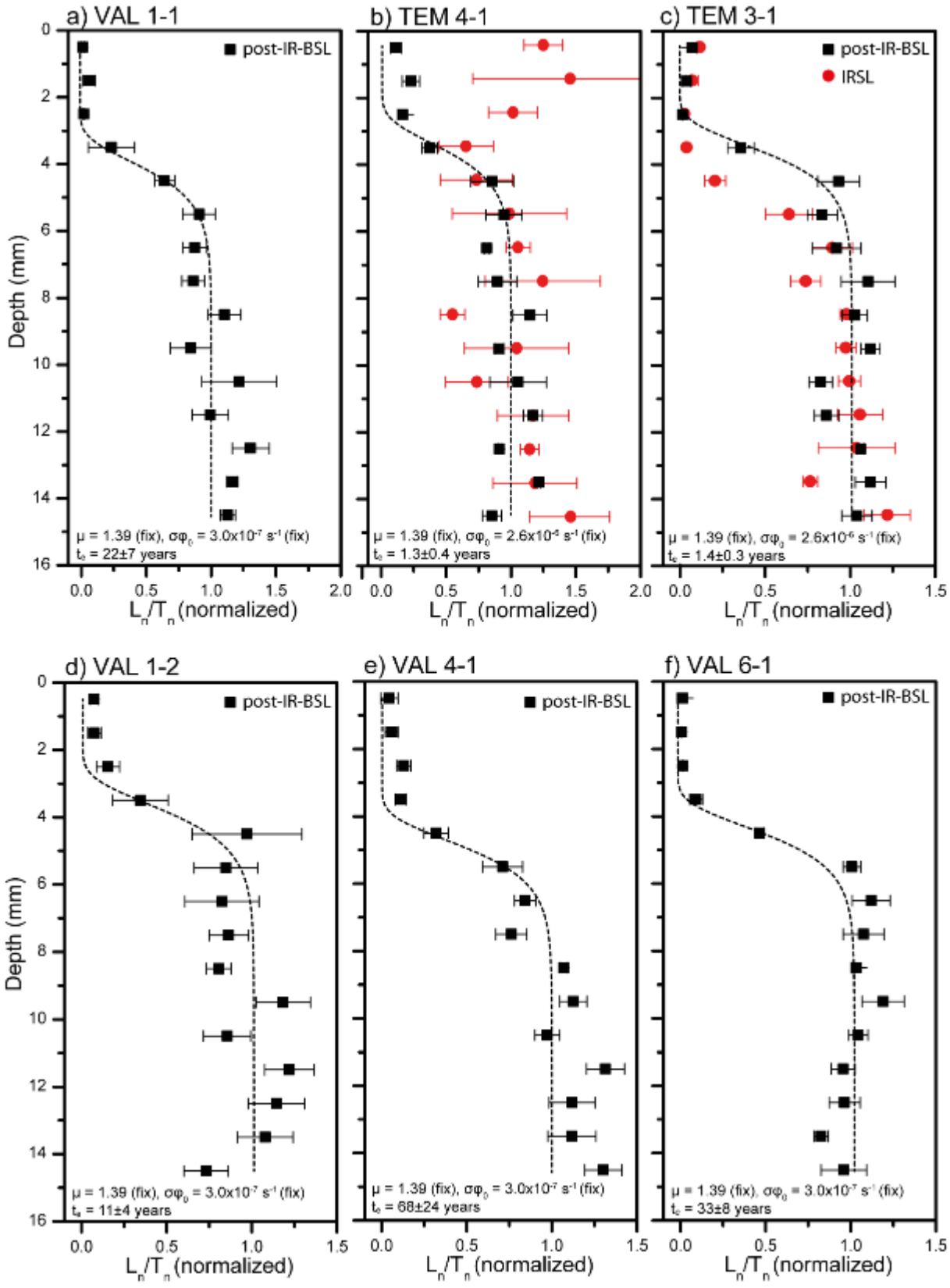

Fig. A15: Fitted p~~P~~ost-IRSL-BSL signal-depth curves for ~~all cores of~~ boulder samples TEM 3-1, TEM 4-1, VAL 1-1, VAL 1-2, VAL 4-1 and VAL 6-1. ~~Black squares = cores included in calculation of mean signal-depth curves, grey circles = cores excluded from calculation of mean signal-depth curves, red squares =~~ All data points represent mean values plus standard error of 3-5 cores. For samples with sensitive IRSL signals, these were plotted for comparison.

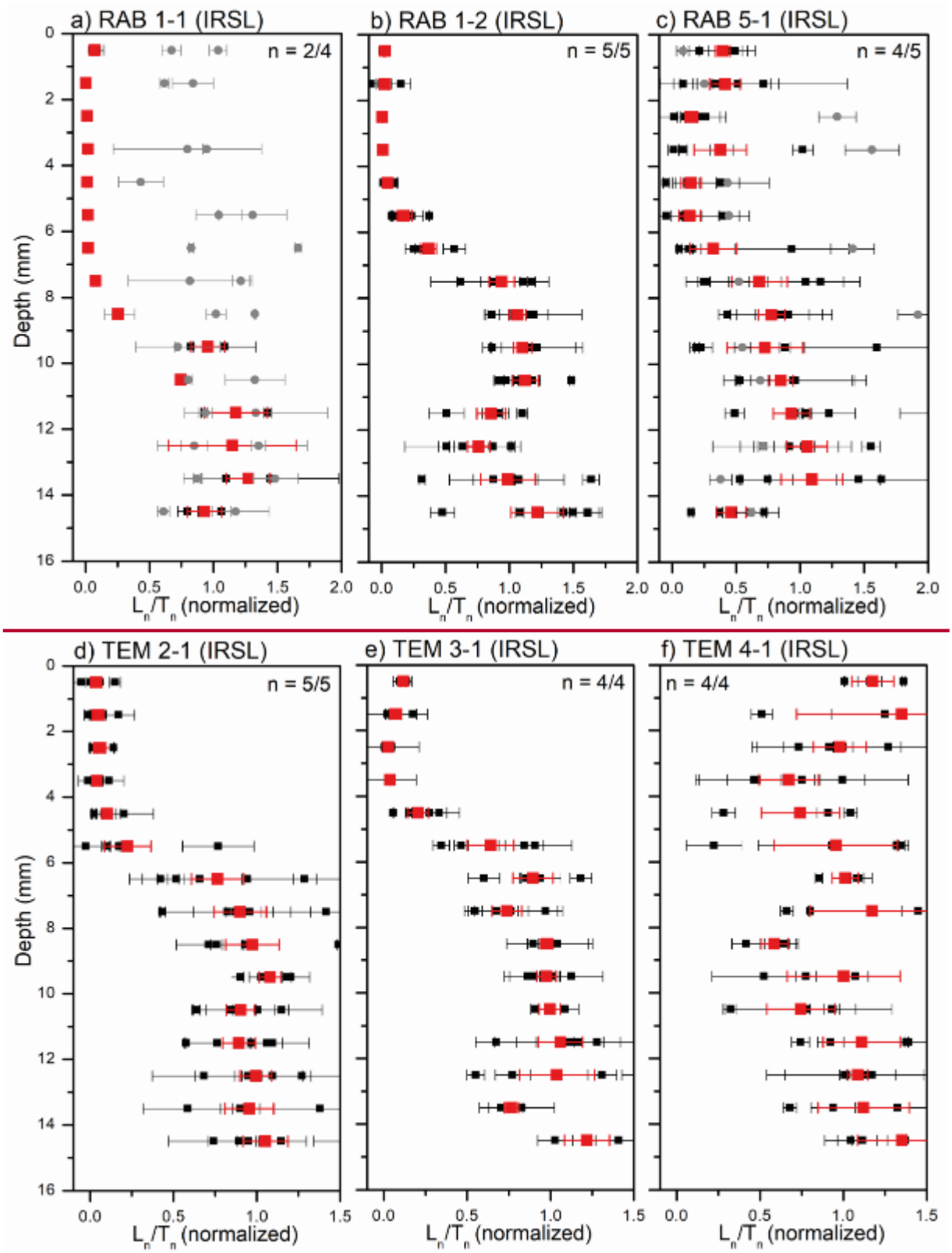

Fig. A16: IRSL signal-depth curves for all cores of boulder samples with adequate feldspar signals (RAB and TEM). Black squares = cores included in calculation of mean signal-depth curves, grey circles = cores excluded from calculation of mean signal-depth curves, red squares = mean values.

Fig. A167: Calibration samples. a) Roof top sample VAL 4-1 CAL I. b) Surface on boulder VAL 4 exposed during first field survey in July 2016 by removing at least 10 cm of rock. c) Roof of the house used for artificially exposing rock samples; samples VAL 4-1 CAL I and HAR 1-1 CAL were placed on top of the highest roof shown in the photo. d) Surface of boulder TEM 3 exposed during the first field survey in July 2016; at least 10 cm of rock were removed.

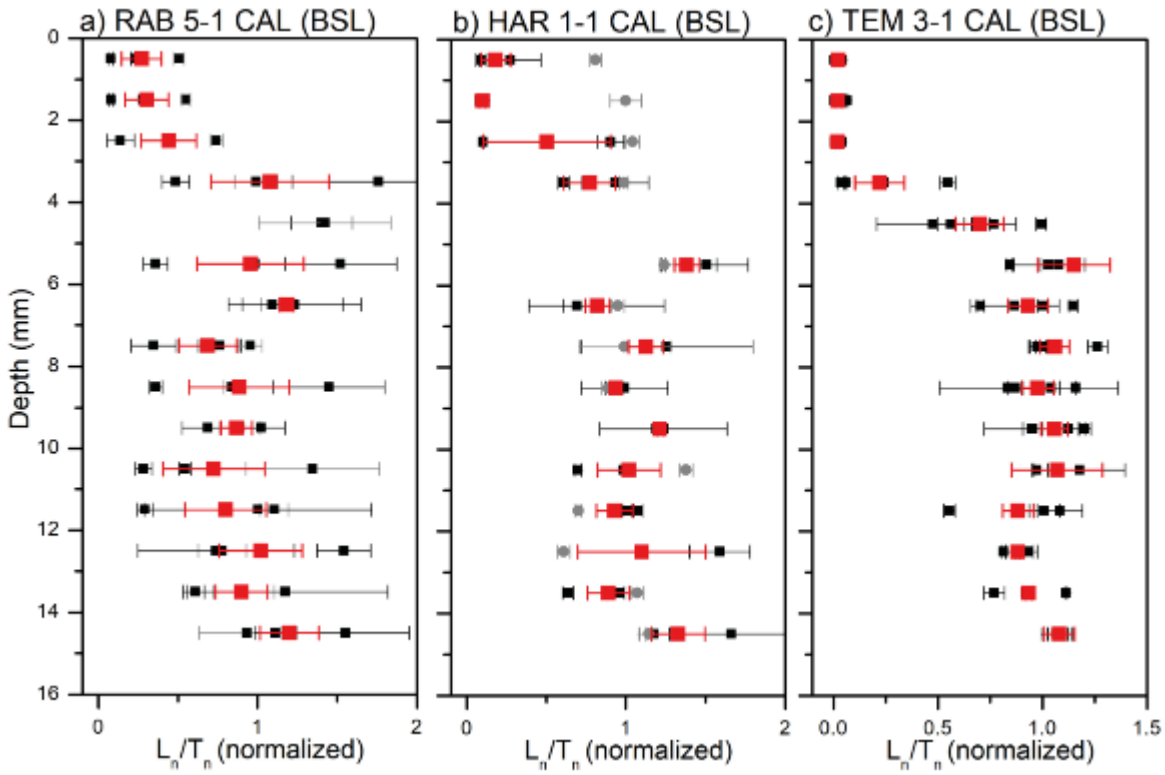

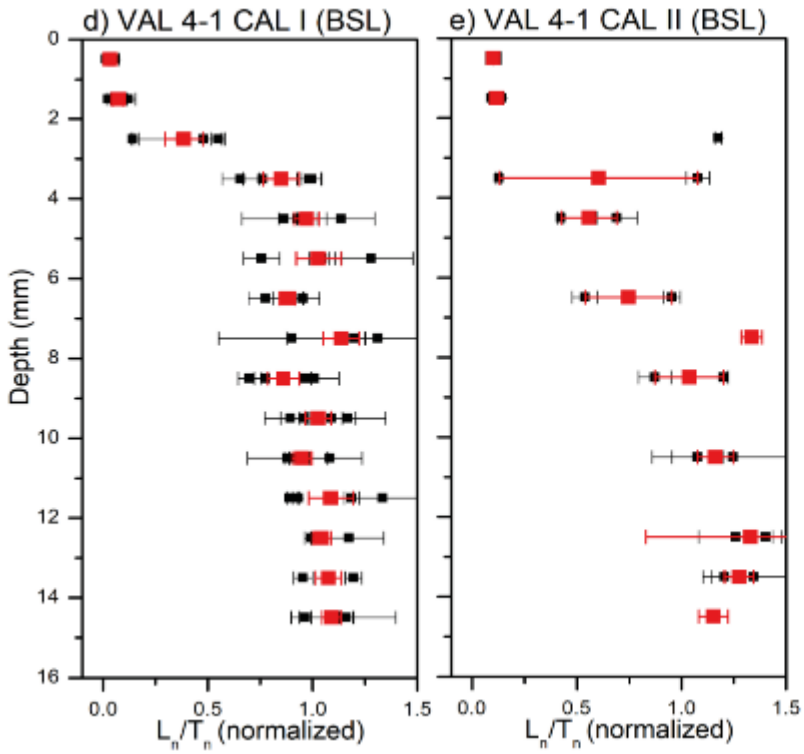

~~**Fig. A18: Post-IRSL-BSL signal-depth curves for all cores of the calibration samples. Black squares = cores included in calculation of mean signal-depth curves, grey circles = cores excluded from calculation of mean signal-depth curves, red squares = mean values.**~~

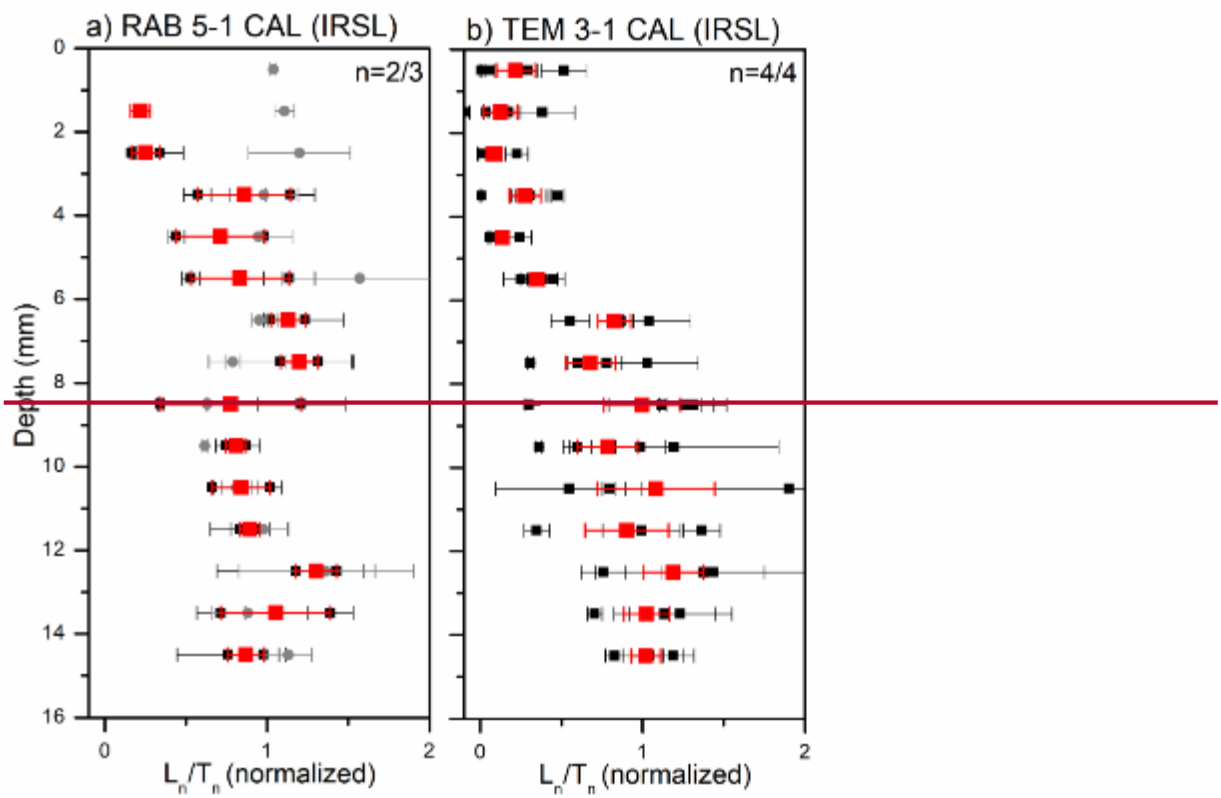

~~Fig. A19: IRSL signal-depth curves for all cores of calibration samples with adequate feldspar signals (RAB 5-1 CAL and TEM 3-1 CAL). Black squares = cores included in calculation of mean signal-depth curves, grey circles = cores excluded from calculation of mean signal-depth curves, red squares = mean values.~~

Step	Treatment	Signal
1	Preheat (220 °C for 10 s)	
2	Blue LEDs (40 s @ 125 °C)	L_x (BSL)
3	Test dose (~6 Gy)	
4	Preheat (220 °C for 10 s)	
5	Blue LEDs (40 s @ 125 °C)	T_x (BSL)
6	Regenerative dose (R1 to R4, R0, R1)	
7	Return to Step 1	

Tab. A3: SAR protocol used for equivalent dose measurement of quartz extracts.

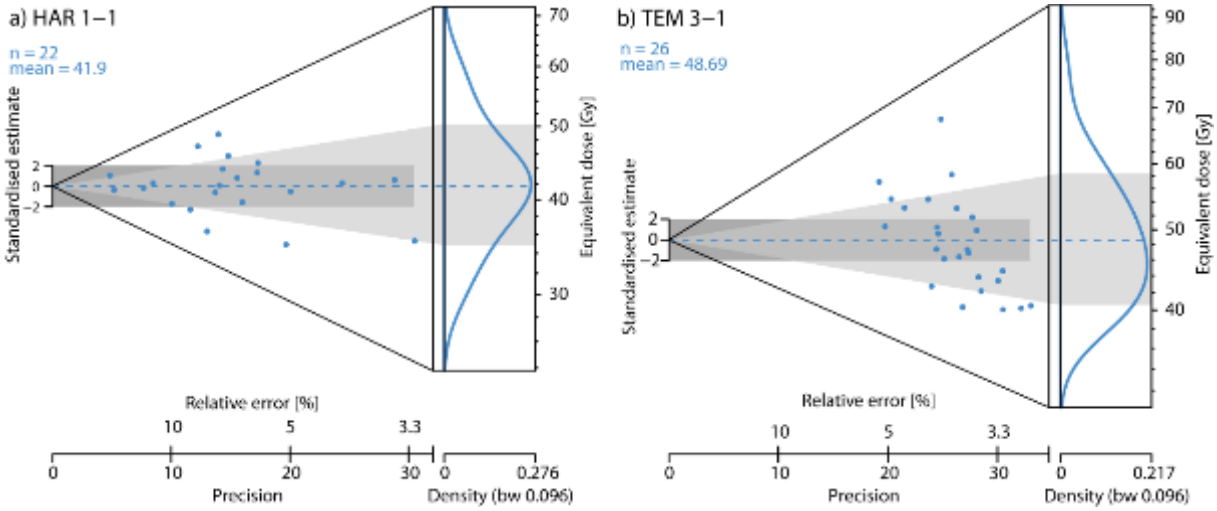

Fig. A17~~20~~: Equivalent dose distributions determined on quartz extracts of samples HAR 1-1 and TEM 3-1 (presented as Abanico plots).

Sample	U (ppm)	Th (ppm)	K (%)	Dose rate (Gy/ka)	Grain size (µm)	N	OD (%)	CAM De (Gy)	Age (ka)
HAR 1-1	0.91±0.06	0.62±0.06	0.11±0.01	0.53±0.02	100-200	22	16±3	41.7±1.6	81.0±4.1
TEM 3-1	0.86±0.05	0.62±0.05	0.10±0.01	0.51±0.02	100-200	26	17±2	48.6±1.7	98.1±4.8

Tab. A4: Dose rates, equivalent doses and conventional burial ages for samples HAR 1-1 and TEM 3-1.

Sample	Control age (years)	Erosion rate (mm/year)
VAL 1-1	50	~~<0.01~~0.0~~2~~7
VAL 1-1	450	0.0~~3~~0
VAL 1-1	6000	~~0.3~~20.0~~3~~7
VAL 1-2	50	0.~~05~~07
~~VAL 1-2~~	~~450~~	~~0.2014~~
~~VAL 1-2~~	~~6000~~	~~0.4014~~
HAR 1-1	15	0.18~~0~~6
HAR 2-1	50	0.04~~9~~6
RAB 1-2	50	0.0612~~3~~

Tab. A5: Modelling of post-transport erosion for samples with exposure ages that underestimate the minimum control ages (VAL 1-1, VAL 1-2, RAB 1-2, HAR 1-1 and HAR 1-2) and t_s equal to the control age (i.e. constant erosion rates for the entire exposure duration).